

## **SUPPORTING INFORMATION**

### **Organic photocatalyst for ppm-level visible-light-driven reversible addition-fragmentation chain transfer (RAFT) polymerization with excellent oxygen tolerance**

Yuna Song,<sup>1,†</sup> Youngmu Kim,<sup>1,†</sup> Yeonjin Noh,<sup>1</sup> Varun Kumar Singh,<sup>1</sup> Santosh Kumar Behera,<sup>2</sup> Abasi Abudulimu,<sup>2</sup> Kyeongwoon Chung,<sup>3</sup> Reinhold Wannemacher,<sup>2</sup> Johannes Gierschner,<sup>2</sup> Larry L  er,<sup>2</sup> and Min Sang Kwon<sup>1,\*</sup>

<sup>1</sup>Department of Materials Science and Engineering, Ulsan National Institute of Science and Technology (UNIST), Ul-san 689-798, Korea

<sup>2</sup>Madrid Institute for Advanced Studies, IMDEA Nanoscience, Calle Faraday 9, Campus Cantoblanco, 28049 Madrid, Spain

<sup>3</sup>3D Printing Materials Center, Korea Institute of Materials Science (KIMS), Changwon, 51508, South Korea

#### **Corresponding Author**

\*E-mail: kwonms@unist.ac.kr

# TABLE OF CONTENTS

## I. Supplementary Methods

- A. General information*
- B. Procedures of PET-RAFT polymerizations of MMA*
- C. Syntheses of 4DP-IPN used in this work*

## II. Supplementary Figures and Tables

## III. UV-vis and PL spectra, CV curves, and $^1\text{H}$ -NMR and $^{13}\text{C}$ -NMR spectra of selected OPCs and GPC traces and $^1\text{H}$ -NMR spectra of the resulting polymers

## IV. Supplementary References

## I. Supplementary Methods

### A. General Information

#### A-1. Sample Preparations

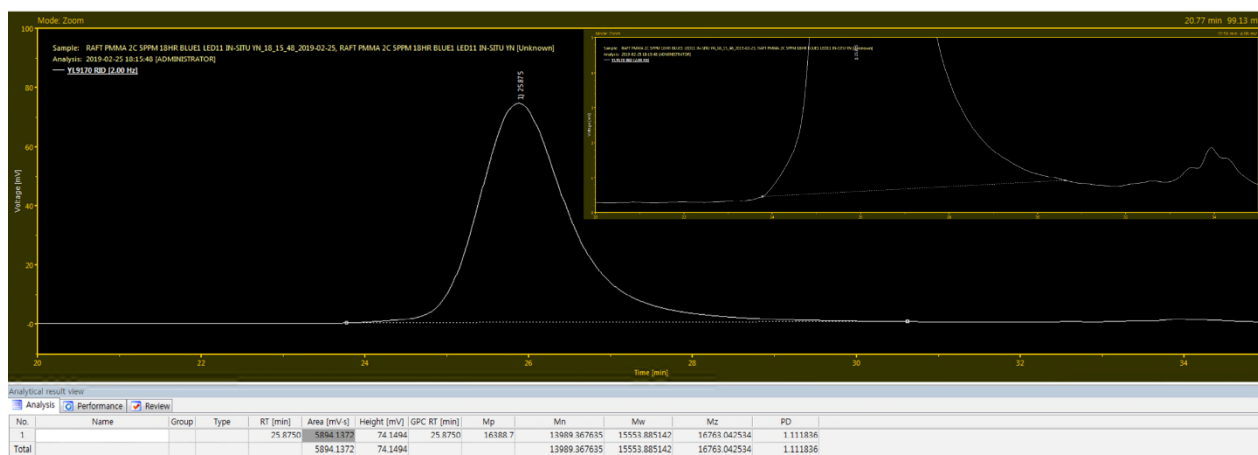
All OPCs were synthesized according to the procedures previously reported by our group.<sup>1</sup> Tris(2-phenylpyridinato) iridium(III) (*fac*-Ir(ppy)<sub>3</sub>, TCI), tetrabromofluorescein (eosin Y, TCI), and fluorescein (Aldrich) were purchased commercially, and used without further purifications. Unless otherwise specified, all chemicals and solvents were purchased commercially, and used without further purification. The inhibitor in methyl methacrylate (MMA, Aldrich, contains  $\leq 30$  ppm MEHQ as inhibitor, 99%) was removed by percolating over an aluminum oxide (Aldrich, activated, basic, Brockmann I) column. Pre-prepared stock solutions of the PCs and the chain transfer agents (CTAs) were used for the higher reproducibility.

#### A-2. Sample Measurements

##### A-2-1. Characterization of Synthesized Polymers

Newly synthesized polymers were characterized by <sup>1</sup>H NMR and gel permeation chromatography (GPC). The molecular weights (MWs) and MW distribution of polymers synthesized were determined by GPC (Young Lin YL9100 HPLC system) coupled with a refractive index (RI) detector (Young Lin YL9170 RI detector) and three columns. Tetrahydrofuran (THF, Samchun Chemicals, HPLC, stabilized, >99.9%) was used as the eluent at 35 °C with a flow rate of 0.8 mL/min. Polymethylmethacrylate (PMMA) standards were used for calibration. The polymer composition was determined using a <sup>1</sup>H NMR spectrometer (Bruker, AVANCE III HD (400 MHz)) with chloroform-d (CDCl<sub>3</sub>, contains 0.05% v/v tetramethylsilane (TMS), 99.8%) as the solvent.

##### ■ Example of calibration of GPC system



##### A-2-2. Photophysical Measurements

Absorbance measurements were done with a Cary 5000 UV-Vis-NIR spectrometer. Room temperature photoluminescence (PL) emission spectra were obtained using a HORIBA Jobin Yvon Fluoromax-4 spectrofluorimeter equipped with a 150 W Xe short arc lamp and Hamamatsu R928P PMT detector; the emission spectra were corrected for the sensitivity of the photomultiplier.

PL quantum yield at r.t. under N<sub>2</sub> atmosphere was measured relative to the QY of 0.1M H<sub>2</sub>SO<sub>4</sub> quinine sulfate solution (with absorbance 0.11 at 387 nm) by using following equation:

$$\phi_S = \phi_R \times \frac{\int I_S}{\int I_R} \times \frac{A_R}{A_S} \times \frac{\eta_S^2}{\eta_R^2}$$

Where,  $\phi_S$  is the quantum yield of the samples,  $\phi_R$  is the quantum yield (0.577) of quinine sulfate solution in 0.1M H<sub>2</sub>SO<sub>4</sub>,  $I_S$  and  $I_R$  are the integrated fluorescence area,  $A_S$  and  $A_R$  are the absorbed amount of light (which relates to the absorbance via  $A = 1-10^{-E}$ ) for the sample and reference solutions, respectively.  $\eta_S$  and  $\eta_R$  are the refractive indices of the solvent for the sample and reference solutions.

Low temperature PL measurements were carried out in CH<sub>3</sub>CN solvent. Emission was dispersed in wavelength using an Acton SP2500 spectrometer and detected either by a Princeton Instruments Spec10:400BR CCD camera attached or by a low dark current hybrid photomultiplier (PMA 06, PicoQuant), both attached to the spectrometer. Gated phosphorescence spectra were acquired using a cw 405 nm laser module with TTL modulation input (maximum modulation frequency 20 kHz) and suitable triggering of the CCD. Trigger pulses for the laser and the CCD camera were provided by a Stanford Research Systems DG645 pulse and delay generator with 5 ps resolution. Phosphorescence spectra were acquired with a delay of 30ms after a 2s excitation pulse.

PL decay measurements were carried out by the time-correlated single photon counting (TCSPC) technique. The excitation source was a 405 nm pulsed diode laser (LDH-D-C-405 PicoQuant) of pulse width (FWHM) < 49 ps controlled by a PDL828 driver (PicoQuant) at a repetition rate of 2.5 MHz. A HydraHarp-400 TCSPC event timer with 1 ps time resolution and a Picoquant TimeHarp 260 nano TCSPC electronics with 1 ns resolution were employed to measure decays on short (nanosecond to microsecond) and long (microsecond to second) time scales, respectively. The decay time fitting procedure was carried out with the measured IRF by using the Fluofit software (PicoQuant). Smallest residual values were obtained in the fitting procedure. The phosphorescence decay measurements were carried out by using gated 405 nm cw excitation.

### A-2-3. Transient absorption spectroscopy

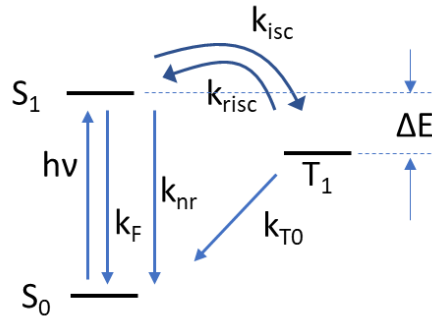
#### ■ Calculation of intersystem crossing rates and yields

Scheme 1 summarizes the photophysical processes that have to be considered for the actual system. It leads to the following system of ordinary differential equations (ODE) that define the dynamics of the concentration of excited singlet and triplet states (S and T, respectively):

$$\begin{cases} \frac{dS}{dt} = -(k_F + k_{nr} + k_{isc}) \cdot S + k_{risc} \cdot T \\ \frac{dT}{dt} = -(k_{T0} + k_{risc}) \cdot T + k_{isc} \cdot S \end{cases} \quad (S1)$$

In eq. S1,  $k_F$  and  $k_{nr}$  are rate constants for the radiative (by fluorescence) and non-radiative singlet deactivation, respectively,  $k_{isc}$  and  $k_{risc}$  are the forward and backward (return) intersystem crossing rate constants, and the rate constant  $k_{T0}$  summarizes phosphorescence and radiation-less deactivation into the electronic ground state S<sub>0</sub>.





**Scheme 1.** Photophysical model to describe the dynamics and yields. States are given as capital letters; rate constants use the symbol “k”. The energy difference between the lowest excited singlet and triplet states is given as  $\Delta E$ .

### ■ By Fluorescence Transient

Time-resolved photoluminescence can be used as a probe for the time-resolved concentration of  $S(t)$ :

$$PL(t) = \left( \frac{dS}{dt} \right)_{PL} = r \cdot k_r \cdot S(t) \quad (S2)$$

ODE systems of the form of eq. S1 lead to biexponential kinetics for both  $S(t)$  and  $T(t)$ . Therefore, PL decay traces will not suffice to quantify the 5 rate constants of scheme 1. We used the following strategy to obtain reliable rate constants: The radiative rate constant  $k_r$  was calculated using the formula of Strickler and Berg, which in simplified form reads  $k_{F,SB} = 4.34 \cdot 10^7 [s^{-1}eV^{-2}] \frac{E_{F,vert}^3}{E_{A,vert}} f$ . Starting from the TD-DFT calculated oscillator strength of  $f = 0.079$  and a vertical absorption and emission energies  $E_{A,vert} = 2.43$  eV and  $E_{F,vert} \approx 1.9$  eV, respectively for the lowest energetic CT transition, we obtain  $k_r = 1 \times 10^7 s^{-1}$ . By spectral modeling of the early transient absorption spectra, which are entirely dominated by the  $S_1$  state, we find that the oscillator strength for stimulated emission is approximately equal to that of the corresponding absorption band, for which we find  $f = 0.082$ , very close to the calculated value.

The PL quantum yield was measured as  $\phi_{PL} = 0.18$  in  $CH_3CN$ . Assuming  $k_{T0} \equiv 0$  (we will verify this assumption below), all photoexcited states must decay through the singlet channel, for which the PL quantum yield is defined as  $\phi_{PL} = \frac{k_F}{(k_F + k_{nr})}$ . From this relation, we get  $k_{nr} = 4.6 \times 10^7 s^{-1}$ .

As noted above, the decay of  $S(t)$  follows biexponential kinetics, producing a fast and a slow decay time ( $\tau_1$  and  $\tau_2$ , respectively). The fast process is caused by equilibration kinetics:

$$\frac{1}{\tau_1} = k_F + k_{nr} + k_{isc} \quad (S3)$$

We found  $\tau_1 = 3.3$  ns for both DMSO and  $CH_3CN$  so that  $k_{isc} = 2.5 \times 10^8 s^{-1}$ . Therefore, the total yield of triplet states  $\phi_T = \frac{k_{isc}}{(k_F + k_{nr} + k_{isc})} = 0.82$ , signifying the upper limit to the overall photochemical polymerization yield when this material is used as a photocatalyst.

For the slower time constant of the PL traces we found  $\tau_2 \approx 100$   $\mu s$ . This represents the lifetime of the triplet state, detected by thermally activated delayed fluorescence (TADF)<sup>2</sup> controlled by the thermodynamic equilibrium constant

$$K = \frac{k_{risc}}{k_{isc}} = \frac{1}{3} \exp\left(\frac{-\Delta E}{k_B T}\right) \quad (S4)$$

In eq. S4,  $\Delta E$  is the energy difference between the lowest excited singlet and triplet state,  $k_B = 8.617 \times 10^{-5}$  eV/K is Boltzmann's constant and  $T = 293$  K is the temperature. The first-order ODE system with constant coefficients S1 (setting  $k_{T0} = 0$ ) can be easily solved, resulting in two decay rates which are the eigenvalues of the matrix of coefficients:

$$\lambda_{1/2} = -\frac{k_s + K \cdot k_{ISC}}{2} \pm \sqrt{\left(\frac{k_s + K \cdot k_{ISC}}{2}\right)^2 - K \cdot k_{ISC}(k_s - k_{ISC})} \quad (S5)$$

Here, the plus sign corresponds to the slow decay component and the minus sign to the fast one. Setting  $\tau_2 = -\lambda_1^{-1} = 100\mu s$ ,  $\tau_1 = -\lambda_2^{-1} = 3.3ns$ ,  $T = 293K$  and solving for  $\Delta E$  results in

$$\Delta E = -kT \cdot \ln\left(\frac{3}{k_{ISC}\tau_T} \cdot \frac{k_s\tau_T - 1}{(k_r + k_{nr})\tau_T - 1}\right) \approx -kT \cdot \ln\left(\frac{3}{k_{ISC}\tau_T} \cdot \frac{k_s}{k_r + k_{nr}}\right) \quad (S6)$$

Inserting the values given above finally results in

$$\Delta E \approx 0.186eV \quad (S7)$$

Considering the long triplet lifetimes in the range of seconds measured at low temperature we can confirm that, at room temperature, it is perfectly legitimate to neglect any direct radiative decay of the triplet to the ground state. As the triplet-singlet splitting determined above is consistent with the one determined from the onsets of the photoluminescence and phosphorescence spectra ( $\Delta E \approx 0.2eV$ ), we can conclude that also non-radiative decay does not contribute significantly to the measured lifetime at room temperature and that the decay happens exclusively through the TADF pathway.

### ■ By Transient Absorption

Similar results are obtained by an independent study of transient absorption (TA) dynamics in the same sample. The differential absorption is defined as

$$\Delta A = A_{pu} - A_0, \quad (S8)$$

where  $A = -\ln T$  is the natural absorbance (base e) with the transmission  $T$ , and the suffixes “0” and “pu” refer to the unperturbed sample (all molecules in electronic ground state) and the sample perturbed by a pump pulse, respectively. In the latter case, some of the molecules are in an excited state. All states, whether ground or excited states, have characteristic resonance energies, leading to characteristic absorption spectra that can be interrogated by a broadband (white) probe pulse.

The fact that the probe pulse is broadband allows us to measure  $A$  at various probe energies  $E_{pr}$ , thus obtaining a TA spectrum  $\Delta A(E_{pr})$ ; the fact that it is a pulse allows us to measure time-resolved TA spectra  $\Delta A(E_{pr}, t)$  where  $t$  is the pump-probe delay time. According to the Beer-Lambert Law,

$$A(E_{pr}) = \sum_i (\sigma_i(E_{pr}) \cdot s_i) \quad (S9)$$

every electronic state  $i \in \{1, \dots, n_{st}\}$  contributes additively to the overall natural absorbance due to its characteristic spectrum of absorption cross-sections  $\sigma_i(E_{pr})$  times the area density  $s = c \cdot d$ , where  $c$  is the concentration and  $d$  is the sample thickness. We consider a total of  $n_{st}$  contributing states. Inserting S9 into S8 yields

$$\Delta A = \sum_i (\sigma_i(E_{pr}) \cdot s_{i,pu}(t)) - \sum_i (\sigma_i(E_{pr}) \cdot s_{i,0}(t)) = \sum_i (\sigma_i(E_{pr}) \cdot \Delta s_i(t)) \quad (S10)$$

In the last term, we introduced  $\Delta s_i(t) = s_{i,pu}(t) - s_{i,0}(t)$  as the pump-induced change of concentration remaining at time  $t$  after the pump. Since the continuous functions  $\sigma_i(E_{pr})$  and  $\Delta s_i(t)$ , and thus  $\Delta A$ , are experimentally probed only at  $n_E$  probe energy points and at  $n_t$  time points, it is convenient to restate S10 in matrix notation. Introducing two-dimensional matrices  $\sigma$  ( $n_{st}$  column vectors of absorption cross-sections  $\sigma_i(E_{pr})$ ) and  $s$  ( $n_{st}$  row vectors of concentration-time dependences  $\Delta s_i(t)$ ), we obtain

$$A = \sigma \times s, \quad (S11)$$

where  $A$  is now an ( $n_E \times n_t$ ) matrix of differential absorptions  $\Delta A(E_{pr}, t)$  measured at  $n_E$  probe energies and  $n_t$  time

points. We can isolate  $\mathbf{s}$  by left-multiplying the inverse matrix  $\sigma^{-1}$ :

$$\mathbf{s} = \sigma^{-1} \times \mathbf{A} \quad (\text{S12})$$

Eq. S12 shows that we can obtain the complete dynamics of all photoexcited states (i.e., the solution of ODE S1) if we know the set of characteristic spectra  $\sigma$  for all contributing states, by multiplying the matrix inverse  $\sigma^{-1}$  with the experimental differential absorption spectrum  $\mathbf{A}$ . However, since generally  $n_E \neq n_{st}$ ,  $\sigma$  is not square, we cannot rigorously calculate its inverse. Here, we use the property of a *truncated singular value decomposition (t-SVD)* that it is always optimal in the least-squares sense, the  $n_s$  strongest singular values of an SVD,

$$\mathbf{A}_{exp} = \mathbf{U} \times \mathbf{s} \times \mathbf{V} = \mathbf{U}_s \times \mathbf{s}_s \times \mathbf{V}_s + \mathbf{U}_n \times \mathbf{s}_n \times \mathbf{V}_n = \mathbf{U}_s \times \mathbf{s}_s \times \mathbf{V}_s + \mathbf{N}; s \in \{1..n_{st}\}, \quad (\text{S13})$$

are automatically selected such as to minimize the square  $\mathbf{N}^2$  of the residuals (noise)  $\mathbf{N}$ . In eq. S13, suffixes  $s$  and  $n$  refer to “signal-related” and “noise-related”, respectively. This means that performing a t-SVD on an experimental differential absorption matrix  $\mathbf{A}_{exp}$  will yield a matrix of  $n_s$  column vectors  $\mathbf{U}_s$ , and a matrix of  $n_s$  row vectors  $\mathbf{T}_s = \mathbf{s}_s \times \mathbf{V}_s$ , that together represent a *bias-free global fit* to  $\mathbf{A}_{exp}$ .

The matrices  $\mathbf{U}_s$  and  $\mathbf{T}_s$  are closely related to our desired matrices  $\sigma$  and  $\mathbf{s}$  in eq. S11, respectively, as we can see by inserting the identity  $\mathbf{R} \times \mathbf{R}^{-1}$  into eq. S13:

$$\mathbf{A}_{exp} = \mathbf{U}_s \times \mathbf{R} \times \mathbf{R}^{-1} \times \mathbf{T}_s + \mathbf{N} \quad (\text{S14})$$

We find that S14 is identical with S11 if

$$\mathbf{A} = \mathbf{A}_{exp} - \mathbf{N}; \quad \sigma = \mathbf{U}_s \times \mathbf{R}; \quad \mathbf{s} = \mathbf{R}^{-1} \times \mathbf{T}_s \quad (\text{S15})$$

The matrix  $\mathbf{R}$  is called the *rotation matrix*; as shown by eq. S12, its matrix elements  $R_{ij}$  are the spectral weights of the  $i$ -th SVD spectrum  $\mathbf{U}_{s,i}$  in the characteristic spectrum of state  $j$ ,  $\sigma_j$ .  $\mathbf{R}$  can therefore also be called the *spectral weights matrix*.

In our experiment, we expect 3 states to contribute to  $\mathbf{A}$  in eq. S11: the singlet ground state  $S_0$ , the first excited singlet state  $S_1$  and the lowest energetic triplet state  $T_1$ . However, due to the conservation rule

$$c(T_1) + c(S_1) + c(S_0) = c_{tot}, \quad (\text{S16})$$

where  $c_{tot}$  is the total concentration of molecules that can be either in the ground state or in one of the excited states, we will obtain only two linearly independent SVD spectra in eq. S13. Due to the linear dependence of one of the concentrations on the other ones, in our kinetic scheme 1 the number of signal-related SVD states is therefore  $n_s = n_{st} - 1 = 2$ .

Due to this linear dependence, we will define the characteristic spectra for  $S_1$  and  $T_1$  by incorporating the associated reduction of ground state absorption (“ground state bleach”):

$$\sigma'_{S1}(E_{pr}) = \sigma_{S1}(E_{pr}) - \sigma_{S0}(E_{pr}); \quad \sigma'_{T1}(E_{pr}) = \sigma_{T1}(E_{pr}) - \sigma_{S0}(E_{pr}) \quad (\text{S17})$$

Eq. S17 can be validated by introducing it into S10; one finds that the conservation rule eq. S16 is automatically respected.

Now that the mathematical formalism is clear, we need to find  $\sigma'_{S1}(E_{pr})$  and  $\sigma'_{T1}(E_{pr})$  to solve eq. S12 to obtain the complete photoexcitation dynamics in  $\mathbf{s}$ . Looking at Scheme 1, we can take advantage of the fact that due to the spin selection rule, the pump pulse exclusively generates  $S_1$  states. Hence, we can use eq. S10 to obtain the characteristic spectrum of  $S_1$  states if we measure  $\Delta A$  at short enough times so that triplet states have not yet been formed. In this case eq. S10 simplifies to:

$$\Delta A(t \rightarrow 0) = \sigma_{S1}(E_{pr}) \cdot \Delta S_{S1}(t) + \sigma_{S0}(E_{pr}) \cdot \Delta S_{S0}(t) = \sigma'_{S1}(E_{pr}) \cdot \Delta S_{S1}(t), \quad (\text{S18})$$

because in this case the conservation law simplifies to  $\Delta c(S_1) = -\Delta c(S_0)$ . As long as no decay to the ground state has yet occurred, the area density of excited states equals the area density (flux) of absorbed photons  $J_{ph,abs}$ . Therefore, we get:

$$\sigma'_{S1}(E_{pr}) = \frac{\Delta A(t \rightarrow 0)}{J_{ph,abs}}, \quad (S19)$$

showing the usefulness of eq. 14. In practice, we took the  $\Delta A$  spectrum at  $t=20$  ps to accommodate internal vibrational relaxation and solvent relaxation after impulsive excitation.

The characteristic spectrum of  $T_1$  states is obtained in a similar way. According to Scheme 1, for times much longer than the equilibration time  $\tau_1$ , there will be an equilibrium between  $S_1$  and  $T_1$  states that will be far on the side of  $T_1$ . As the experimentally detected energy difference is  $\Delta E = 0.2$  eV, the equilibrium ratio  $c(S_1)/c(T_1)$  will be less than 1/1000 allowing us to neglect singlet states in eq. S10 in this case:

$$\Delta A(t \gg \tau_1) = \sigma'_{T1}(E_{pr}) \cdot \Delta s_{T1}(t). \quad (S20)$$

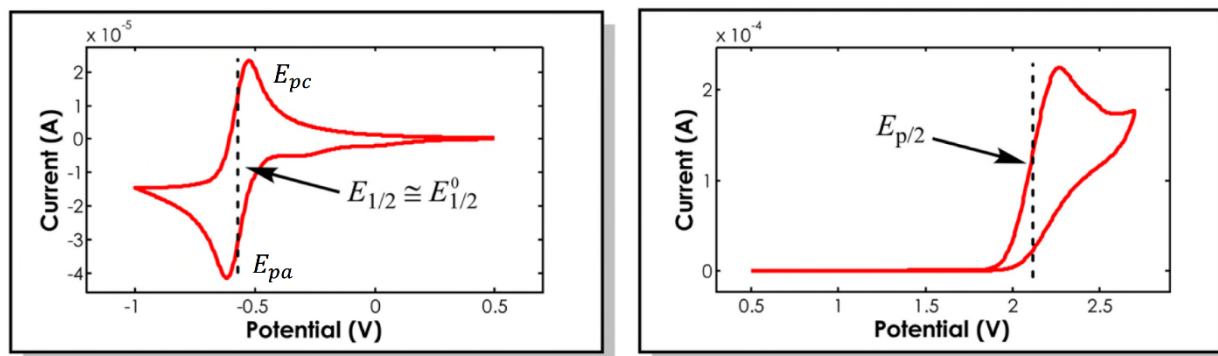
The problem here is that we do not know a priori the remaining triplet concentration at time  $t$ . Again, the definition of  $\sigma'_{T1}(E_{pr})$  in eq. S17 turns out very helpful: As we know the absolute cross-sections of the ground state  $\sigma_{S0}(E_{pr})$ , we can find both  $\Delta s_{T1}(t)$  and  $\sigma'_{T1}(E_{pr})$  at the same time by a curve optimization scheme, varying the spectral shape  $\sigma_{T1}(E_{pr})$  by introducing one or more positive Gaussians, taking advantage of the fact that triplet states do not show stimulated emission (formally negative TA).

Finally, having obtained the absolute time-resolved concentrations of  $S_1$  and  $T_1$  states, we can reproduce their dynamics by numerically solving ODE system S1 and varying the rate constants in a non-linear optimization algorithm, thus obtaining all rate constants except  $k_r$  and  $k_{nr}$ , which cannot be distinguished and are summarized into  $k_m = k_r + k_{nr}$ .

#### **A-2-4. Electrochemical Measurements**

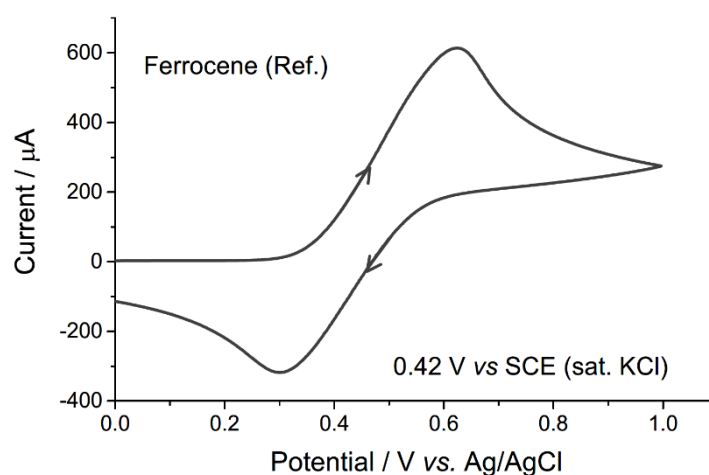
Cyclic voltammetry experiments were carried out with a VersaSTAT3-200 (Princeton Applied Research) using an one-compartment electrolysis cell consisting of a glassy carbon working electrode, a platinum wire counter electrode, and a quasi  $Ag^+/Ag$  (sat. KCl) reference electrode bought from AT FRONTIER (Part No. R303). Specifically, the electrode is a silver wire that is coated with a thin layer of silver chloride and an insulated lead wire connects the silver wire with measuring instrument. The electrode also consists of a porous plug on the one end which will allow contact between the field environment with the silver chloride electrolyte. Saturated potassium chloride is added inside the body of the electrode to stabilize the silver chloride concentration and in this condition the electrode's reference potential is known to be +0.197 V at 25 °C.

■ *Representative CV demonstrating a reversible (left) and an irreversible (right) redox behavior.*<sup>3</sup>



For our OPCs and *fac*-Ir(ppy)<sub>3</sub>, the measurements were done in 2 mM CH<sub>3</sub>CN (Alfa aesar, anhydrous, 99.8+%) solution with 0.1 M tetrabutylammonium hexafluorophosphate (n-Bu<sub>4</sub>NPF<sub>6</sub>, Aldrich, Electrochemical grade) as supporting electrolyte at a scan rate of 100 mV/s. For fluorescein and eosin Y, the measurements were done in 2 mM CH<sub>3</sub>CN:H<sub>2</sub>O (1:1 v/v) solution with 0.1 M n-Bu<sub>4</sub>NPF<sub>6</sub> as supporting electrolyte at a scan rate of 100 mV/s. The redox potential was calibrated after each experiment against the ferrocenium/ferrocene couple (Fc<sup>+</sup>/Fc), which allowed conversion of all potentials to the aqueous saturated calomel electrode (SCE) scale by using  $E^0(\text{Fc}^+/\text{Fc}) = 0.42 \text{ V vs. SCE in CH}_3\text{CN}$ . The working solution was degassed with N<sub>2</sub> for 15 min (30 min for fluorescein and eosin Y) before measurement and then kept under a positive N<sub>2</sub> pressure during the measurement.

■ CV curve of ferrocene recored in our lab.



For the compounds showing a reversible redox behavior, the standard reduction potentials of PC<sup>+</sup> ( $E_{ox}^0$ ) and PC ( $E_{red}^0$ ) in the ground state were obtained from CV as the half sum of anodic ( $E_{pa}$ ) and cathodic ( $E_{pc}$ ) peak potentials such as following:

$$E_{ox}^0 \approx E_{1/2}^o = \frac{(E_{pa} + E_{pc})}{2}$$

$$E_{red}^0 \approx E_{1/2}^o = \frac{(E_{pa} + E_{pc})}{2}$$

For the compounds exhibiting an irreversible redox behavior, the standard reduction potentials of PC<sup>+</sup> and PC in the ground state were taken from half-peak potentials ( $E_{1/2}^0$ ), which correspond to the potential at half the maximum current

in the CV as a way to estimate  $E_{1/2}^0$ .<sup>19</sup> However, in such compounds having an irreversible redox behavior, it should be noted that the values are not truly reflective of  $E_{1/2}^0$  due to the issues explained in the previous literature.<sup>4</sup>

Basically, we conducted all experiments with a standard condition to maintain internal consistency; this includes that all measurements were performed with the same scan rate (100 mV/s) and the same solution of electrolytes. In addition, following the suggestion by Addison,<sup>5</sup> we converted measured potential values from silver–silver chloride into saturated calomel electrode (SCE) and the redox potentials of the compounds including OPCs and substrates are reported in volts against the SCE.

### ***A-3. Quantum-chemical Calculations***

Geometrical, electronic and optical properties of the 4DP-IPN catalyst and of initiators CPADB, CDTPA were carried out by (time-dependent) density functional theory, (TD)DFT, using the Gaussian09 program package, using the B3LYP functional with the 6-311+G\* basis set.<sup>6-8</sup> For this, the geometries were optimized in vacuum, all single point calculations were carried out in dimethylformamid (DMF) solution, using the polarizable continuum model (PCM).

## **B. Procedures of PET-RAFT polymerizations of MMA**

### ***B-1. Procedure for negative control experiment in the presence of argon and air***

#### ***B-1-1. In the presence of argon***

A procedure for the standard reaction conditions [MMA]:[CTA]:[PC] = [200]:[1]:[0] under argon was carried out as follows. A 20 mL glass vial equipped with a stirring bar was charged with MMA (1.0 mL, 9.29 mmol) and CPADB (0.046 mmol), and anhydrous DMSO (1 mL; Aldrich, anhydrous, 99.9%) as the solvent, inside a glove box, for the polymerization. Afterwards, the vial was capped with a rubber septum and sealed with parafilm, and bubbled with argon for 30 min outside the glove box. Subsequently, the polymerization was carried out under a 3 W 455 nm LED (ca. 2.5 mW/cm<sup>2</sup>) irradiation at room temperature. After 18 h, a 0.1 mL aliquot of the reaction mixture was removed via syringe and dissolved in a vial containing CDCl<sub>3</sub>. Without storing, the aliquot was then immediately analyzed by <sup>1</sup>H NMR for conversion. The sample used for <sup>1</sup>H NMR analysis was then dried under reduced pressure and re-dissolved in THF for the  $M_n$  and polydispersity analyses by GPC.

#### ***B-1-2. In the presence of air***

A procedure for the standard reaction conditions [MMA]:[CTA]:[PC] = [200]:[1]:[0] under air was carried out as follows. A 4 mL glass vial equipped with a stirring bar was charged with MMA (1.5 mL, 13.9 mmol), CPADB (0.070 mmol) and DMSO (1.5 mL) as the solvent. After, the vial was capped with a rubber septum and sealed with parafilm, and bubbled with air (DEOKYANG, O<sub>2</sub> 21 mol%, H<sub>2</sub>O 2 x 10<sup>-6</sup> mol%) for 30 min outside the glove box. Subsequently, the polymerization was carried out under a 3 W 455 nm LED (ca. 2.5 mW/cm<sup>2</sup>) irradiation at room temperature. After 18 h, a 0.1 mL aliquot of the reaction mixture was removed via syringe and dissolved in a vial containing CDCl<sub>3</sub>. Without storing, the aliquot was then immediately analyzed by <sup>1</sup>H NMR for conversion. The sample used for <sup>1</sup>H NMR analysis was then dried under reduced pressure and re-dissolved in THF for the  $M_n$  and polydispersity analyses by GPC.

### ***B-2. General procedure for PET-RAFT polymerizations of MMA in the presence of argon and air***

### ***B-2-1. In the presence of argon***

A typical PET-RAFT procedure for the standard reaction conditions  $[MMA]:[CTA]:[OPC] = [200]:[1]:[0.001]$  and  $[MMA]:[CTA]:[Ir(ppy)_3] = [200]:[1]:[0.0002]$  under argon was carried out as follows. A 20 mL glass vial equipped with a stirring bar was charged with MMA (1.0 mL, 9.29 mmol), CPADB (0.046 mmol), OPC ( $4.65 \times 10^{-5}$  mmol) and DMSO (1.0 mL) as the solvent, inside a glove box, for reaction condition  $[MMA]:[CTA]:[OPC] = [200]:[1]:[0.001]$ . For reaction condition  $[MMA]:[CTA]:[Ir(ppy)_3] = [200]:[1]:[0.0002]$ ;  $Ir(ppy)_3$  ( $9.29 \times 10^{-6}$  mmol) in DMSO (1.0 mL) was used. After, the vial was capped with a rubber septum and sealed with parafilm, and bubbled with argon for 30 min outside the glove box. Subsequently, the polymerization was carried out under a 3 W 455 nm LED (ca. 2.5 mW/cm<sup>2</sup>) irradiation at room temperature. After 18 h, a 0.1 mL aliquot of the reaction mixture was removed via syringe and dissolved in a vial containing CDCl<sub>3</sub>. Without storing, the aliquot was then immediately analyzed by <sup>1</sup>H NMR for conversion. The sample used for <sup>1</sup>H NMR analysis was then dried under reduced pressure and re-dissolved in THF for the M<sub>n</sub> and polydispersity analyses by GPC.

For experiments under green LED, a 20 mL glass vial equipped with a stirring bar was charged with MMA (1.0 mL, 9.29 mmol), CDTPA (0.046 mmol), 4DP-IPN ( $4.65 \times 10^{-5}$  mmol) and DMSO (1.0 mL) as the solvent inside a glove box. After, the vial was capped with a rubber septum and sealed with parafilm, and bubbled with argon for 30 min outside the glove box. Subsequently, the polymerization was carried out under a 3 W 515 nm LED (ca. 0.5 mW/cm<sup>2</sup>) irradiation at room temperature. After 6 h, a 0.1 mL aliquot of the reaction mixture was removed via syringe and dissolved in a vial containing CDCl<sub>3</sub>. Without storing, the aliquot was then immediately analyzed by <sup>1</sup>H NMR for conversion. The sample used for <sup>1</sup>H NMR analysis was then dried under reduced pressure and re-dissolved in THF for the M<sub>n</sub> and polydispersity analyses by GPC.

### ***B-2-2. In the presence of air***

A typical PET-RAFT procedure for the standard reaction conditions  $[MMA]:[CTA]:[OPC] = [200]:[1]:[0.001]$  and  $[MMA]:[CTA]:[Ir(ppy)_3] = [200]:[1]:[0.0002]$  under air was carried out as follows. A 4 mL glass vial equipped with a stirring bar was charged with MMA (1.5 mL, 13.9 mmol), CPADB (0.070 mmol), OPC ( $6.97 \times 10^{-5}$  mmol) and DMSO (1.5 mL) as the solvent, inside a glove box, for reaction condition  $[MMA]:[CTA]:[OPC] = [200]:[1]:[0.001]$ . For reaction condition  $[MMA]:[CTA]:[Ir(ppy)_3] = [200]:[1]:[0.0002]$ ;  $Ir(ppy)_3$  ( $1.39 \times 10^{-5}$  mmol) in DMSO (1.5 mL) was used. Pre-prepared stock solution of the PCs and the RAFT agent were used for the higher reproducibility of results. After, the vial was capped with a rubber septum and sealed with parafilm, and bubbled with air for 30 min outside the glove box. Subsequently, the polymerization was carried out under a 3 W 455 nm LED (ca. 2.5 mW/cm<sup>2</sup>) irradiation at room temperature. After 18 h, a 0.1 mL aliquot of the reaction mixture was removed via syringe and dissolved in a vial containing CDCl<sub>3</sub>. Without storing, the aliquot was then immediately analyzed by <sup>1</sup>H NMR for conversion. The sample used for <sup>1</sup>H NMR analysis was then dried under reduced pressure and re-dissolved in THF for the M<sub>n</sub> and polydispersity analyses by GPC.

For experiments under green LED, a 4 mL glass vial equipped with a stirring bar was charged with MMA (1.5 mL, 13.9 mmol), CDTPA (0.070 mmol), 4DP-IPN ( $6.97 \times 10^{-5}$  mmol) and DMSO (1.5 mL) as solvent inside a glove box. After, the vial was capped with a rubber septum and sealed with parafilm, and bubbled with air for 30 min outside the glove box. Subsequently, the polymerization was carried out under a 3 W 515 nm LED (ca. 0.5 mW/cm<sup>2</sup>) irradiation at room temperature. After 6 h, a 0.1 mL aliquot of the reaction mixture was removed via syringe and dissolved in a vial

containing CDCl<sub>3</sub>. Without storing, the aliquot was then immediately analyzed by <sup>1</sup>H NMR for conversion. The sample used for <sup>1</sup>H NMR analysis was then dried under reduced pressure and re-dissolved in THF for the M<sub>n</sub> and polydispersity analyses by GPC.

### ***B-3. Experimental procedure for kinetic studies in the presence of argon and air***

#### ***B-3-1. In the presence of argon***

A typical PET-RAFT procedure for the standard reaction conditions [MMA]:[CTA]:[4DP-IPN] = [200]:[1]:[0.001] and [MMA]:[CTA]:[Ir(ppy)<sub>3</sub>] = [200]:[1]:[0.0002] under argon were carried out as follows. A 20 mL glass vial equipped with a stirring bar was charged with MMA (1.5 mL, 13.9 mmol), CPADB (0.070 mmol), 4DP-IPN (6.97 x 10<sup>-5</sup> mmol) and DMSO (1.5 mL) as solvent, inside a glove box, for reaction condition [MMA]:[CTA]:[OPC] = [200]:[1]:[0.001]. For reaction condition [MMA]:[CPADB]:[Ir(ppy)<sub>3</sub>] = [200]:[1]:[0.0002]; Ir(ppy)<sub>3</sub> (1.39 x 10<sup>-5</sup> mmol) in DMSO (1.5 mL) was used. After, the vial was capped with a rubber septum and sealed with parafilm, and bubbled with argon for 30 min outside the glove box. Subsequently, the polymerization was carried out under a 3 W 455 nm LED (ca. 2.5 mW/cm<sup>2</sup>) irradiation at room temperature. A 0.1 mL aliquot of the reaction mixture was taken via syringe at predetermined interval times and dissolved in a vial containing CDCl<sub>3</sub>. Without storing, each aliquot was then immediately analyzed by <sup>1</sup>H NMR for conversion. The samples used for <sup>1</sup>H NMR analyses were then dried under reduced pressure and re-dissolved in THF for M<sub>n</sub> and polydispersity analyses by GPC.

#### ***B-3-2. In the presence of air***

A typical PET-RAFT procedure for the standard reaction conditions [MMA]:[CTA]:[4DP-IPN] = [200]:[1]:[0.001] and [MMA]:[CTA]:[Ir(ppy)<sub>3</sub>] = [200]:[1]:[0.0002] under air were carried out as follows. A 4 mL glass vial equipped with a stirring bar was charged with MMA (1.5 mL, 13.9 mmol), CPADB (0.070 mmol), 4DP-IPN (6.97 x 10<sup>-5</sup> mmol) and DMSO (1.5 mL) as solvent, inside a glove box, for reaction condition [MMA]:[CTA]:[OPC] = [200]:[1]:[0.001]. For reaction condition [MMA]:[CTA]:[Ir(ppy)<sub>3</sub>] = [200]:[1]:[0.0002]; Ir(ppy)<sub>3</sub> (1.39 x 10<sup>-5</sup> mmol) in DMSO (1.5 mL) was used. After, the vial was capped with a rubber septum and sealed with parafilm, and bubbled with air for 30 min outside the glove box. Subsequently, the polymerization was carried out under a 3 W 455 nm LED (ca. 2.5 mW/cm<sup>2</sup>) irradiation at room temperature. A 0.1 mL aliquot of the reaction mixture was taken via syringe at predetermined interval times and dissolved in a vial containing CDCl<sub>3</sub>. Without storing, each aliquot was then immediately analyzed by <sup>1</sup>H NMR for conversion. The samples used for <sup>1</sup>H NMR analyses were then dried under reduced pressure and re-dissolved in THF for M<sub>n</sub> and polydispersity analyses by GPC. However, because of the weakness of the small rubber septa for 4 mL vials, kinetic study in the presence of air was done by dividing time intervals into three parts to prevent further addition of oxygen from atmosphere; 0 min ~ 1 h, 2 h ~ 6 h, 9 h ~ 18 h. The experiments were done under the same LED set-up for the same catalyst.

### ***B-4. Experimental procedure for temporal control in the presence of argon***

A typical PET-RAFT procedure for the standard reaction conditions [MMA]:[CPADB]:[4DP-IPN] = [200]:[1]:[0.001] and [MMA]:[CPADB]:[Ir(ppy)<sub>3</sub>] = [200]:[1]:[0.0002] under argon were carried out as follows. A 20 mL glass vial equipped with a stirring bar was charged with MMA (1.5 mL, 13.9 mmol), CPADB (0.070 mmol), 4DP-IPN (6.97 x 10<sup>-5</sup> mmol) and DMSO (1.5 mL) as solvent, inside a glove box, for reaction condition [MMA]:[CTA]:[OPC] =



[200]:[1]:[0.001]. For reaction conditions [MMA]:[CPADB]:[Ir(ppy)<sub>3</sub>] = [200]:[1]:[0.0002]; Ir(ppy)<sub>3</sub> (1.39 x 10<sup>-5</sup> mmol) in DMSO (1.5 mL) was used. After, the vial was capped with a rubber septum and sealed with parafilm, and bubbled with argon for 30 min outside the glove box. Subsequently, the polymerization was carried out by switching the irradiation source on and off for predetermined interval times (under a 3 W 455 nm LED (ca. 2.5 mW/cm<sup>2</sup>) irradiation at room temperature). The total reaction time including both “ON” and “OFF” steps was 22 h. A 0.1 mL aliquot of the reaction mixture was taken via syringe at each interval and dissolved in a vial containing CDCl<sub>3</sub>. Without storing, the aliquot was then immediately analyzed by <sup>1</sup>H NMR for conversion.

## ***B–5. Experimental procedure for chain extension in the presence of argon and air***

### ***B–5–1. In the presence of argon***

A typical PET-RAFT procedure for the standard reaction conditions [MMA]:[CPADB or Macroinitiator]:[4DP-IPN] = [200]:[1]:[0.001] under argon was carried out as follows. A 20 mL glass vial equipped with a stirring bar was charged with MMA (1.0 mL, 9.29 mmol), CPADB (0.046 mmol), 4DP-IPN (4.65 x 10<sup>-5</sup> mmol) and DMSO (1.0 mL) as solvent, inside a glove box. After, the vial was capped with a rubber septum and sealed with parafilm, and bubbled with argon for 30 min outside the glove box. Subsequently, the polymerization was carried out under a 3W 455 nm LED (ca. 2.5 mW/cm<sup>2</sup>) irradiation at room temperature. For the first chain, the reaction was carried out for 12 h. To isolate the first chain, the reaction mixture was first diluted with 3 mL of THF and dissolved completely, then poured into beaker containing methanol (75 mL) which caused the polymer to precipitate. Subsequent stirring for 30 min followed by vacuum filtration resulted in dried polymer which can be used as a macroinitiator ( $M_n = 12,500$  Da,  $\bar{D} = 1.07$ ). Again, a 20 mL glass vial equipped with a stirring bar was charged with MMA (0.2 mL, 1.86 mmol), macroinitiator (0.116 g, 9.29 x 10<sup>-3</sup> mmol), 4DP-IPN (9.29 x 10<sup>-6</sup> mmol) and DMSO (1.2 mL) as solvent. After, the vial was capped with a rubber septum and sealed with parafilm, and bubbled with argon for 30 min outside the glove box. Subsequently, the polymerization was carried out under a 3 W 455 nm LED (ca. 2.5 mW/cm<sup>2</sup>) irradiation at room temperature. For the second chain, the reaction was carried out for 8 h. A 0.1 mL aliquot of the reaction mixture was removed via syringe and dissolved in a vial containing CDCl<sub>3</sub>. Without storing, the aliquot was then immediately analyzed by <sup>1</sup>H NMR for conversion. The sample used for <sup>1</sup>H NMR analysis was then dried under reduced pressure and re-dissolved in THF for  $M_n$  and polydispersity analysis by GPC.

### ***B–5–2. In the presence of air***

A typical PET-RAFT procedure for the standard reaction conditions [MMA]:[CDTPA or Macroinitiator]:[4DP-IPN] = [200]:[1]:[0.001] under air was carried out as follows. A 4 mL glass vial equipped with a stirring bar was charged with MMA (1.5 mL, 13.9 mmol), CDTPA (0.070 mmol), 4DP-IPN (6.97 x 10<sup>-5</sup> mmol) and DMSO (1.5 mL) as solvent, inside a glove box. After, the vial was capped with a rubber septum and sealed with parafilm, and bubbled with air for 30 min outside the glove box. Subsequently, the polymerization was carried out under a 3 W 515 nm LED (ca. 0.5 mW/cm<sup>2</sup>) irradiation at room temperature. For the first chain, the reaction was carried out for 5 h. To isolate the first chain, the reaction mixture was first diluted with 4.5 mL of THF and dissolved completely, then poured into beaker containing methanol (120 mL) which caused the polymer to precipitate. Subsequent stirring for 30 min followed by vacuum filtration resulted in dried polymer which can be used as a macroinitiator ( $M_n = 15,800$ ,  $\bar{D} = 1.15$ ). Again, a 20 mL glass vial equipped with a stirring bar was charged with MMA (0.378 mL, 3.51 mmol), macroinitiator (0.278 g,

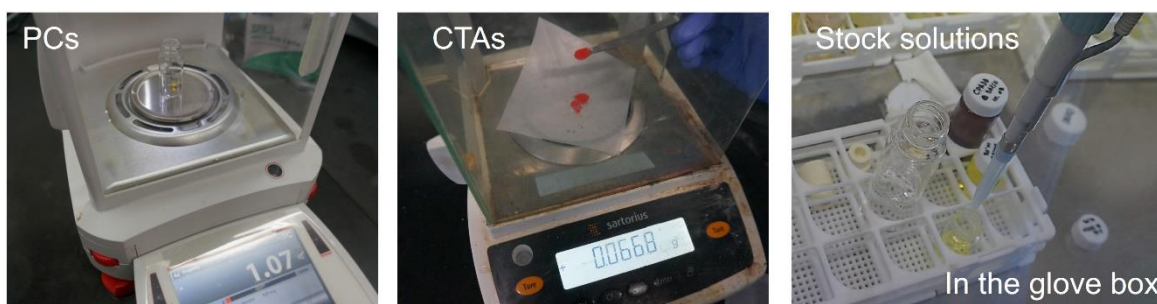
0.018 mmol), 4DP-IPN ( $1.76 \times 10^{-5}$  mmol) and DMSO (2.482 mL) as solvent. After, the vial was capped with a rubber septum and sealed with parafilm, and bubbled with air for 30 min outside the glove box. Subsequently, the polymerization was carried out under a 3 W 515 nm LED (ca.  $0.5 \text{ mW/cm}^2$ ) irradiation at room temperature. For the second chain, the reaction was carried out for 3 h. A 0.1 mL aliquot of the reaction mixture was removed via syringe and dissolved in a vial containing  $\text{CDCl}_3$ . Without storing, the aliquot was then immediately analyzed by  $^1\text{H}$  NMR for conversion. The sample used for  $^1\text{H}$  NMR analysis was then dried under reduced pressure and re-dissolved in THF for  $M_n$  and polydispersity analysis by GPC.

#### ***B–6. Experimental procedure for molecular weight control experiments in the presence of argon***

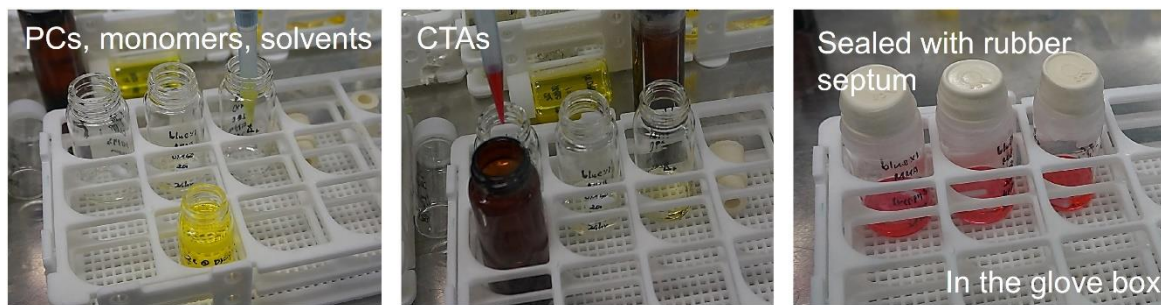
A typical PET-RAFT procedure for the standard reaction conditions of molecular weight control  $[\text{MMA}]:[\text{CPADB}]:[\text{4DP-IPN}] = [200]:[4]:[0.001]$  (target degree of polymerization (DP) = 50, MMA (1.0 mL, 9.29 mmol), CPADB (0.186 mmol), 4DP-IPN ( $4.65 \times 10^{-5}$  mmol) and DMSO (1.0 mL) as solvent),  $[\text{MMA}]:[\text{CPADB}]:[\text{4DP-IPN}] = [200]:[2]:[0.001]$  (target DP = 100, MMA (1.0 mL, 9.29 mmol), CPADB (0.093 mmol), 4DP-IPN ( $4.65 \times 10^{-5}$  mmol) and DMSO (1.0 mL) as solvent), and  $[\text{MMA}]:[\text{CPADB}]:[\text{4DP-IPN}] = [200]:[0.5]:[0.001]$  (target DP = 400, MMA (1.0 mL, 9.29 mmol), CPADB (0.023 mmol), 4DP-IPN ( $4.65 \times 10^{-5}$  mmol) and DMSO (1.5 mL) as solvent) under argon were carried out as follows. A 20 mL glass vial equipped with a stirring bar was charged with predetermined amounts of reagents, inside a glove box. After, the vial was capped with a rubber septum and sealed with parafilm, and bubbled with argon for 30 min outside the glove box. Subsequently, the polymerization was carried out under a 3 W 455 nm LED (ca.  $2.5 \text{ mW/cm}^2$ ) irradiation at room temperature. After 36 h (6 h for reaction condition  $[\text{MMA}]:[\text{CPADB}]:[\text{4DP-IPN}] = [200]:[0.5]:[0.001]$ ), a 0.1 mL aliquot of the reaction mixture was removed via syringe and dissolved in a vial containing  $\text{CDCl}_3$ . Without storing, the aliquot was then immediately analyzed by  $^1\text{H}$  NMR for conversion. The sample used for  $^1\text{H}$  NMR analysis was then dried under reduced pressure and re-dissolved in THF for  $M_n$  and polydispersity analysis by GPC.

#### ***B–7. Graphical Supporting Information for General Procedure for PET-RAFT Polymerization of MMA***

■ **STEP 1:** Prepare stock solutions of PCs and CTA in the glove box.



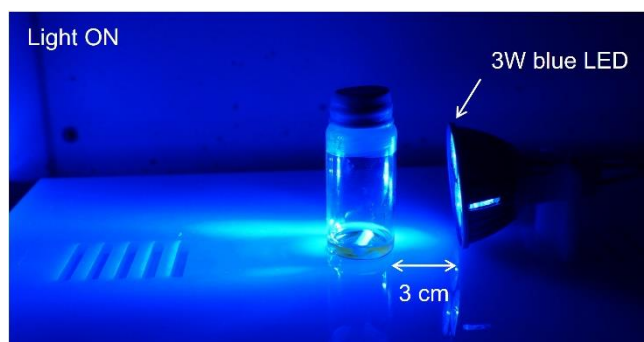
■ **STEP 2:** Add PC, CTA, monomer, and solvent to 20 mL (of 4 mL for the polymerizations under air) vial with magnetic bar and seal with rubber septum inside the glove box.



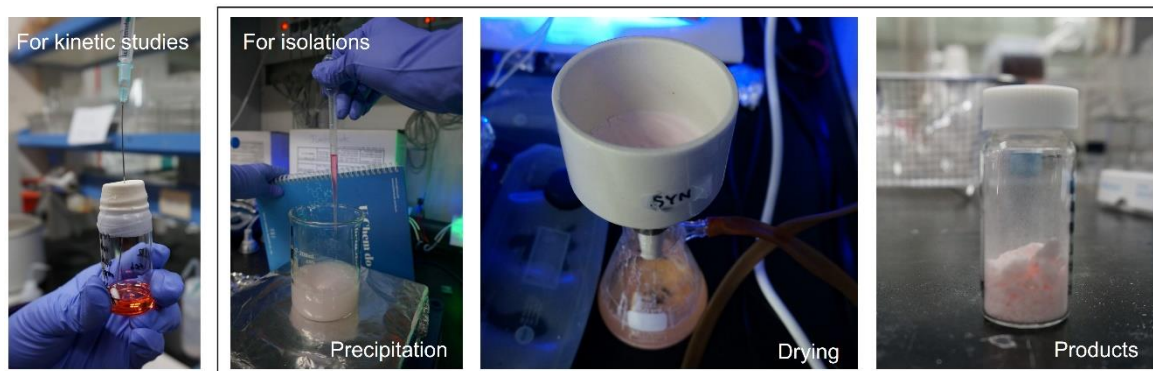
■ **STEP 3:** Cover with aluminum foils and degas with argon (or air) for 30 min.



■ **STEP 4:** Irradiate under a 3W blue (or green) LED with stirring at r.t. for predetermined time.

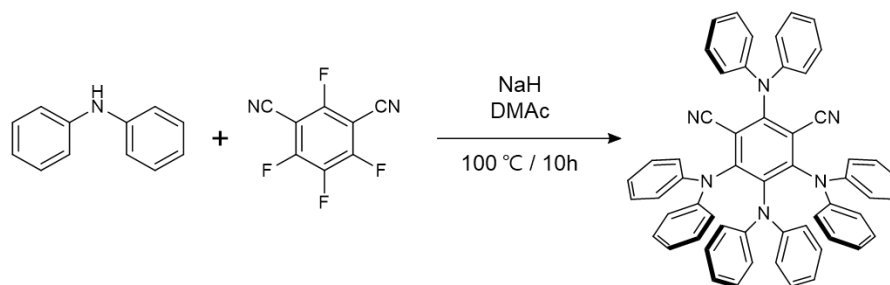


■ **STEP 5:** For kinetic studies (or in-situ monitoring of polymerizations), aliquot of the reaction mixture is taken by syringe and dissolve in a vial containing  $\text{CDCl}_3$  for  $^1\text{H}$  NMR. The samples used for  $^1\text{H}$  NMR analyses are then dried under reduced pressure and re-dissolved in THF for  $M_n$  and polydispersity analyses by GPC. For isolations, the reaction mixture is first diluted with 3 mL of THF and dissolve completely. Then, pour into beaker containing methanol (75 mL) and stir for 30 min and collect the polymers by vacuum filtration.



## C. Syntheses of 4DP-IPN used in this work

### ■ Syntheses scheme of 4DP-IPN.



**2,4,5,6-tetrakis(diphenylamino)benzene-1,3-dinitrile (4DP-IPN):** A solution of NaH (60% in oil, 0.477 g, 11.94 mmol) and diphenylamine (1.48 g, 8.75 mmol) in anhydrous dimethyl acetamide DMAc (5 mL) was stirred for 30 min in ice bath under a argon atmosphere. After 30 min, tetrafluoroisophthalonitrile (0.4 g, 1.99 mmol) dissolved in DMAc (5 mL) was slowly added to the reaction mixture and stirred further for 10 hours at 100 °C. Afterwards, distilled water (2 mL) was poured into the reaction mixture to quench the leftover NaH and methanol was added to precipitate the crude product, which was further purified by column chromatography on silica gel (CH<sub>2</sub>Cl<sub>2</sub>:hexane, 2:3 v/v) to give pure product (1.32 g, 83.4% yield). <sup>1</sup>H NMR (400 MHz, CDCl<sub>3</sub>): δ 7.31-7.27 (t, 4H), 7.12-7.08 (t, 12H), 7.07-7.03 (t, 2H), 6.95-6.88 (m, 8H), 6.73 (d, 10H), 6.57 (d, 4H). <sup>13</sup>C NMR (CDCl<sub>3</sub>, 100 MHz, ppm): δ 154.15, 151.68, 145.47, 144.61, 143.06, 140.24, 129.34, 128.56, 127.52, 124.11, 123.87, 122.91, 122.57, 121.02, 113.11, 112.97. HRMS m/z (ESI<sup>+</sup>) Calculated for C<sub>56</sub>H<sub>40</sub>N<sub>6</sub> (M<sup>+</sup>+1) 797.33, found: 797.33. analysis (calcd., found for C<sub>56</sub>H<sub>40</sub>N<sub>6</sub>): C (84.40, 82.51), H (5.06, 4.94), N (10.55, 9.97). For <sup>1</sup>H NMR and <sup>13</sup>C NMR are in Figure S25, S26.

## II. Supplementary Figures and Tables

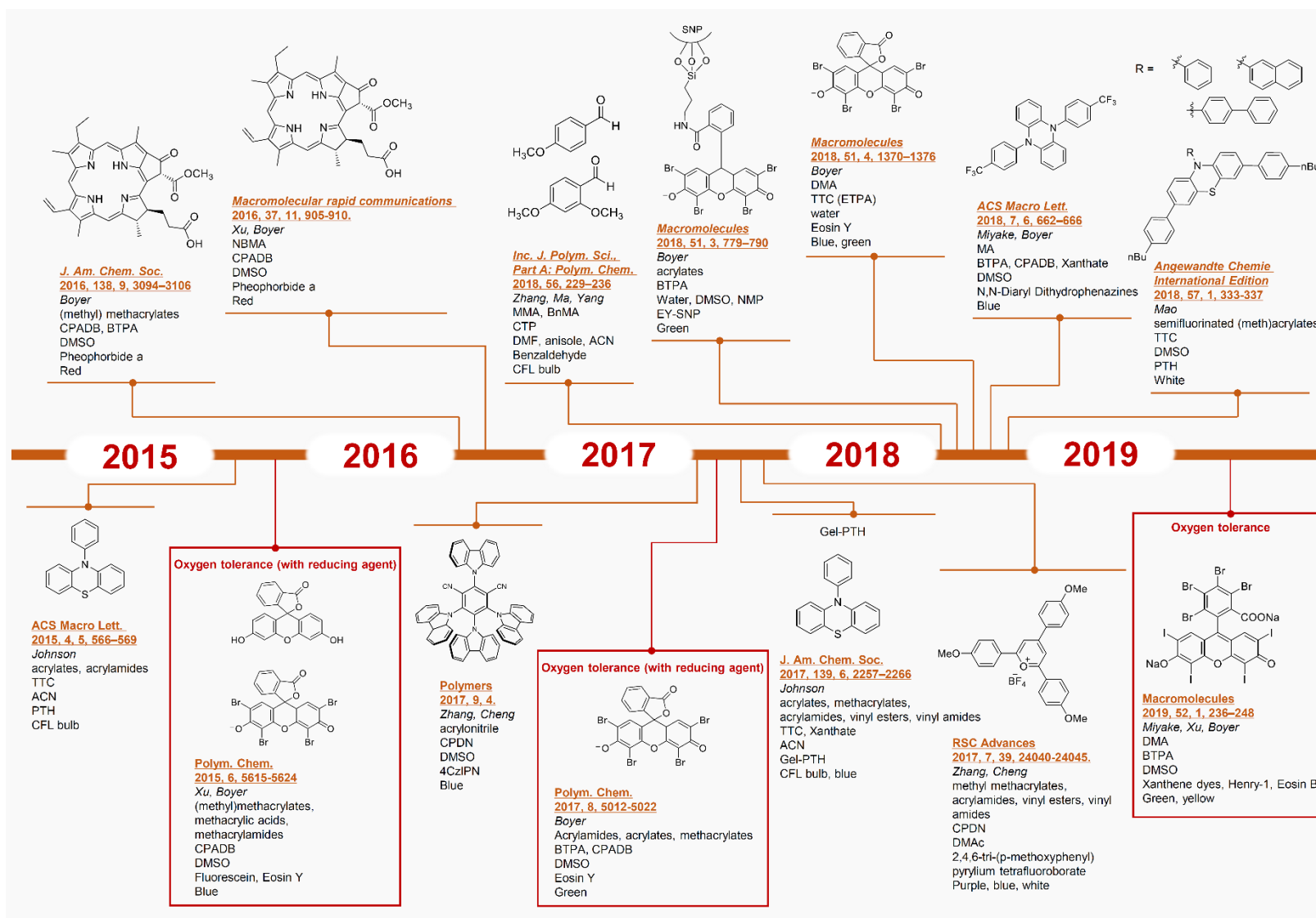


**Figure S1.** Summary of the development of organic photocatalysts for PET-RAFT polymerizations.

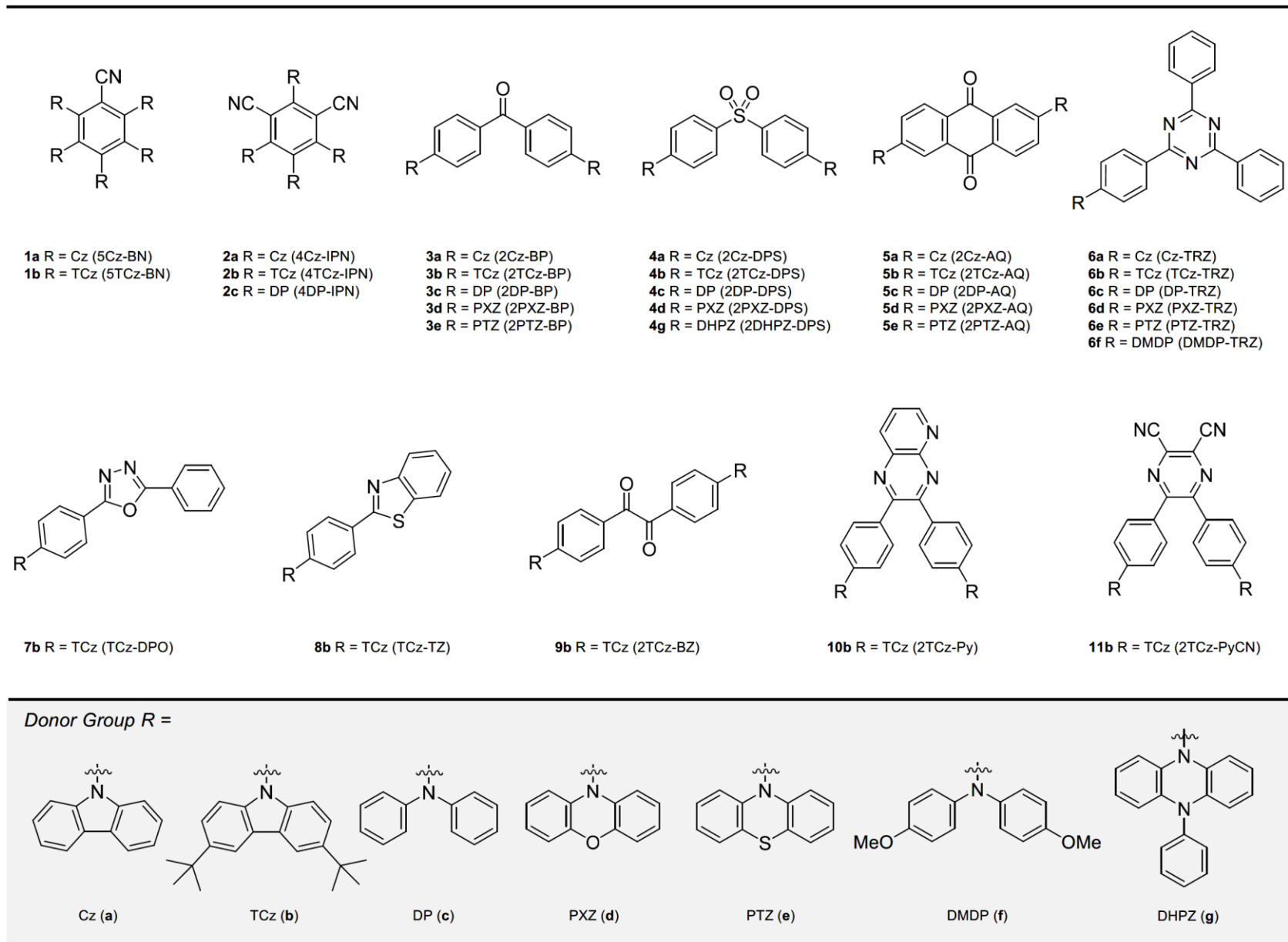


**Figure S2.** OPCs library developed in our recent work.



**Table S1.** Photophysical and electrochemical properties of OPCs in our library.

Entry	Absorption (nm)	Excited state energies (eV)			Ground state redox potentials (V vs SCE)		Excited state redox potentials (V vs SCE)				CV reversibility	
	$\lambda_{max}(\lambda_{onset})$	$E_{00}(S_1)$	$E_{00}(T_1)$	$\Delta E_{ST}$	$E_{ox}^0$	$E_{red}^0$	$E_{ox}^*(S_1)$	$E_{ox}^*(T_1)$	$E_{red}^*(S_1)$	$E_{red}^*(T_1)$	$PC^{+ \cdot}$	$PC^{- \cdot}$
1a	384 (450)	2.93	2.86	0.07	+1.41	-1.50	-1.52	-1.45	1.43	1.36	<i>ir</i>	<i>r</i>
1b	400 (469)	2.84	2.78	0.06	+1.12	-1.61	-1.72	-1.66	1.23	1.17	<i>r</i>	<i>r</i>
2a	431 (485)	2.72	2.75	-0.03	+1.52	-1.21	-1.2	-1.23	1.51	1.54	<i>ir</i>	<i>r</i>
2b	451 (513)	2.62	2.62	0.00	+1.30	-1.31	-1.32	-1.32	1.31	1.31	<i>r</i>	<i>r</i>
3a	360 (418)	3.1	2.95	0.15	+1.28	-1.64	-1.82	-1.67	1.46	1.31	<i>ir</i>	<i>r</i>
3b	363 (436)	3.06	2.93	0.13	+1.05	-1.66	-2.01	-1.88	1.4	1.27	<i>r</i>	<i>r</i>
3c	375 (445)	3.04	2.62	0.42	+1.02	-1.84	-2.02	-1.6	1.2	0.78	<i>r</i>	<i>r</i>
3d	401 (485)	2.71	2.52	0.19	+0.79	-1.61	-1.92	-1.73	1.1	0.91	<i>r</i>	<i>r</i>
3e	343 (433)	3.21	2.93	0.28	+0.74	-1.73	-2.47	-2.19	1.48	1.2	<i>r</i>	<i>r</i>
4a	338 (385)	3.46	3.12	0.34	+1.32	-1.96	-2.14	-1.8	1.5	1.16	<i>lr</i>	<i>ir</i>
4b	346 (397)	3.35	3.08	0.27	+1.26	-2.06	-2.09	-1.82	1.29	1.02	<i>r</i>	<i>ir</i>
4c	346 (399)	3.3	2.85	0.45	+1.06	-2.15	-2.24	-1.79	1.15	0.7	<i>r</i>	<i>ir</i>
4d	383 (454)	2.83	2.81	0.02	+0.84	-1.87	-1.99	-1.97	0.96	0.94	<i>r</i>	<i>ir</i>
4g	431 (524)	2.59	2.56	0.03	+0.26	-1.98	-2.33	-2.30	0.61	0.58	<i>r</i>	<i>r</i>
5a	433 (541)	2.36	2.19	0.17	+1.43	-0.84	-0.93	-0.76	1.52	1.35	<i>lr</i>	<i>r</i>
5b	463 (563)	2.44	2.29	0.15	+1.28	-0.87	-1.16	-1.01	1.57	1.42	<i>r</i>	<i>r</i>
5c	445 (588)	2.27	n.d.	n.d.	+1.20	-0.83	-1.07	n.d.	1.44	n.d.	<i>lr</i>	<i>r</i>
5d	529 (677)	n.d.	n.d.	n.d.	+0.79	-0.74	n.d.	n.d.	n.d.	n.d.	<i>r</i>	<i>r</i>
5e	408 (538)	2.53	n.d.	n.d.	+0.82	-0.91	-1.71	n.d.	1.62	n.d.	<i>r</i>	<i>r</i>
6a	359 (422)	3.27	2.88	0.39	+1.30	-1.63	-1.97	-1.58	1.64	1.25	<i>ir</i>	<i>r</i>
6b	373 (439)	3.1	2.85	0.25	+1.20	-1.65	-1.9	-1.65	1.45	1.2	<i>r</i>	<i>r</i>
6c	388 (465)	2.96	2.59	0.37	+1.0	-1.73	-1.96	-1.59	1.23	0.86	<i>ir</i>	<i>r</i>
6d	411 (481)	2.65	2.43	0.22	+0.73	-1.63	-1.92	-1.7	1.02	0.8	<i>r</i>	<i>r</i>
6e	363 (468)	3.3	2.82	0.48	+0.73	-1.62	-2.57	-2.09	1.68	1.2	<i>r</i>	<i>r</i>
6f	390 (501)	2.66	2.52	0.14	+0.77	-1.76	-1.89	-1.75	0.9	0.76	<i>r</i>	<i>r</i>
7b	348 (406)	3.46	n.d.	n.d.	+1.21	-2.05	-2.25	n.d.	1.41	n.d.	<i>r</i>	<i>r</i>
8b	360 (420)	3.28	n.d.	n.d.	+1.18	-1.91	-2.1	n.d.	1.37	n.d.	<i>r</i>	<i>r</i>
9b	387 (488)	2.93	2.58	0.35	+1.26	-1.07	-1.67	-1.32	1.86	1.51	<i>r</i>	<i>r</i>
10b	396 (507)	2.84	2.35	0.49	+1.20	-1.37	-1.64	-1.15	1.47	0.98	<i>r</i>	<i>r</i>
11b	386 (470)	2.75	2.49	0.26	+1.21	-1.06	-1.54	-1.28	1.69	1.43	<i>r</i>	<i>r</i>

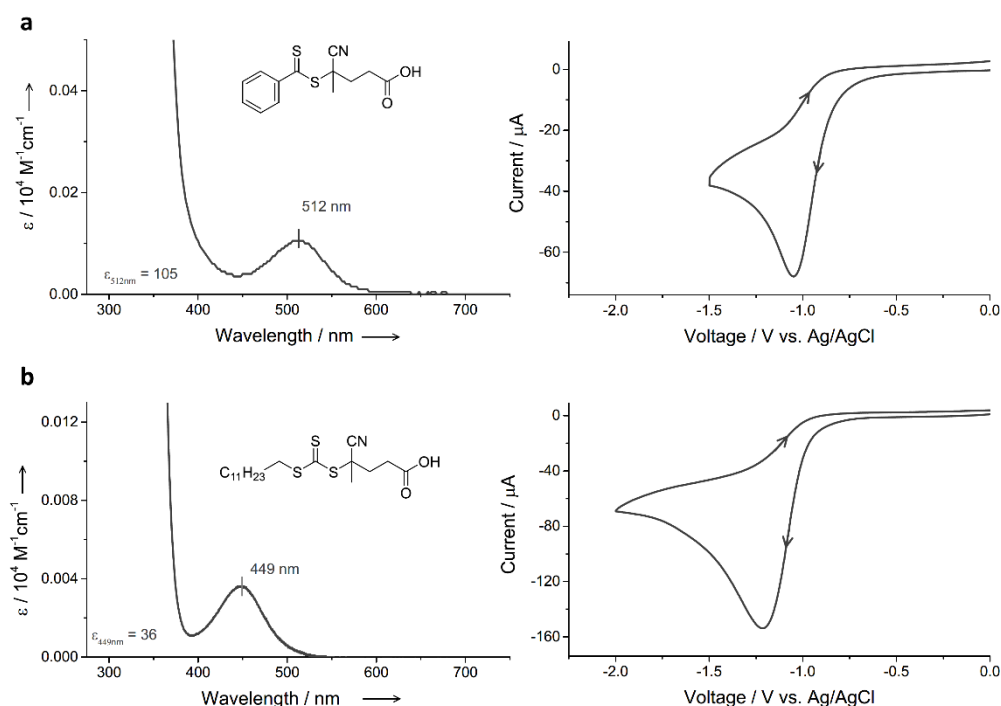


**Figure S3.** UV-vis spectra (left) and CV curves (right) of (a) CPADB and (b) CDTPA. UV-vis measurements were performed in DMSO with  $[\text{CTA}] = 20 \mu\text{M}$ . CV measurements were done in 0.2 mM  $\text{CH}_3\text{CN}$  solution with 0.1 M  $n\text{-Bu}_4\text{NPF}_6$  as supporting electrolyte at a scan rate of 100 mV/s.

in DMF: B3LYP/6-311+G\*

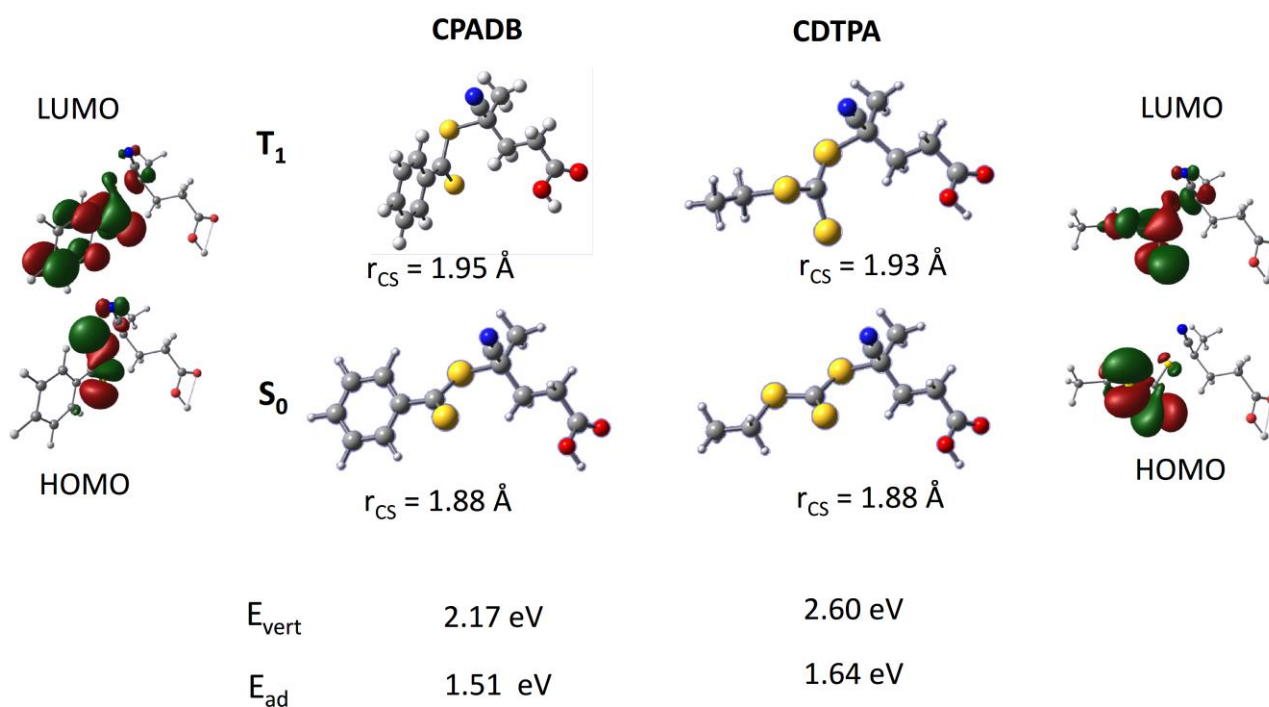


**Figure S4.** Properties of CPADB and CDTPA: Molecular geometries in  $S_0$  and  $T_1$  (the latter is exclusively described by a HOMO→LUMO excitation); corresponding frontier MOs. Adiabatic and vertical transition energies in DMF.



Figure 1 consists of two photographs. The left photograph shows the experimental setup for the LED light source. It includes a power supply unit with two outlets, a halogen socket, an LED holder, an LED stabilizer, and an acryl plate. A yellow arrow points to the LED bulb. The right photograph shows the setup with the light source turned OFF, highlighting the glass plate. A yellow arrow points to the glass plate.

Light ON

LED (3 W, 515 nm)

12.5 cm

1 2 3 4 5

INFORMATION ONLY, NOT FOR MANUFACTURING

Technical drawing of the Thorlabs N/A:PM100D power meter showing dimensions in inches and millimeters.

Dimensions (inches in parentheses):

- Front View:
  - Top: 3.17 (80.40)
  - Right: 2.36 (60)
  - Bottom: 7.09 (180)
  - Left: 4.13 (105)
  - Bottom Left: 1.50 (38)
- Side View:
  - Depth: 1.50 (38)
- Top View:
  - Mounting Hole Spacing: 1.50 (38)

1/4-20 UNC

ALL DIMENSIONS IN PARANTHESES ARE MILLIMETERS

UNFOLLOWS SPECIFIC DIMENSIONS ARE IN INCHES TOLERANCES: FRACTIONS DECIMALS ANGLES SURF FINISH

FEATURES: Ge 12.12.2008, CHG: Go 12.12.2008, APP: Go 12.12.2008

NO PART OF THIS DRAWING CAN BE REPRODUCED OR TRANSMITTED IN ANY FORM OR BY ANY MEANS, ELECTRONIC OR MECHANICAL, INCLUDING PHOTOCOPYING, RECORDING, OR BY ANY INFORMATION STORAGE AND RETRIEVAL SYSTEM.

THORLABS

German

Optical Power and Energy Meter

MODEL: PM100D

CHG: 17454-001

REV: A

The figure consists of two vertically stacked line graphs. Both graphs plot 'Normalized intensity / a.u.' on the y-axis (ranging from 0.0 to 1.0) against 'Wavelength / nm' on the x-axis (ranging from 400 to 650 nm). The top graph, represented by a blue line, shows a sharp peak at approximately 455 nm with a maximum intensity of 1.0. The bottom graph, represented by a green line, shows a broader peak at approximately 515 nm, also reaching a maximum intensity of 1.0.

Supporting-21

**a**

Entry	Atmosphere	[M]:[I]:[PC]	$\alpha$ (%)	$M_{n,theo}$ (Da)	$M_{n,exp}$ (Da)	$\bar{D}$	$I^*$
1	Ar	200:1:0	20	4400	6000	1.17	0.73
2	Air	200:1:0	9	2000	5000	1.28	0.40

For detailed procedures, see supplementary methods; section B.

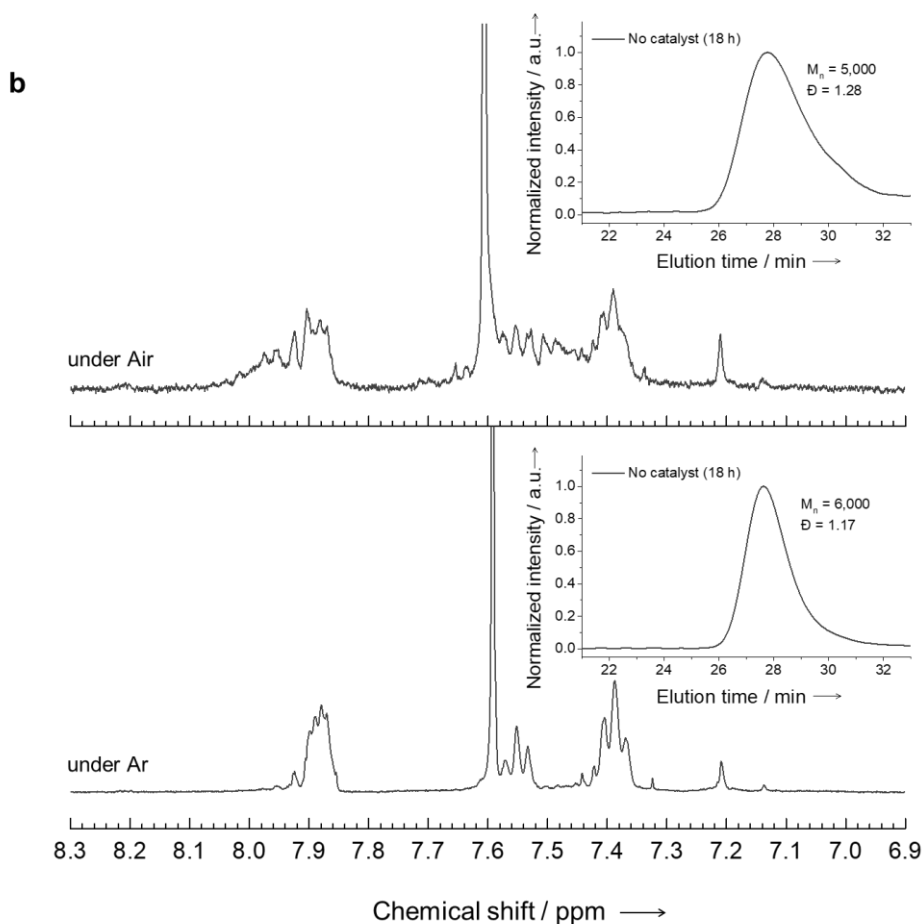


**Figure S6.** (a) Negative control experiments of PET-RAFT of MMA in the presence of argon and air using CPADB. For detailed procedures, see supplementary methods; section B. (b)  $^1\text{H}$ -NMR spectra and GPC traces of the reaction mixtures obtained after PET-RAFT polymerizations of MMA under air (up) and argon (bottom).

**Table S2.** Results of PET-RAFT polymerization of MMA in the presence of CPADB using 4DP-IPN of 1 ppm under argon. All polymerizations were performed at room temperature under a 3 W blue LED (455 nm, ca. 2.5 mW/cm<sup>2</sup>).

Entry <sup>a</sup>	PC	Bubbling	[M]:[I]:[PC]	Conversion (%)	M <sub>n,theo</sub> (Da)	M <sub>n,exp</sub> (Da)	$\bar{D}$	I*
1 <sup>b</sup>	4DP-IPN	Ar	200:1:0.001	62	12700	14000	1.11	0.91
2	4DP-IPN	Ar	200:1:0.0002	41	8500	10300	1.11	0.83
3	4DP-IPN	Ar	200:1:0.0002	41	8600	10400	1.11	0.83

a. For detailed procedures, see supplementary methods; section B in the supporting information. b. Same data as Table 1 entry 11.

**Table S3.** Reproducibility test. For detailed procedures, see supplementary methods; section B. Experiments were performed in many different set-ups by students in our group.

Entry <sup>a</sup>	PC	Bubbling	[M]:[I]:[PC]	Conversion (%)	M <sub>n,theo</sub> (Da)	M <sub>n,exp</sub> (Da)	$\bar{D}$	I*
1 <sup>b</sup>	4DP-IPN	Ar	200:1:0.001	62	12700	14000	1.11	0.91
2	4DP-IPN	Ar	200:1:0.001	63	13000	13900	1.13	0.94
3	4DP-IPN	Ar	200:1:0.001	76	15500	17400	1.14	0.89
4	4DP-IPN	Ar	200:1:0.001	67	13600	15400	1.13	0.88
5	4DP-IPN	Ar	200:1:0.001	69	14000	16600	1.14	0.84
6	4DP-IPN	Ar	200:1:0.001	58	11800	13300	1.13	0.89
7 <sup>b</sup>	4DP-IPN	Air	200:1:0.001	70	14200	24100	1.26	0.59
8	4DP-IPN	Air	200:1:0.001	74	15000	25100	1.22	0.60
9	4DP-IPN	Air	200:1:0.001	88	17900	26700	1.34	0.67
10	4DP-IPN	Air	200:1:0.001	89	18100	23900	1.27	0.76
11	4DP-IPN	Air	200:1:0.001	76	15400	24200	1.37	0.64
12 <sup>c</sup>	4DP-IPN	Air	200:1:0.001	84	17100	36400	1.42	0.47

a. For detailed procedures, see supplementary methods; section B in the supporting information. b. This was used as data for Table 1; entry 11 and 12 in the manuscript. c. As shown in here, reproducibility under air was rather lower than that in argon atmosphere.

**Table S4.** Control of molecular weight of PMMA in the presence of argon using CPADB and 4DP-IPN of 5 ppm. For detailed procedures, see supplementary methods; section B. <sup>1</sup>H-NMR spectra and GPC curves of the resulting polymers are in Figure S26.

Entry <sup>a</sup>	PC	Bubbling	[M]:[I]:[PC]	Conversion (%)	M <sub>n,theo</sub> (Da)	M <sub>n,exp</sub> (Da)	$\bar{D}$	I*
1 <sup>b</sup>	4DP-IPN	Ar	200:4:0.001	64	3500	4200	1.13	0.83
2 <sup>b</sup>	4DP-IPN	Ar	200:2:0.001	78	8100	8300	1.13	0.98
3 <sup>c</sup>	4DP-IPN	Ar	200:1:0.001	62	12700	14000	1.11	0.91
4 <sup>d</sup>	4DP-IPN	Ar	200:0.5:0.001	51	20700	27000	1.20	0.77

a. The reactions were performed at room temperature under a 3 W blue LED (455 nm, ca. 2.5 mW/cm<sup>2</sup>). For detailed procedures, see supplementary methods; section B. b. The reaction was performed for 36 h. c. The reaction was performed for 24 h. d. The reaction was performed for 6 h.

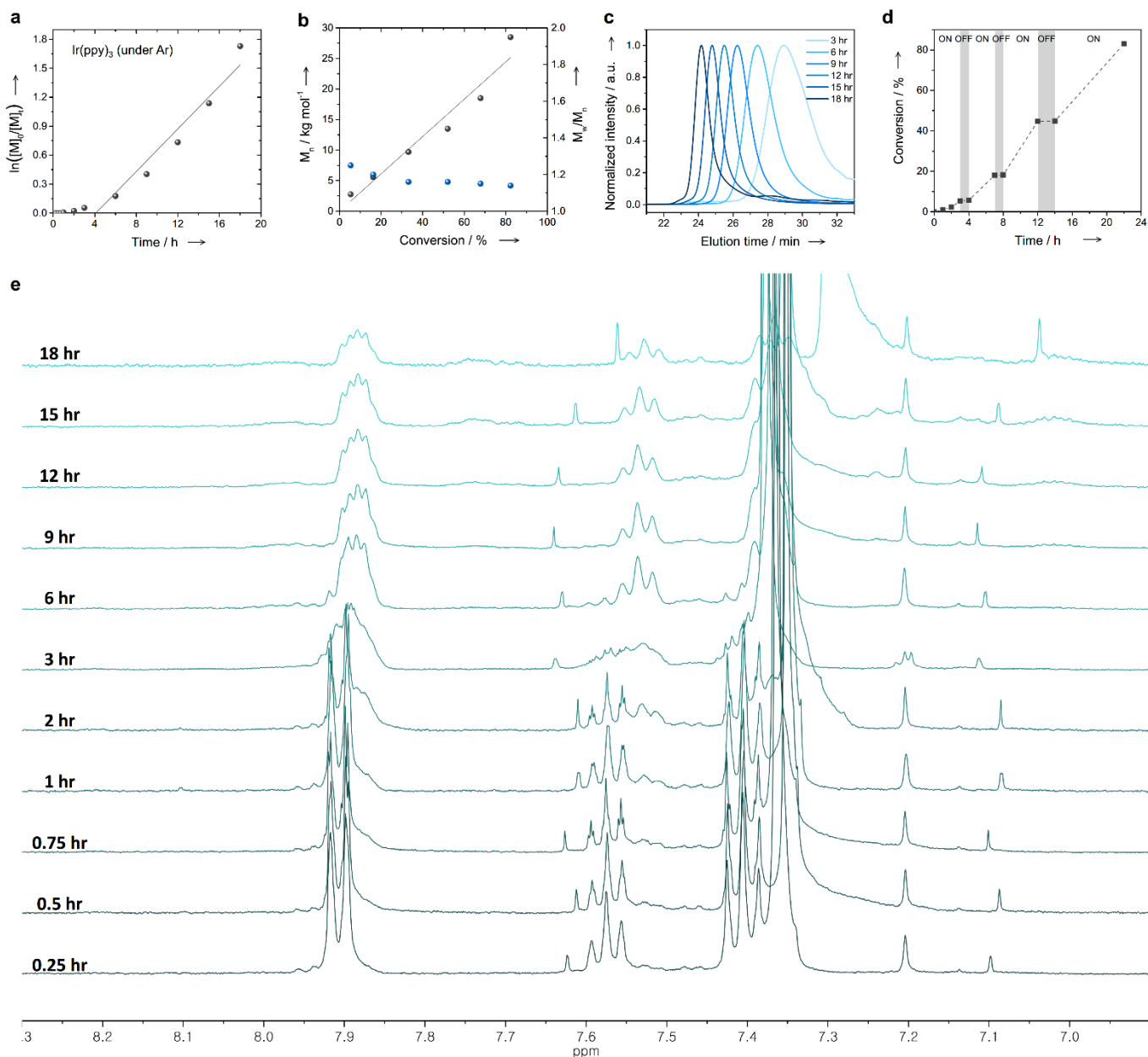


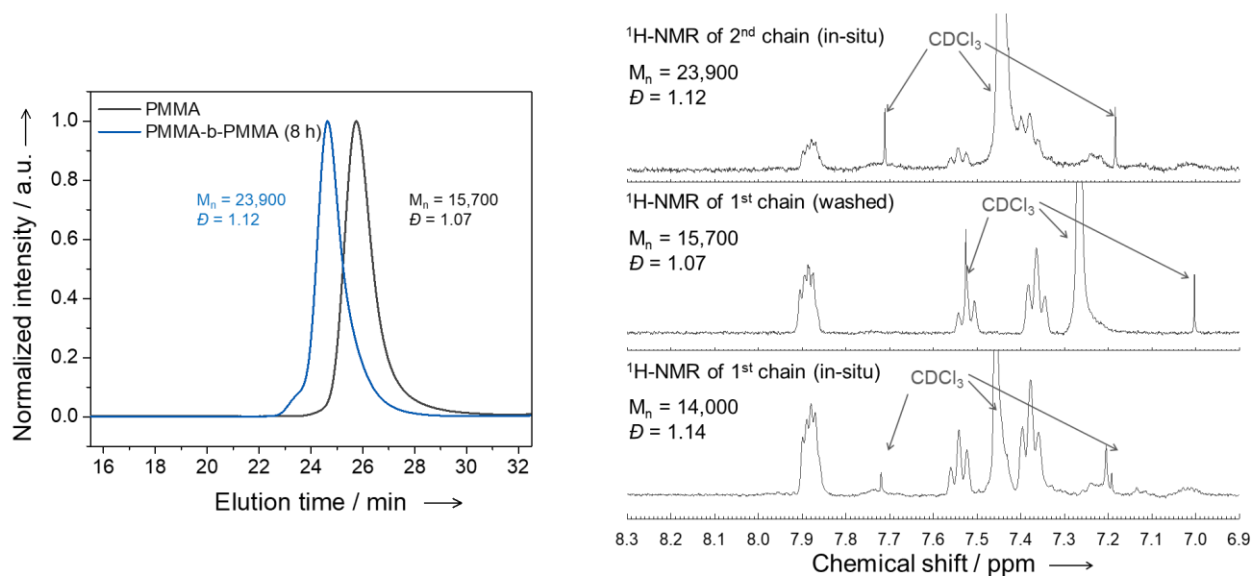
**Figure S7.** Kinetic plots for PET-RAFT polymerizations of MMA in the presence of argon using  $\text{Ir}(\text{ppy})_3$  of 1 ppm. For detailed procedures, see supplementary methods; section B. (a)  $\ln([M]_0/[M]_t)$  versus reaction time. (b)  $M_n$  versus conversion (black circle) and  $M_w/M_n$  versus conversion (blue circle). (c) GPC traces at different reaction time. (d) Light “ON”/“OFF” experiment for PET-RAFT polymerization of MMA using CPADB and  $\text{Ir}(\text{ppy})_3$  of 1 ppm. (e) <sup>1</sup>H NMR spectra at different reaction time.

a

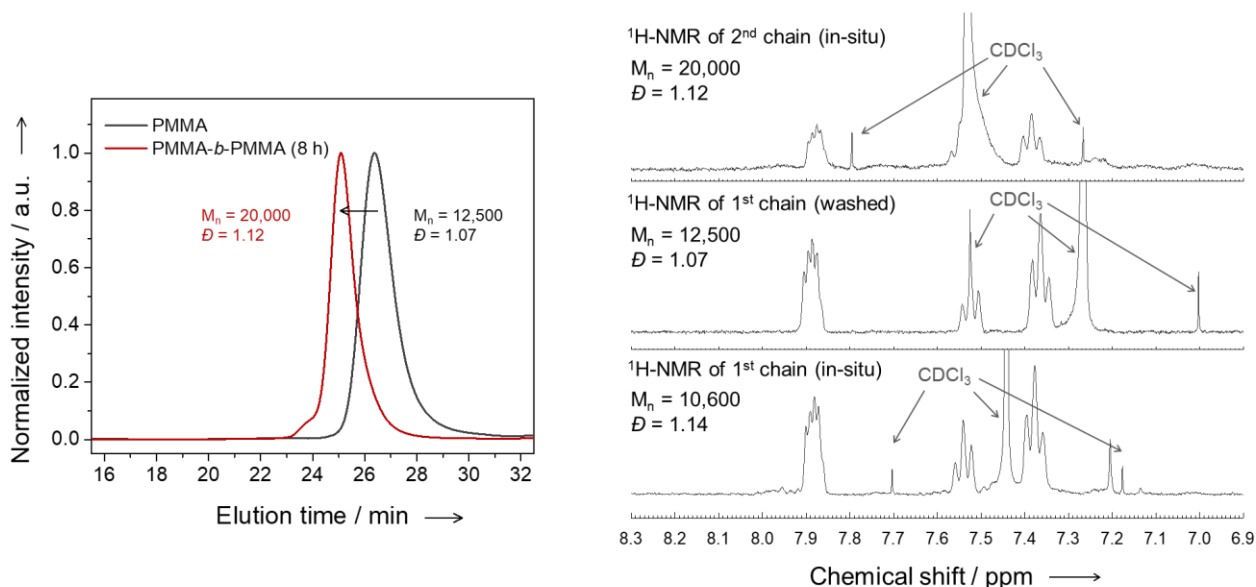
Entry	PC	Atmosphere	[M]:[I]:[PC]	$\alpha$ (%)	$M_{n,theo}$ (Da)	$M_{n,exp}$ (Da)	$\bar{D}$	$I^*$
1 <sup>a</sup>	Ir(ppy) <sub>3</sub>	Ar	200:1:0.0002	53	10800	14000	1.14	0.77
2 <sup>b</sup>	Ir(ppy) <sub>3</sub>	Ar	200:1:0.0002	-	-	15700	1.07	
3 <sup>c</sup>	Ir(ppy) <sub>3</sub>	Ar	200:1:0.0002	-	-	23900	1.12	
4 <sup>a</sup>	4DP-IPN	Ar	200:1:0.001	36	7500	10600	1.14	0.71
5 <sup>b</sup>	4DP-IPN	Ar	200:1:0.001	-	-	12500	1.07	
6 <sup>c</sup>	4DP-IPN	Ar	200:1:0.001	-	-	20000	1.12	

a. The macro-agent were performed at room temperature under a 3 W blue LED (455 nm, 2.5 mW/cm<sup>2</sup>) for 12 h. b. The purified macroinitiator. c. The PMMA-*b*-PMMA were performed at room temperature under a 3 W blue LED (455 nm, 2.5 mW/cm<sup>2</sup>) for 8 h under Ar.

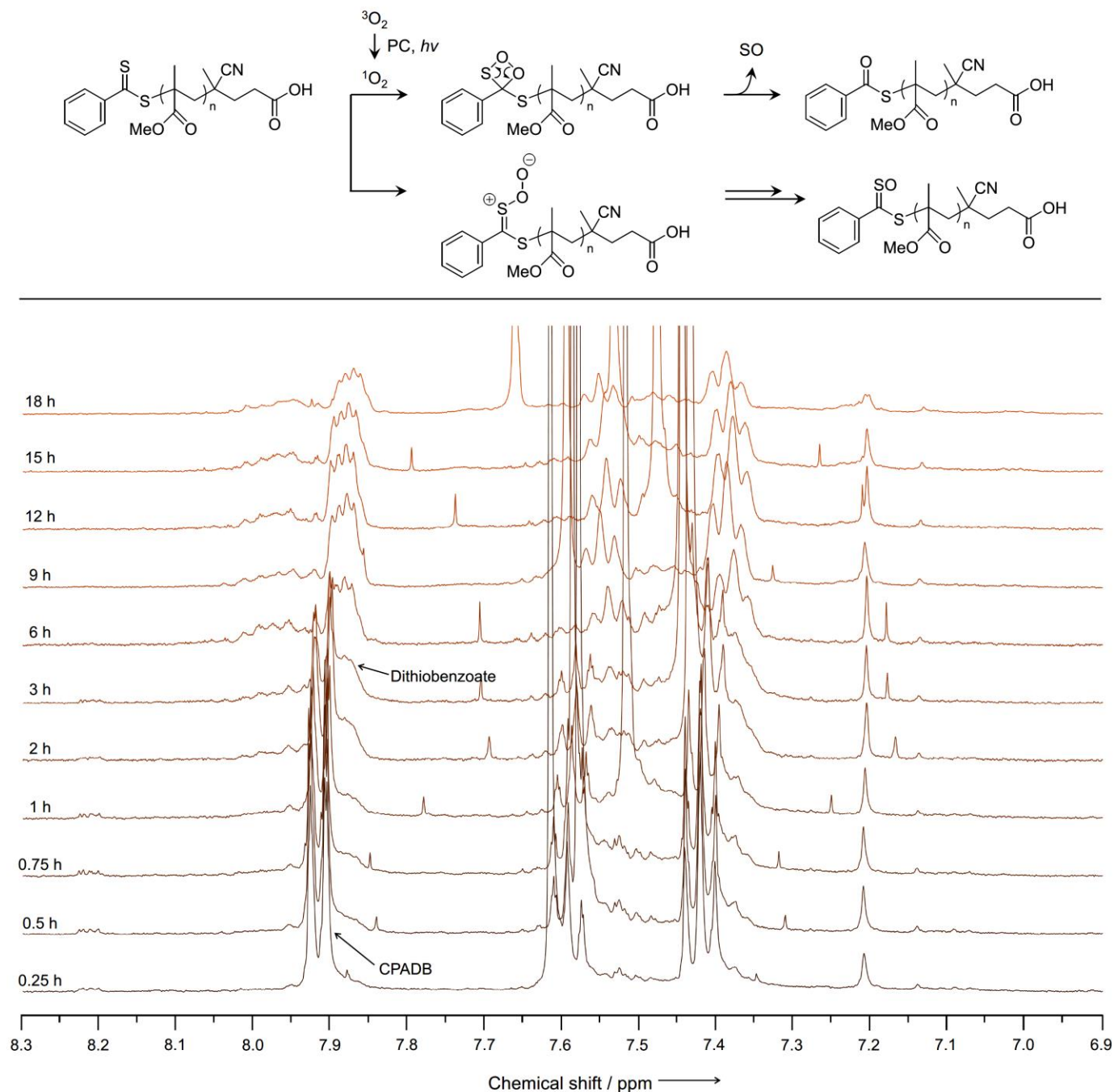
b



c

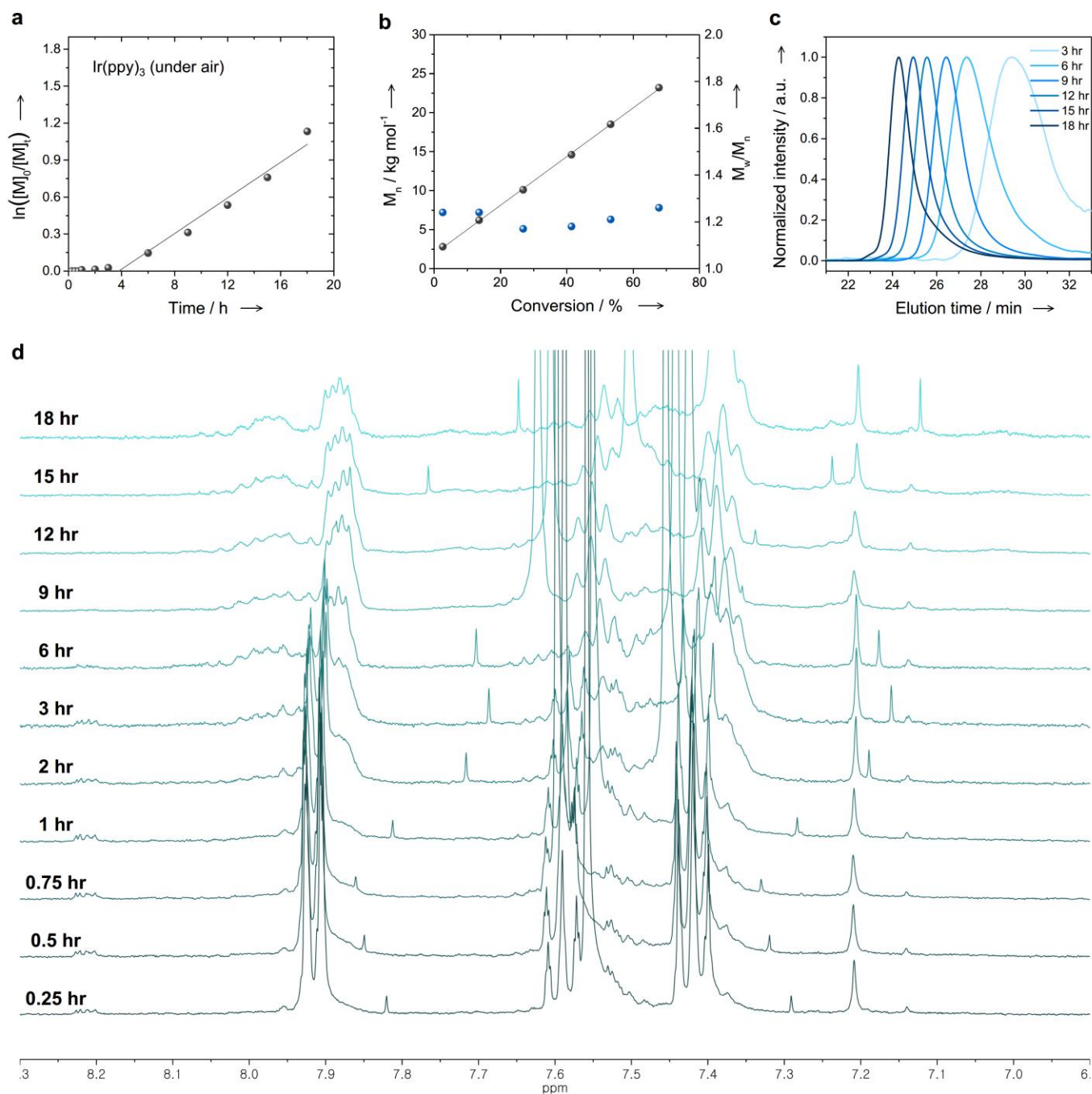


**Figure S8.** (a) Chain extensions of PMMA in the presence of argon using Ir(ppy)<sub>3</sub> of 1 ppm and 4DP-IPN of 5 ppm. For detailed procedures, see supplementary methods; section B. GPC traces of PMMA and diblock of PMMA-*b*-PMMA and <sup>1</sup>H NMR spectra of washed (middle) and in-situ (bottom) 1<sup>st</sup> chain and in-situ (top) 2<sup>nd</sup> chain using (b) Ir(ppy)<sub>3</sub> of 1 ppm and (c) 4DP-IPN of 5 ppm under argon.



**Figure S9.** <sup>1</sup>H-NMR spectra of the polymerization mixtures using CPADB and 4DP-IPN (5 ppm) at different reaction times. For reaction conditions, see main text. Suggested mechanism for the photo-oxidation of CPADB is given in the top.



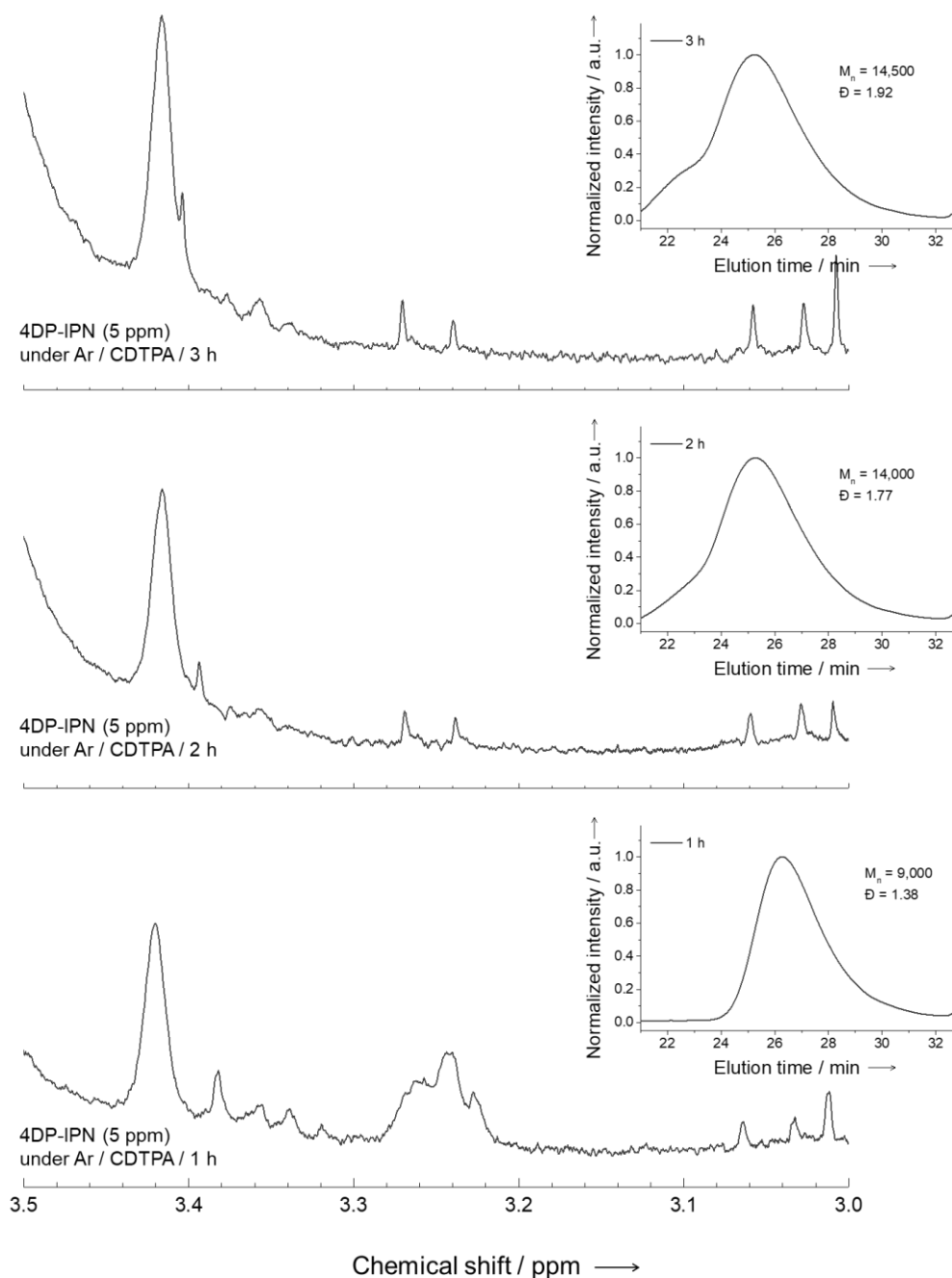


**Figure S10.** Kinetic plots for PET-RAFT polymerizations of MMA in the presence of air using  $\text{Ir(ppy)}_3$  of 1 ppm. For detailed procedures, see supplementary methods; section B. (a)  $\ln([M]_0/[M]_t)$  versus reaction time. (b)  $M_n$  versus conversion (black circle) and  $M_w/M_n$  versus conversion (blue circle). (c) GPC traces at different reaction time. (d) <sup>1</sup>H NMR spectra of kinetic study at different reaction time.

**a**

Entry <sup>a</sup>	PC	Atmosphere	[M]:[I]:[PC]	$\alpha$ (%)	$M_{n,theo}$ (Da)	$M_{n,exp}$ (Da)	$\bar{D}$	$I^*$	Reaction time (h)
1	4DP-IPN	Ar	200:1:0.001	32	6700	9000	1.38	0.74	1
2	4DP-IPN	Ar	200:1:0.001	61	12400	14000	1.77	0.89	2
3	4DP-IPN	Ar	200:1:0.001	64	13100	14500	1.92	0.90	3

a. The reactions were performed at room temperature under a 3 W blue LED (455 nm, ca. 2.5 mW/cm<sup>2</sup>). CDTPA was used as a CTA.

**b**

**Figure S11.** (a) Results of PET-RAFT polymerization of MMA in the presence of CDTPA using 4DP-IPN of 5 ppm under argon. All polymerizations were performed at room temperature under a 3 W blue LED (455 nm, ca. 2.5 mW/cm<sup>2</sup>). For detailed procedures, see supplementary methods; section B. (b) <sup>1</sup>H-NMR spectra and GPC traces of the reaction mixtures obtained after PET-RAFT polymerizations of MMA.



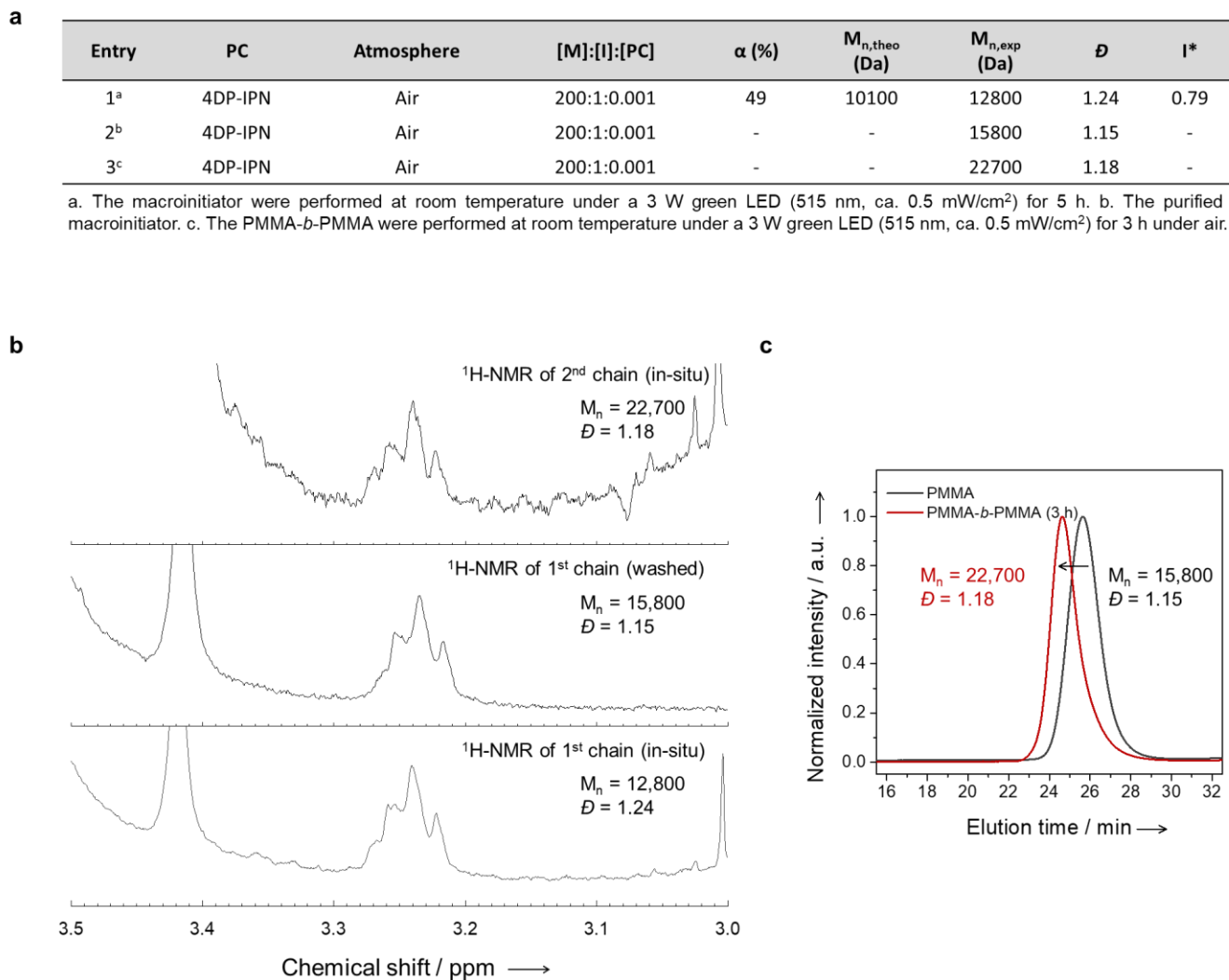


**Figure S12.** (a) Chain extensions of PMMA in the presence of air using CDTPA and 4DP-IPN of 5 ppm. For detailed procedures, see supplementary methods; section B. (b) <sup>1</sup>H NMR spectra of washed (middle) and in-situ (bottom) 1<sup>st</sup> chain and in-situ (top) 2<sup>nd</sup> chain under air. (c) GPC traces (right) of PMMA (black) and diblock of PMMA-*b*-PMMA (red) under air.

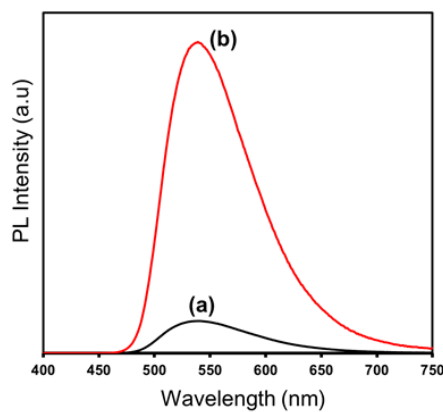


**Figure S13.** PL emission spectra of 4DP-IPN in CH<sub>3</sub>CN at r.t. (a) unpurged (b) after purging 10 min with dry N<sub>2</sub> gas,  $\lambda_{exc}$  = 387 nm.

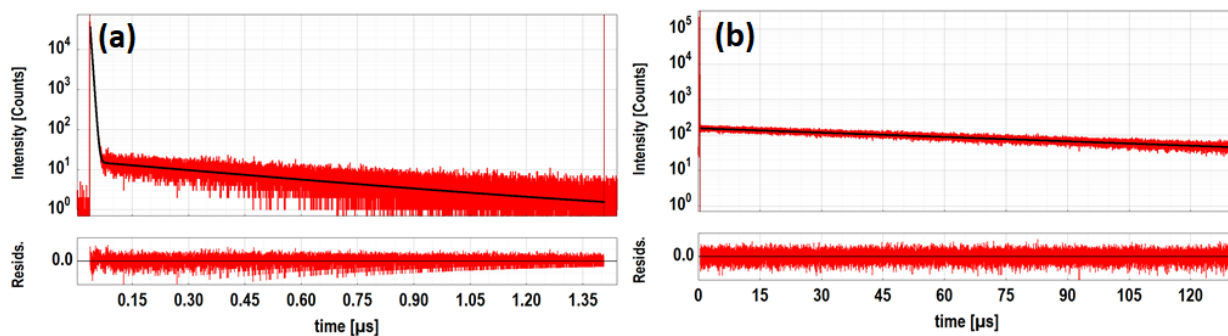


**Figure S14.** PL decay of 4DP-IPN in CH<sub>3</sub>CN at RT, excitation at  $\lambda_{\text{exc}} = 405$  nm, detection at  $\lambda_{\text{det}} = 536$  nm; experiment (red), bi-exponential fits (black). (a) unpurged solution at a repetition rate of  $\nu_{\text{rep}}=300$  kHz;  $\tau_1 = 3.3$  ns ( $A_1 = 9.9 \cdot 10^{-1}$ , 94% and  $\tau_2 = 0.52$   $\mu$ s ( $A_2 = 4.2 \cdot 10^{-4}$ , intensity-weighted fractional amplitude 6 %). (b) after purging (10 min, dry N<sub>2</sub> gas),  $\nu_{\text{rep}}=7$  kHz;  $\tau_1 = 3.3$  ns ( $A_1 = 9.9 \cdot 10^{-1}$ , 3%) and  $\tau_2 = 104$   $\mu$ s ( $A_2 \approx 1 \cdot 10^{-3}$ , 97%).

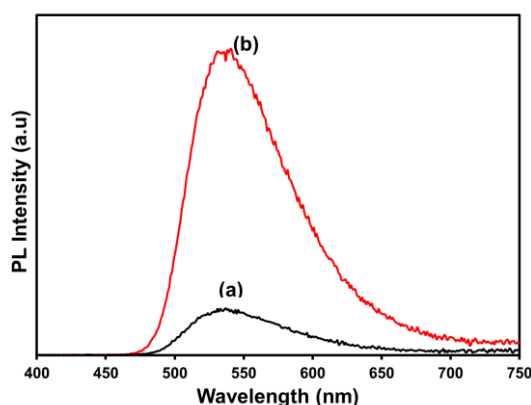


**Figure S15.** PL emission spectra of 4DP-IPN in DMSO at r.t. (a) unpurged (b) after 10 min purging with dry N<sub>2</sub> gas,  $\lambda_{\text{exc}} = 387$  nm.

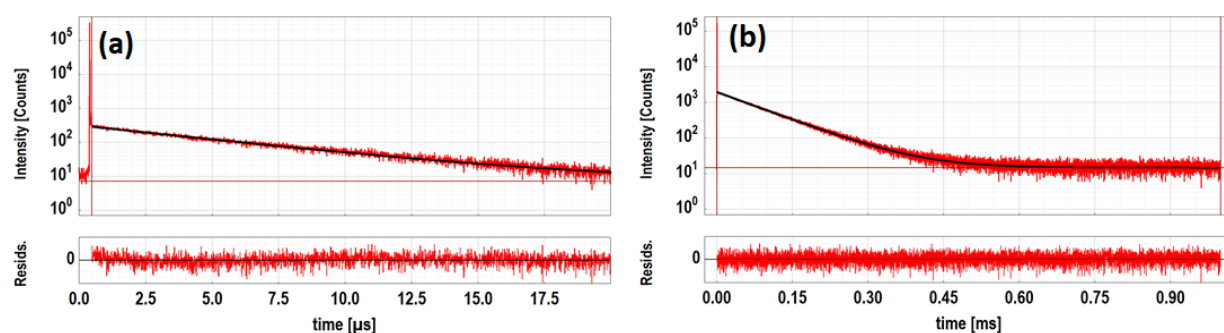


**Figure S16.** PL decays of 4DP-IPN in DMSO at RT,  $\lambda_{\text{exc}} = 405$  nm,  $\lambda_{\text{det}} = 540$  nm; experiment (red), mono-exponential fits (black). (a) unpurged,  $\nu_{\text{rep}}=50$  kHz,  $\tau = 5.1$   $\mu$ s. (b) after purging (10 min, dry N<sub>2</sub> gas),  $\nu_{\text{rep}}=1$  kHz,  $\tau = 82.8$   $\mu$ s.

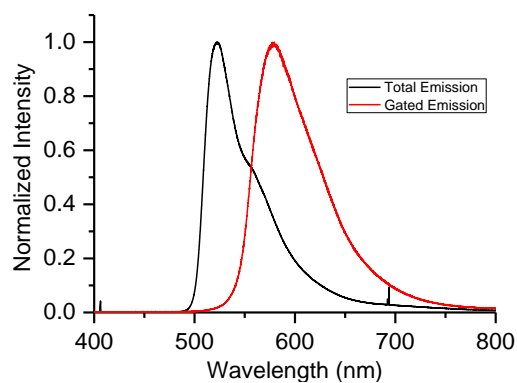


**Figure S17.** Emission under continuous wave excitation and gated emission of 4DP-IPN in CH<sub>3</sub>CN at 65K.

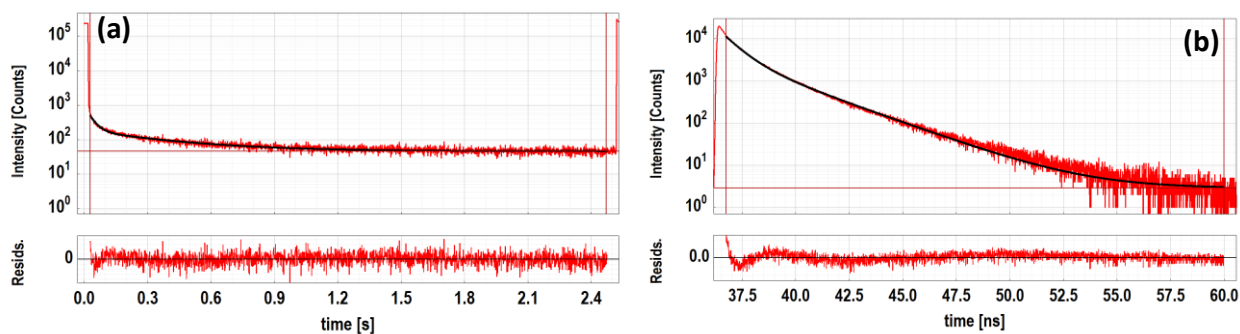


**Figure S18.** PL Decays of 4DP-IPN in CH<sub>3</sub>CN at 65K, experiment (red), bi-exponential fits (black). (a) Phosphorescence decay,  $\lambda_{\text{exc}} = 405$  nm,  $\lambda_{\text{det}} = 560$  nm,  $\nu_{\text{rep}} = 0.33$  Hz.  $\tau_1 = 31$  ms ( $A_1 = 3.0 \cdot 10^{-1}$ , 17 %),  $\tau_2 = 380$  ms ( $A_2 = 7.1 \cdot 10^{-1}$ , 83%). (b) Fluorescence decay,  $\lambda_{\text{exc}} = 405$  nm,  $\lambda_{\text{det}} = 525$  nm,  $\nu_{\text{rep}} = 2.5$  MHz.  $\tau_1 = 2.4$  ns ( $A_1 = 2.9 \cdot 10^{-1}$ , 56%),  $\tau_2 = 0.8$  ns ( $A_2 = 7.1 \cdot 10^{-1}$ , 44%).

**Table S5.** PLQY of 4DP-IPN at r.t. under N<sub>2</sub> purged condition.

solvent	$\Phi_F$
CH <sub>3</sub> CN	0.18
DMSO	0.23

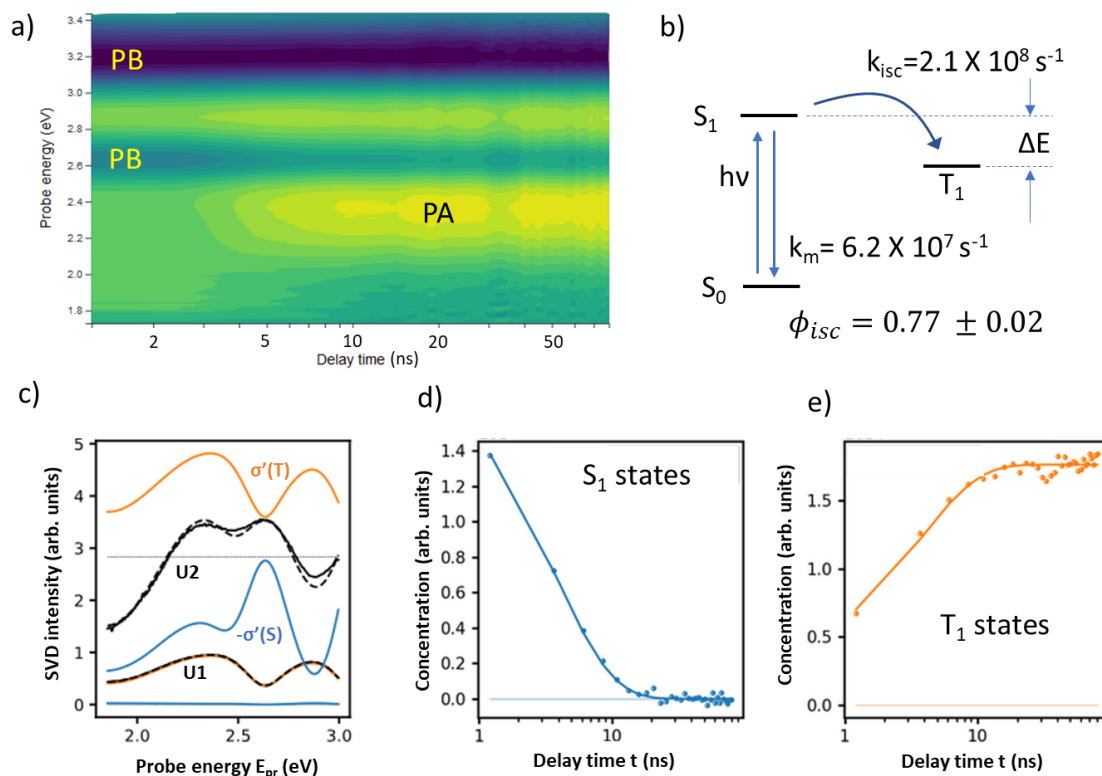


**Figure S19.** Transient absorption (TA) experiment of 4DP-IPN was performed in CH<sub>3</sub>CN at r.t. (a) TA spectrum in the nanosecond temporal range, after pumping with 300 ps monochromatic pump pulses at 355 nm with 2  $\mu$ J pulse energy and a repetition rate of 500 Hz. The false color scale denotes green as zero signal, yellow as positive transient absorption (photo-induced absorption, PA) and blue as negative transient absorption (transient photobleach, PB). (b) Kinetic model for the simulation of the TA dynamics. Note that the slow processes from scheme 1 ( $k_{isc}$  and  $k_{T0}$ ) have been omitted because they cannot be obtained on a 100 ns time scale; note also that  $k_m = k_F + k_{nr}$ . Without measuring the PLQY, one cannot distinguish these processes leading to the same PA and PB dynamics. However, even without knowledge of PLQY, one can still get the ISC yield, defined as  $\phi_{isc} = k_{isc} / (k_m + k_{isc})$ , directly from fitting the TA spectrum in panel (a). (c) t-SVD (eq. S13) of panel (a) (black solid lines in panel (c), and reproduction (black dashed lines) by a weighted superposition of the characteristic spectra for excited singlet and triplet states (blue and orange lines, defined acc. to eq. S14). (d) and (e) resulting dynamics of excited singlet and triplet states, according to eq. S12 (blue and orange symbols, respectively) and fitted dynamics according to panel b) (blue and orange solid lines, respectively).

III. UV-vis and PL spectra, CV curves, and  $^1\text{H}$ -NMR and  $^{13}\text{C}$ -NMR spectra of selected OPCs and GPC traces and  $^1\text{H}$ -NMR spectra of the resulting polymers (Figure S13– 47)

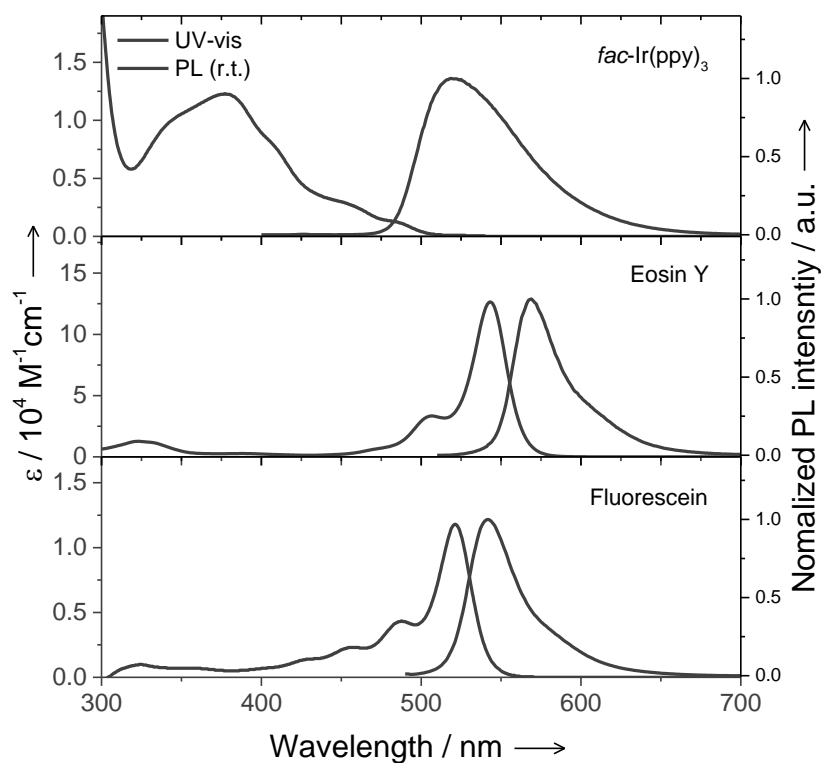


**Figure S20.** UV-vis and PL spectra of PCs purchased commercially in DMSO (20  $\mu\text{M}$ ).

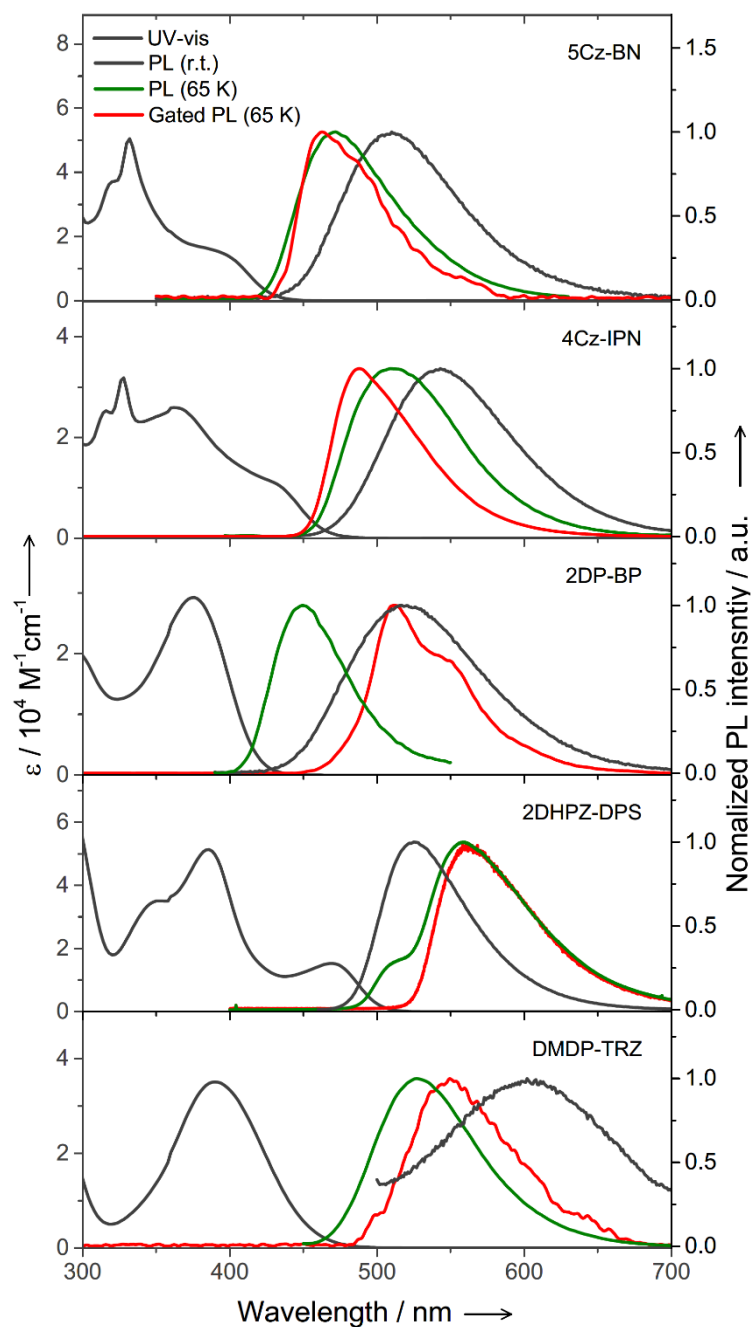


**Figure S21.** UV-vis and PL spectra of selected OPCs in DMF (20  $\mu$ M).

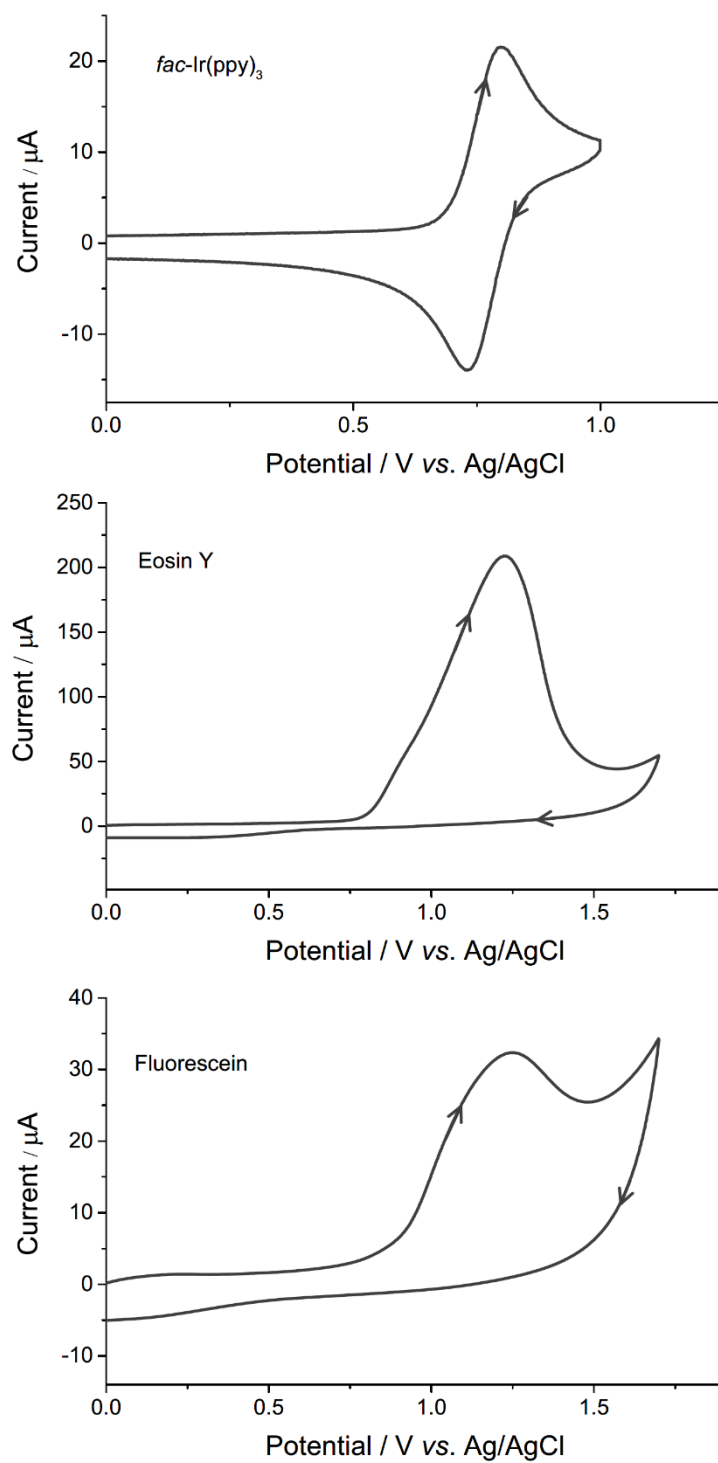


**Figure S22.** CV curves of PCs purchased commercially in CH<sub>3</sub>CN (2 mM). For eosin Y and fluorescein, in CH<sub>3</sub>CN:H<sub>2</sub>O (1:1 v/v) (2 mM).

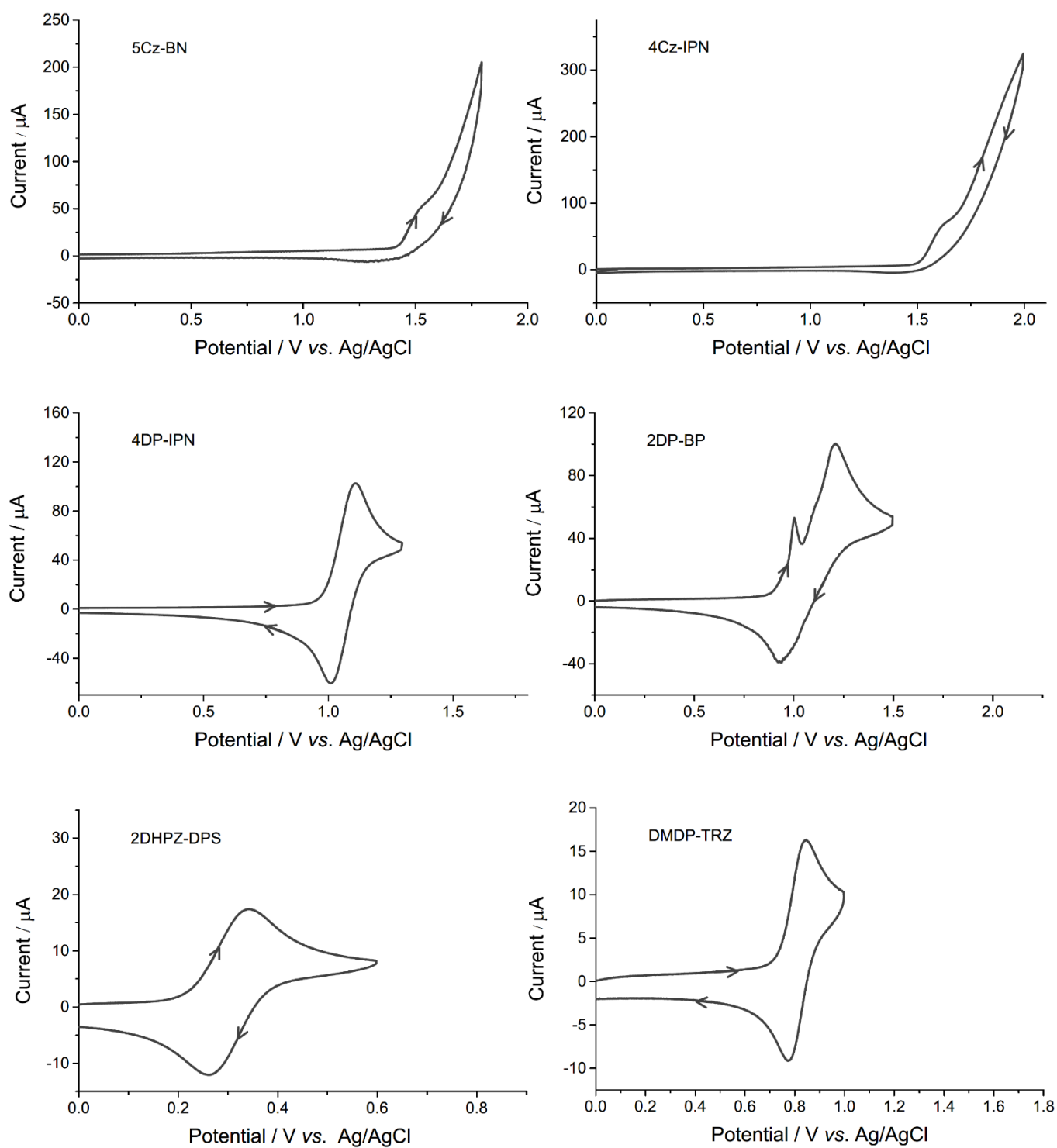


**Figure S23.** CV curves of selected OPCs in  $\text{CH}_3\text{CN}$  (2 mM).



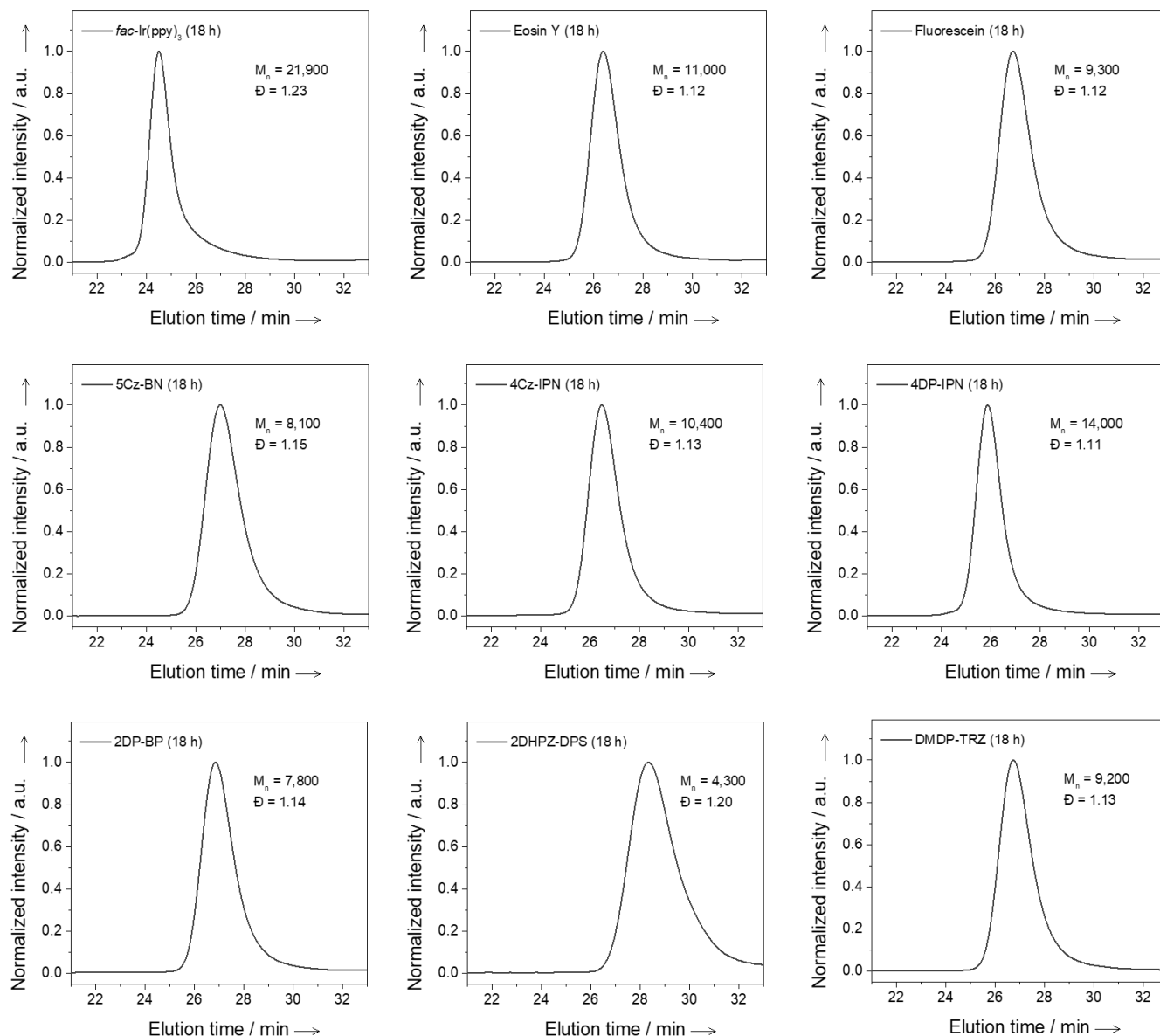


**Figure S24.** GPC traces of PET-RAFT polymerizations of MMA for Table 1 in the manuscript. Experimental condition: [MMA]:[CPADB]:[Ir(ppy)<sub>3</sub>] = 200:1:0.0002 and [MMA]:[CPADB]:[OPC] = 200:1:0.001 in DMSO under a 3W 455 nm LED at room temperature under argon.

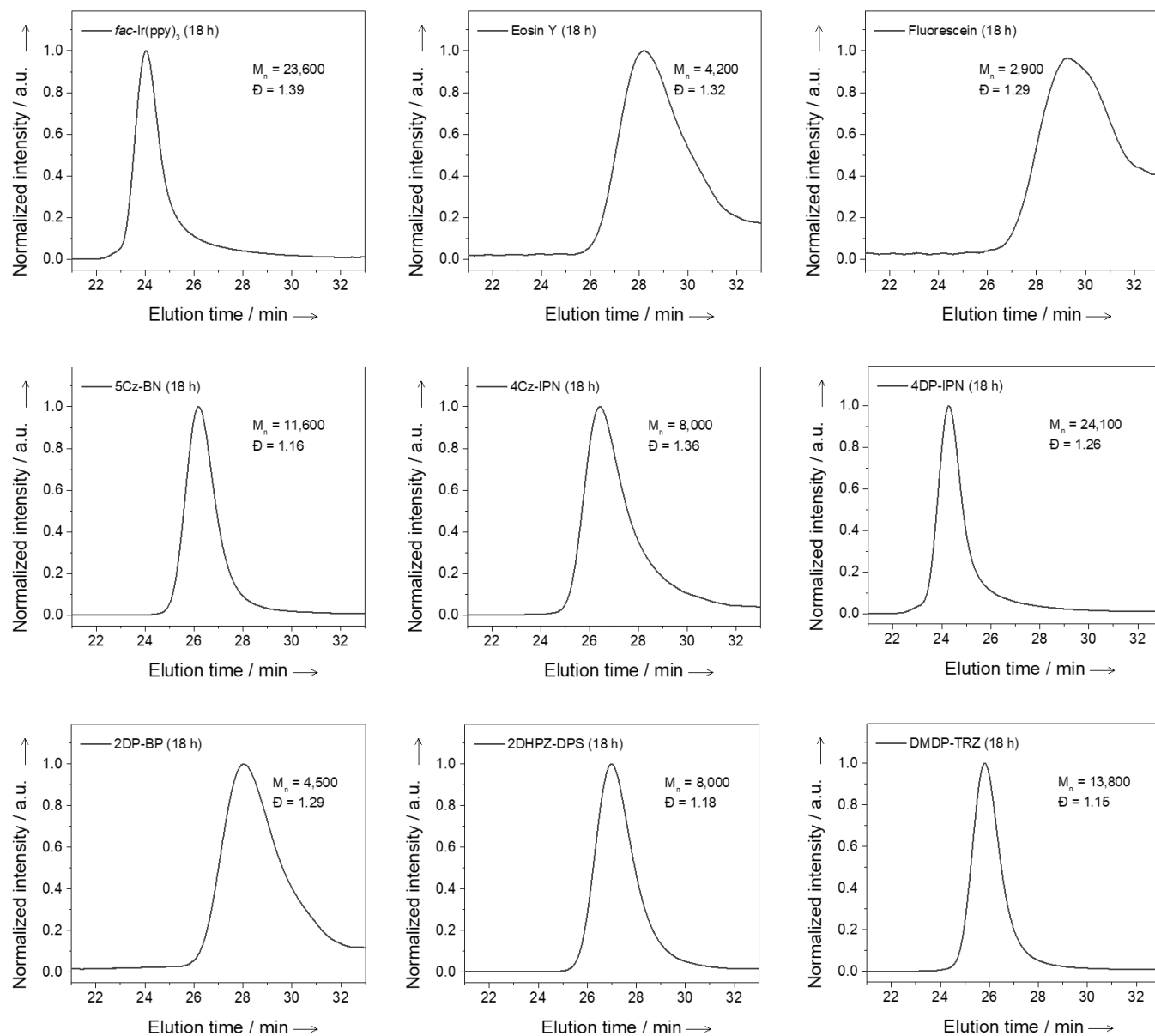


**Figure S25.** GPC traces of PET-RAFT polymerizations of MMA for Table 1 in the manuscript. Experimental condition:  $[MMA]:[CPADB]:[Ir(ppy)_3] = 200:1:0.0002$  and  $[MMA]:[CPADB]:[OPC] = 200:1:0.001$  in DMSO under a 3W 455 nm LED at room temperature under air.

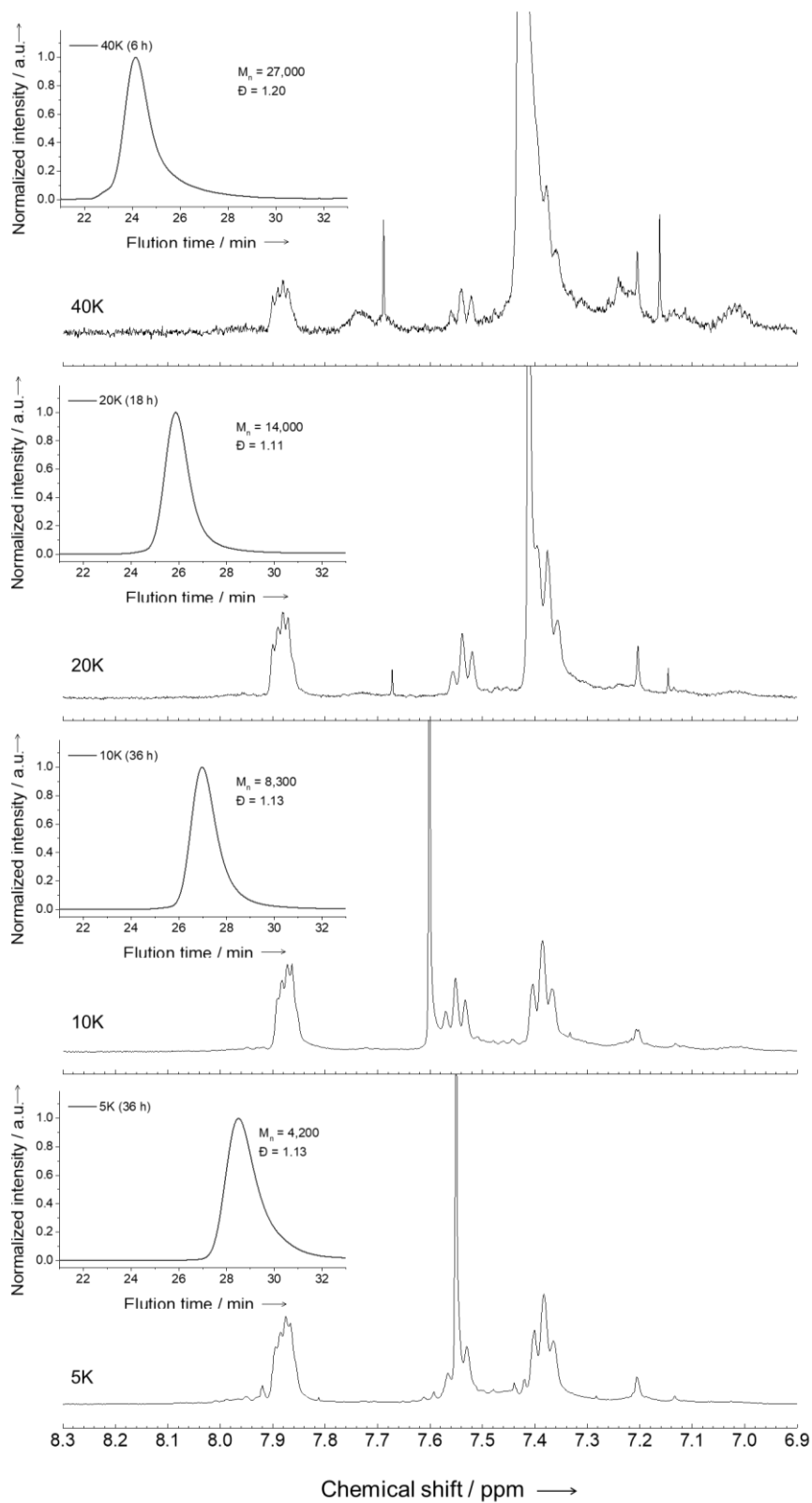


**Figure S26.**  $^1\text{H}$ -NMR spectra and GPC curves of the molecular weight controlled PMMA in the presence of argon using CPADB and 4DP-IPN of 5 ppm.

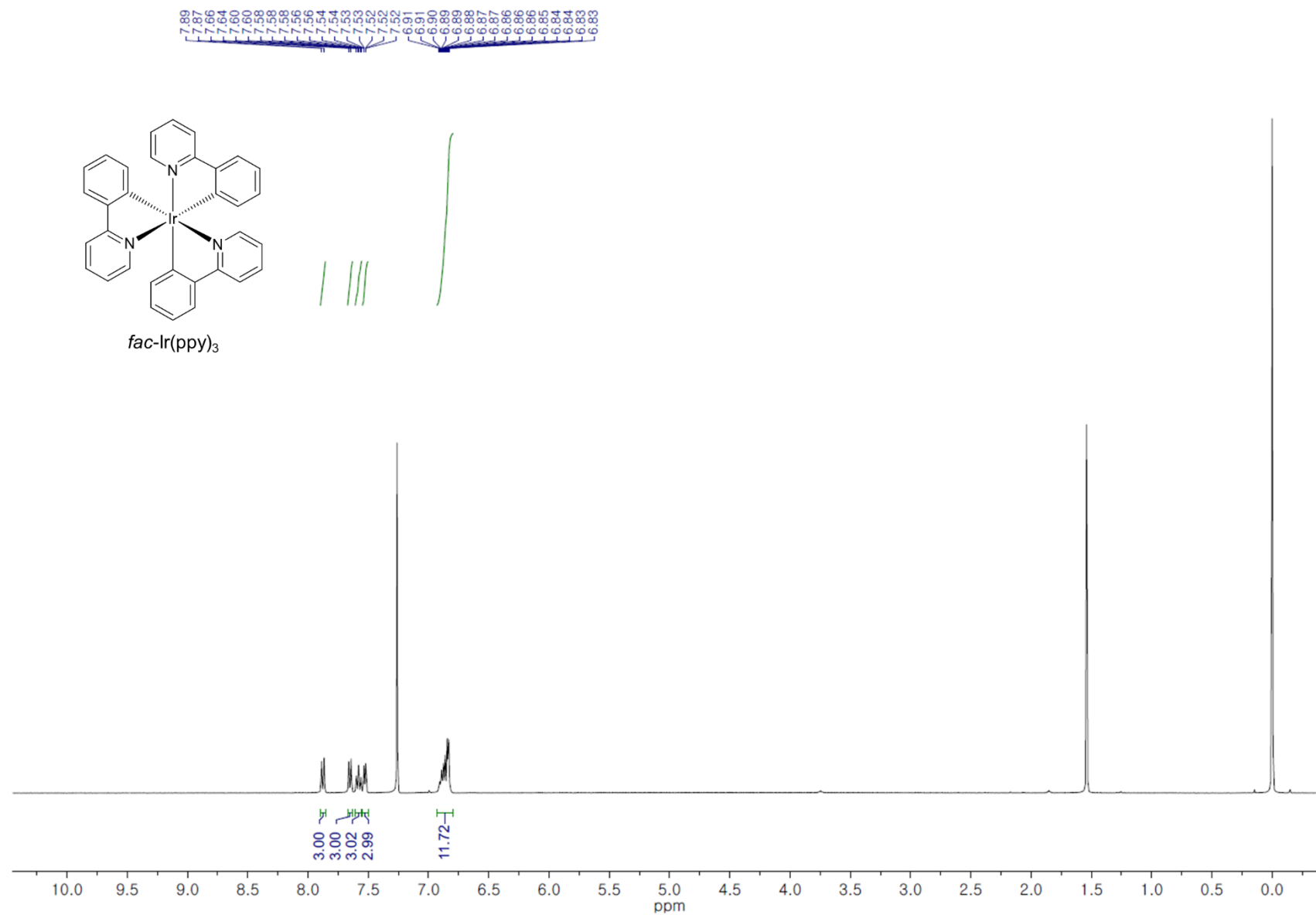


**Figure S27.** <sup>1</sup>H NMR of Ir(ppy)<sub>3</sub> in CDCl<sub>3</sub> at r.t..

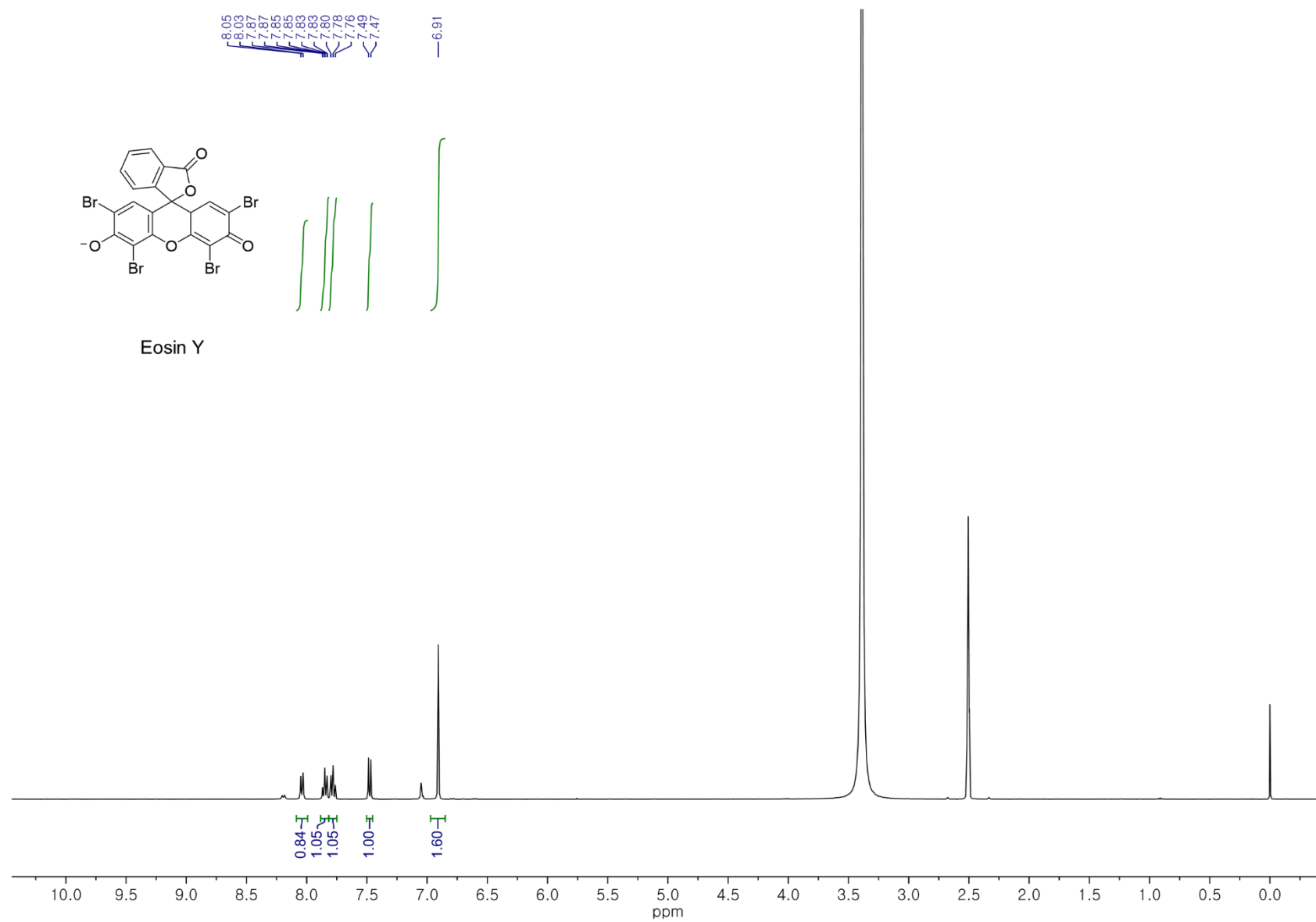


**Figure S28.**  $^1\text{H}$  NMR of eosin Y in  $\text{CDCl}_3$  at r.t..

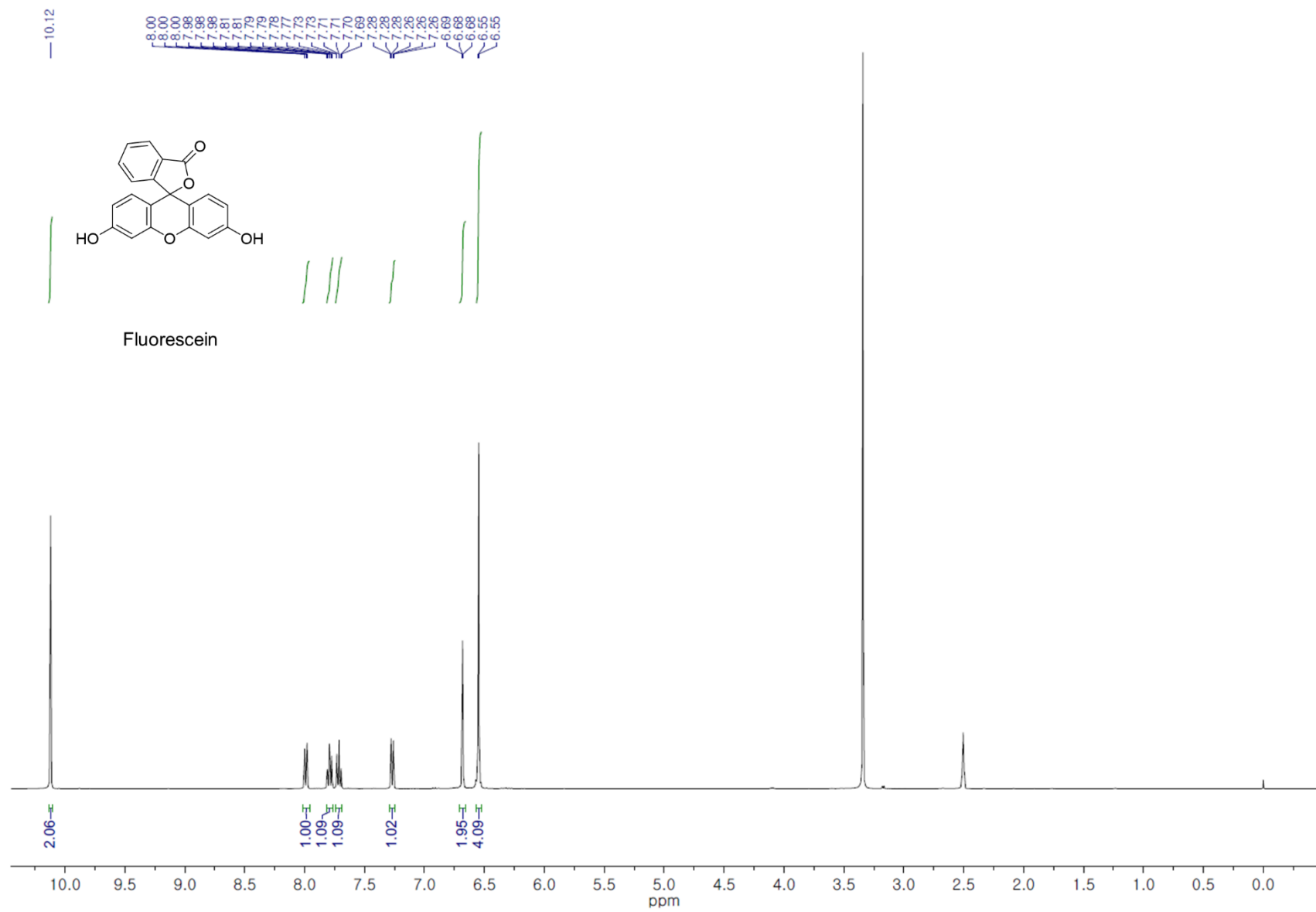


**Figure S29.** <sup>1</sup>H NMR of fluorescein in CDCl<sub>3</sub> at r.t..

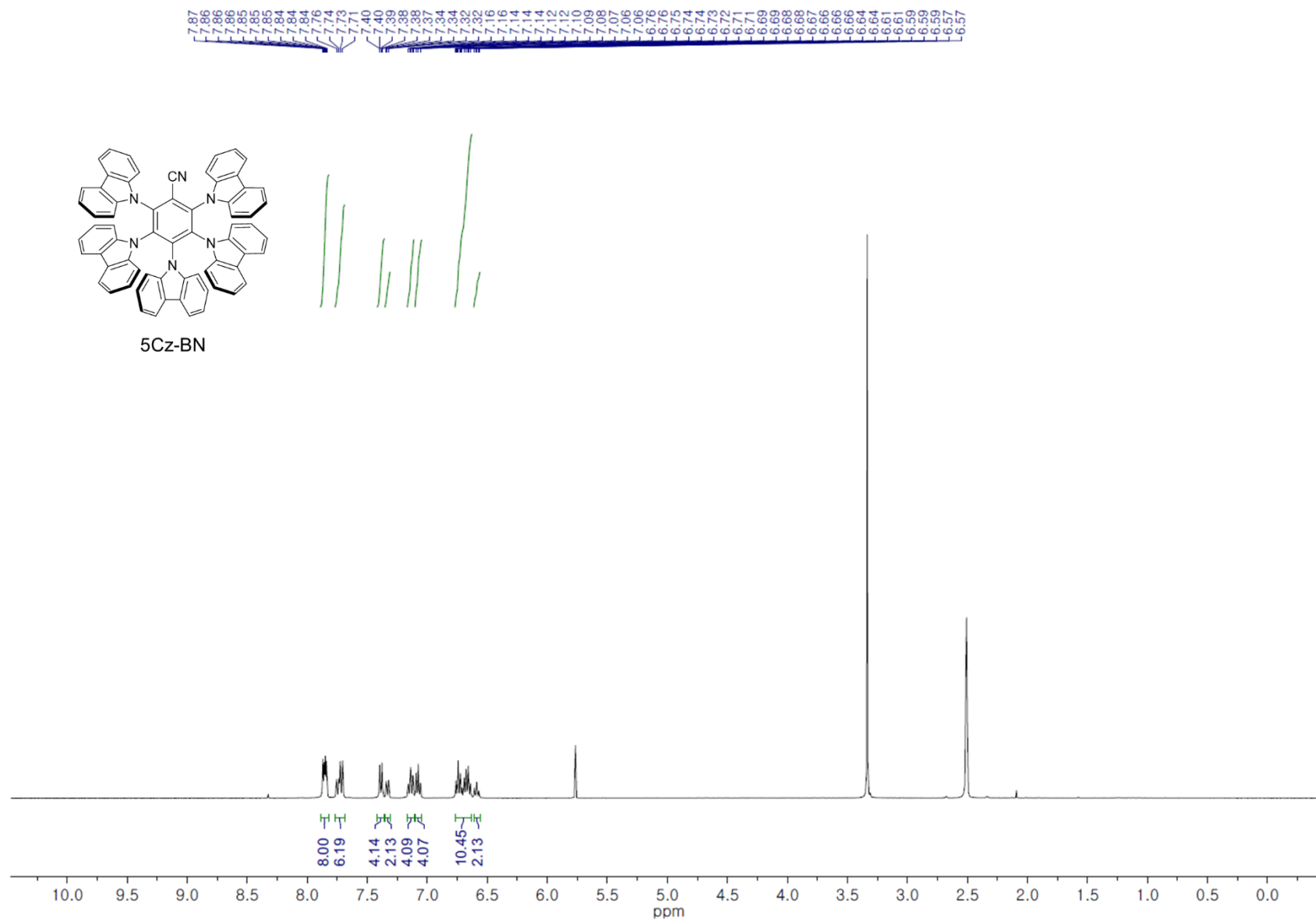


**Figure S30.**  $^1\text{H}$  NMR of 5Cz-BN in  $\text{CDCl}_3$  at r.t..

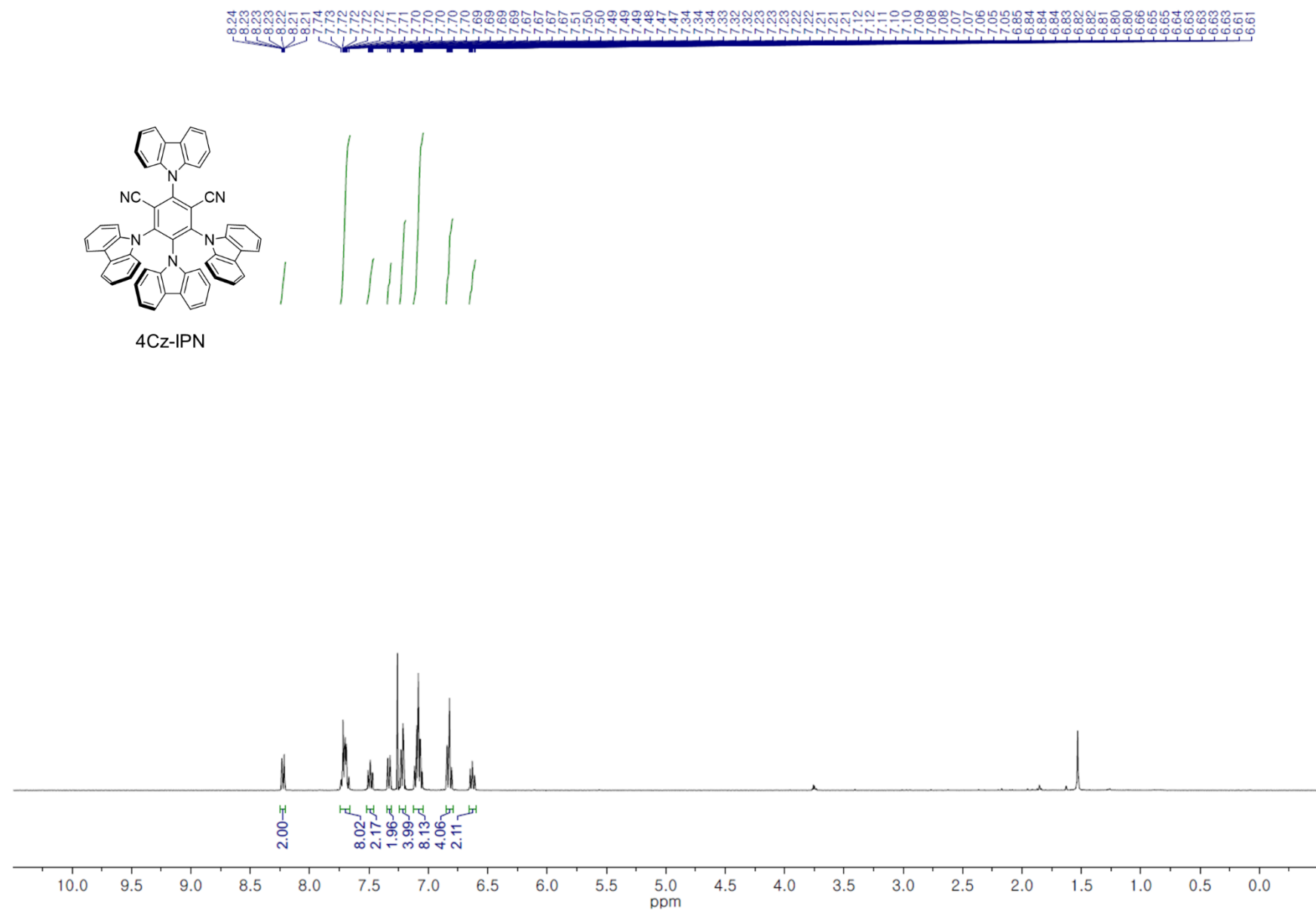


**Figure S31.**  $^1\text{H}$  NMR of 4Cz-IPN in  $\text{CDCl}_3$  at r.t..



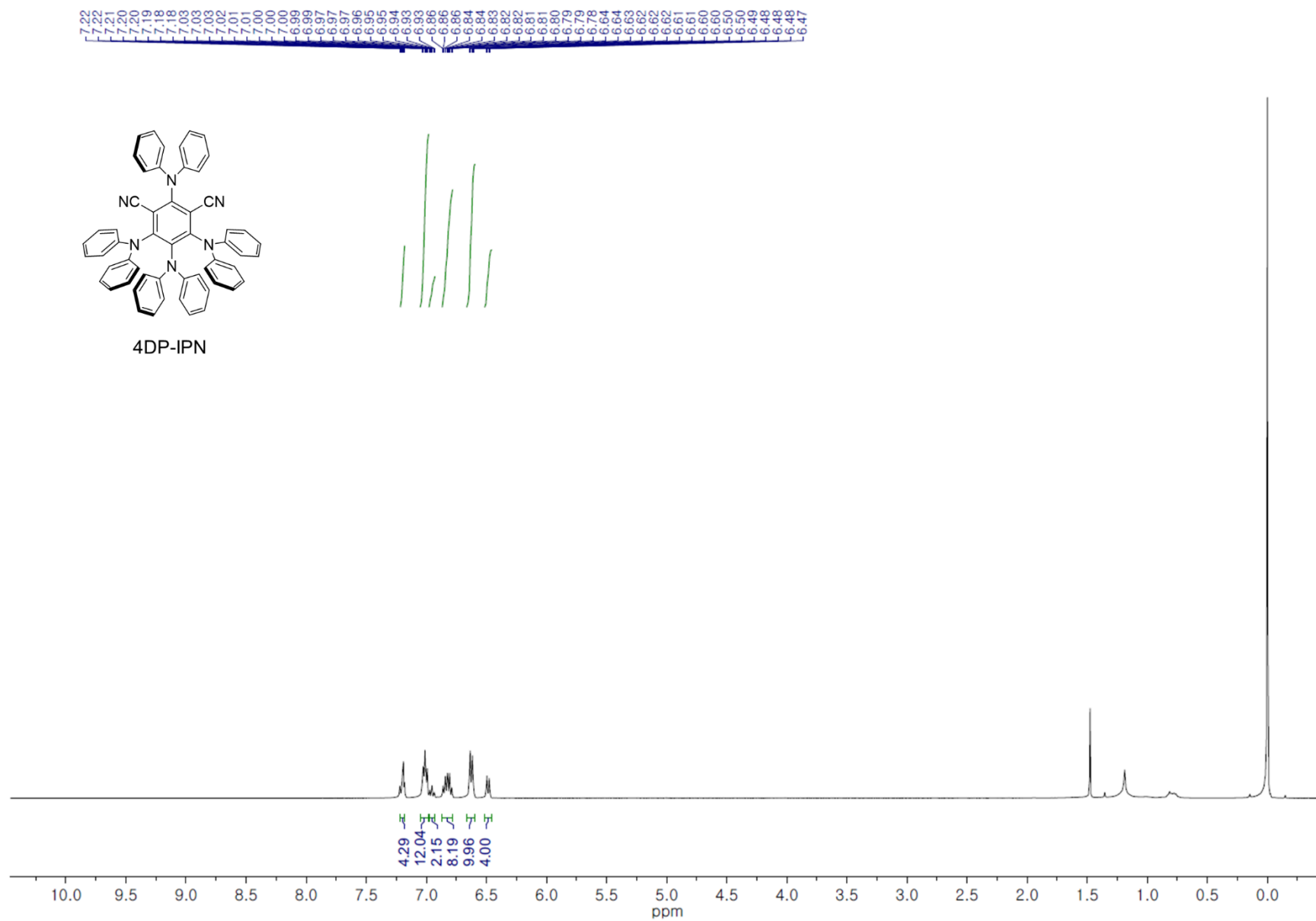


**Figure S32.** <sup>1</sup>H NMR of 4DP-IPN in CDCl<sub>3</sub> at r.t..

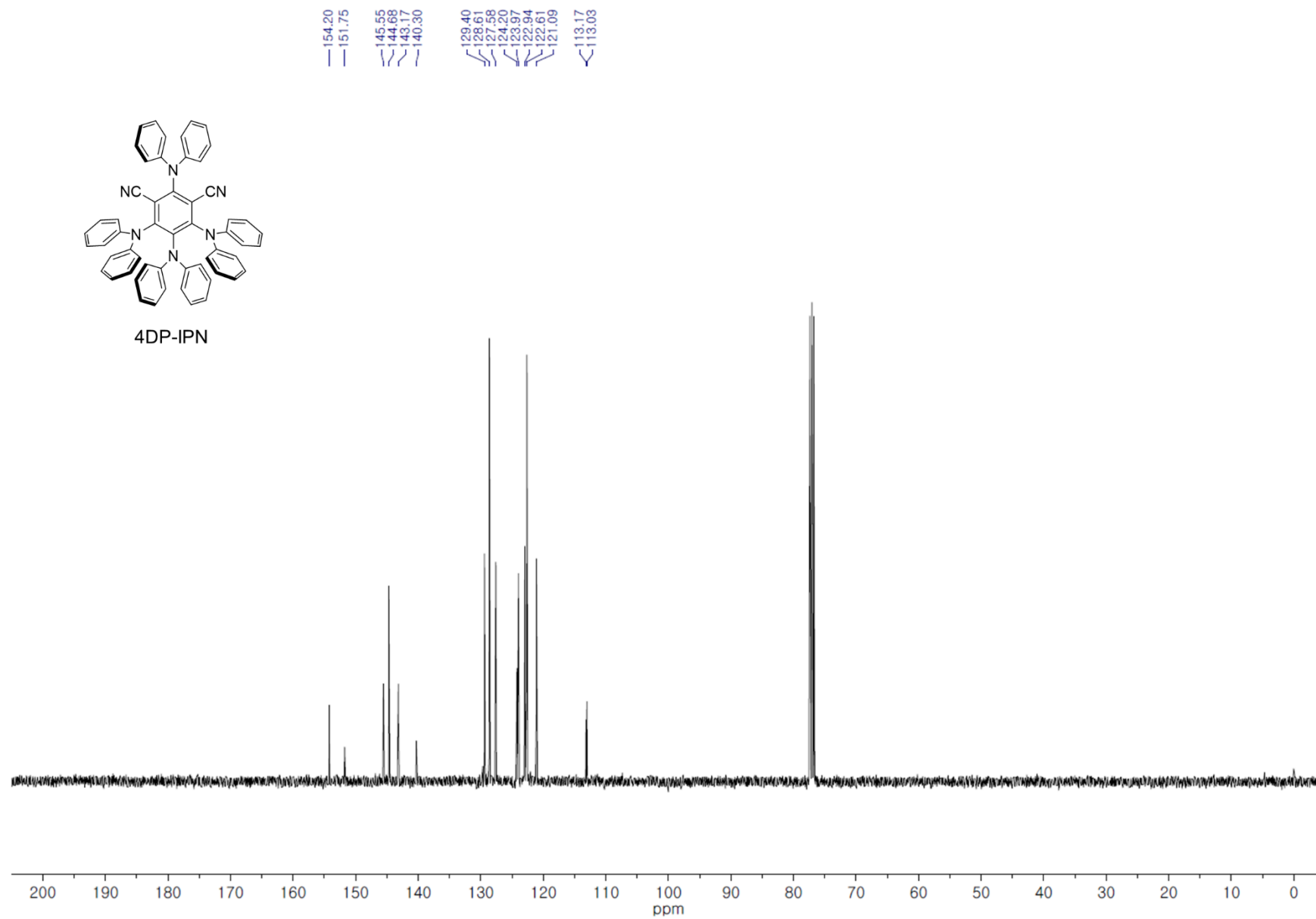


**Figure S33.**  $^{13}\text{C}$  NMR of 4DP-IPN in CDCl<sub>3</sub> at r.t..

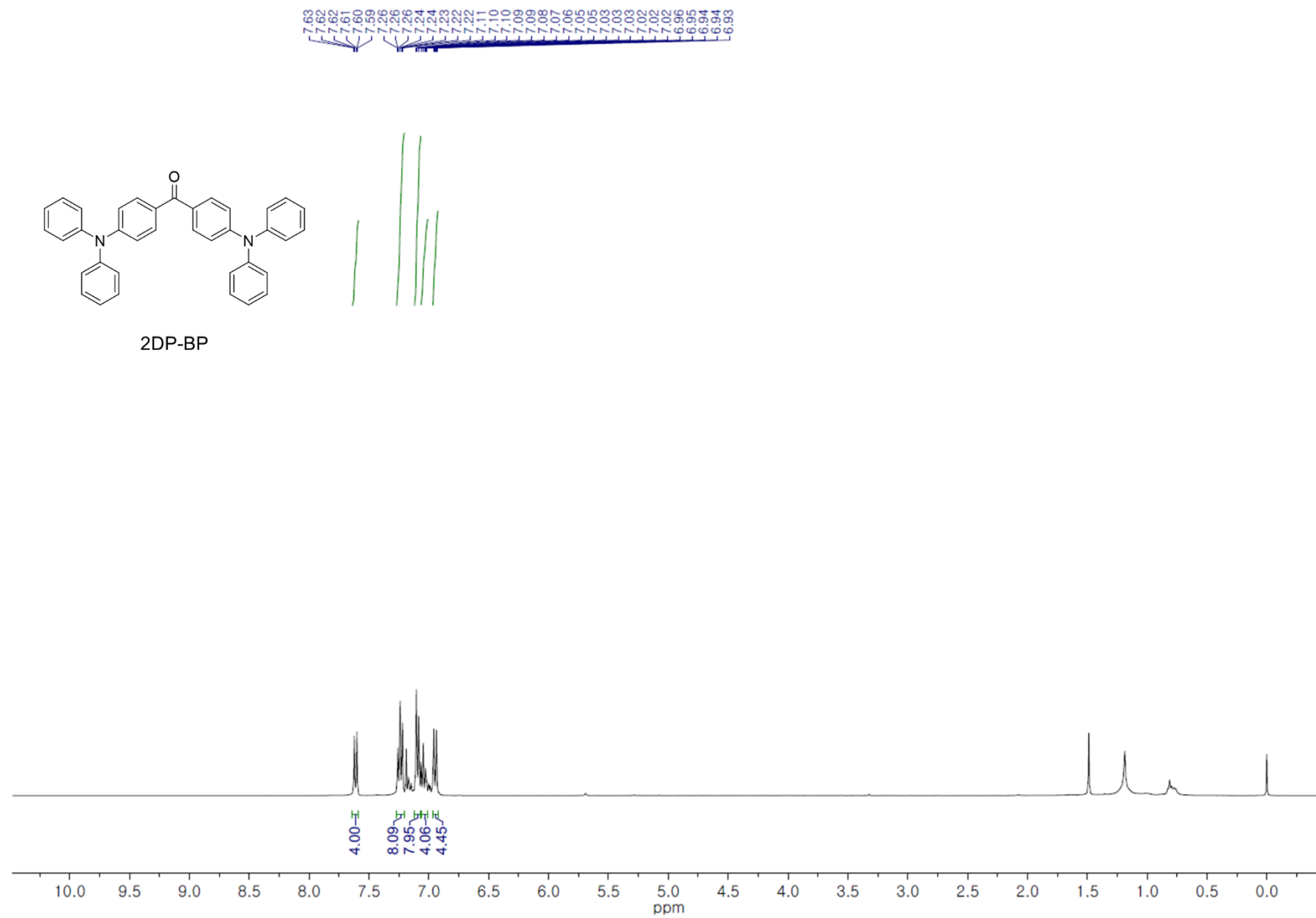


**Figure S34.**  $^1\text{H}$  NMR of 2DP-BP in  $\text{CDCl}_3$  at r.t..

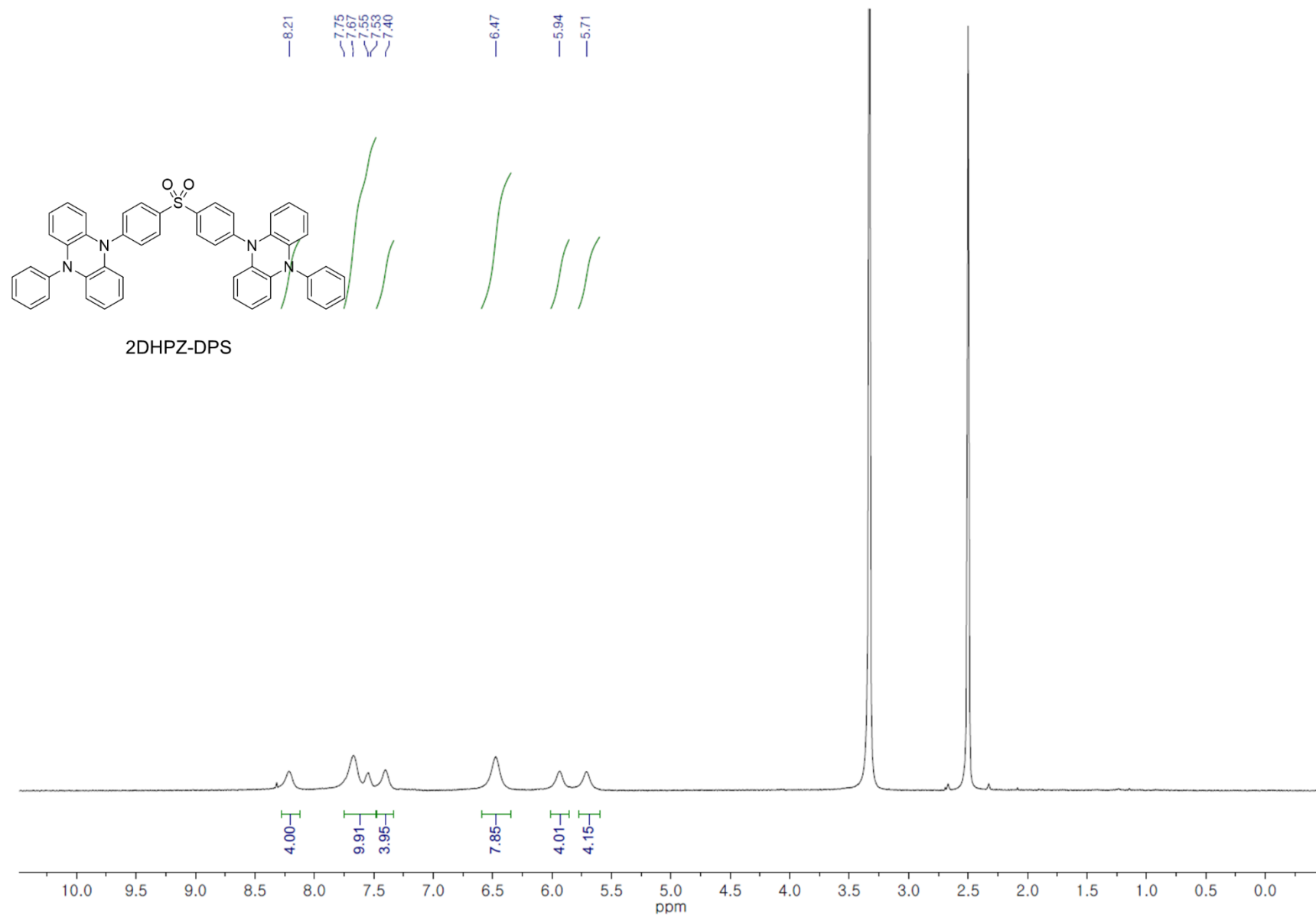


**Figure S35.**  $^1\text{H}$  NMR of 2DHPZ-DPS in CDCl<sub>3</sub> at r.t..

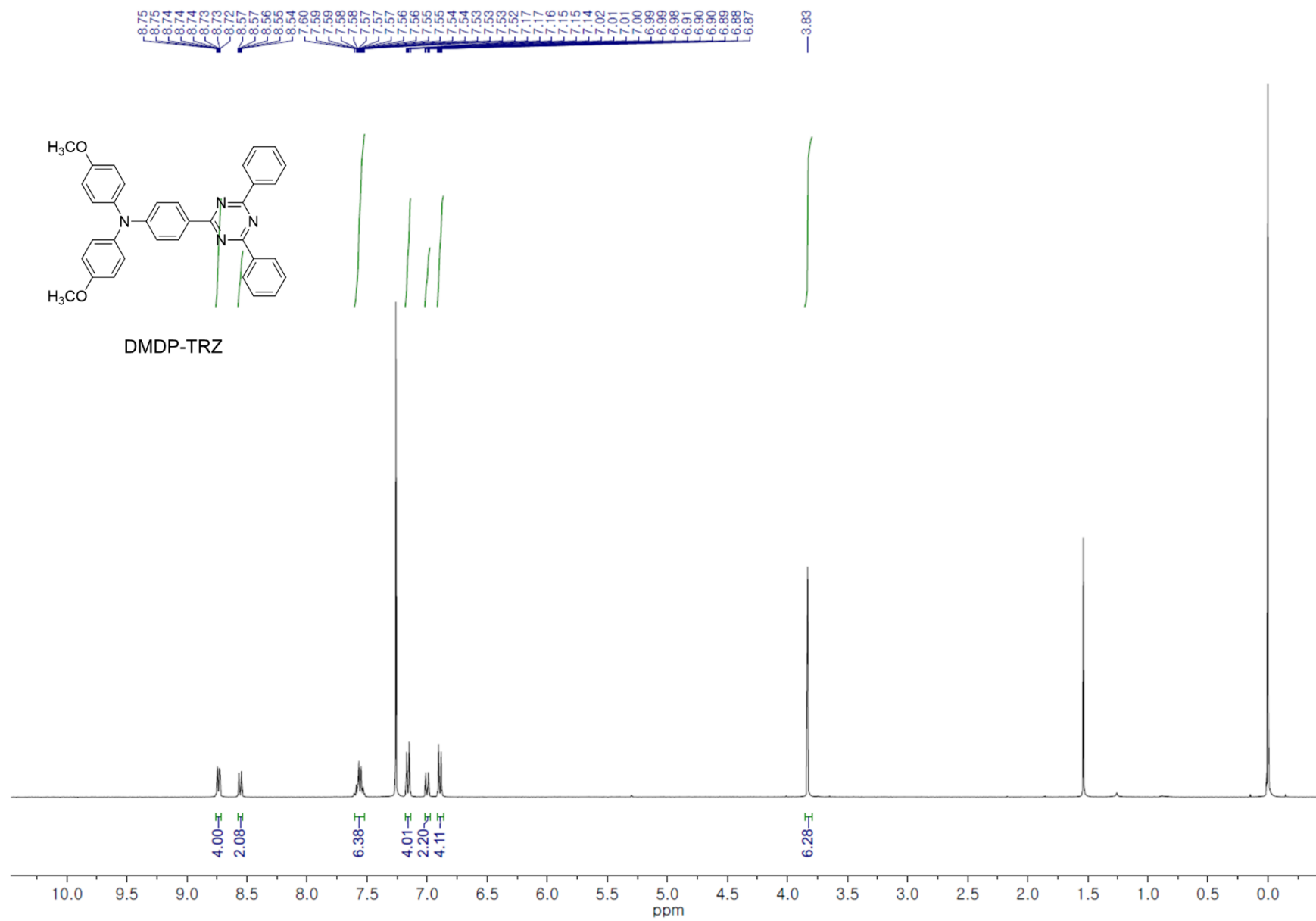


**Figure S36.** <sup>1</sup>H NMR of DMDP-TRZ in CDCl<sub>3</sub> at r.t..

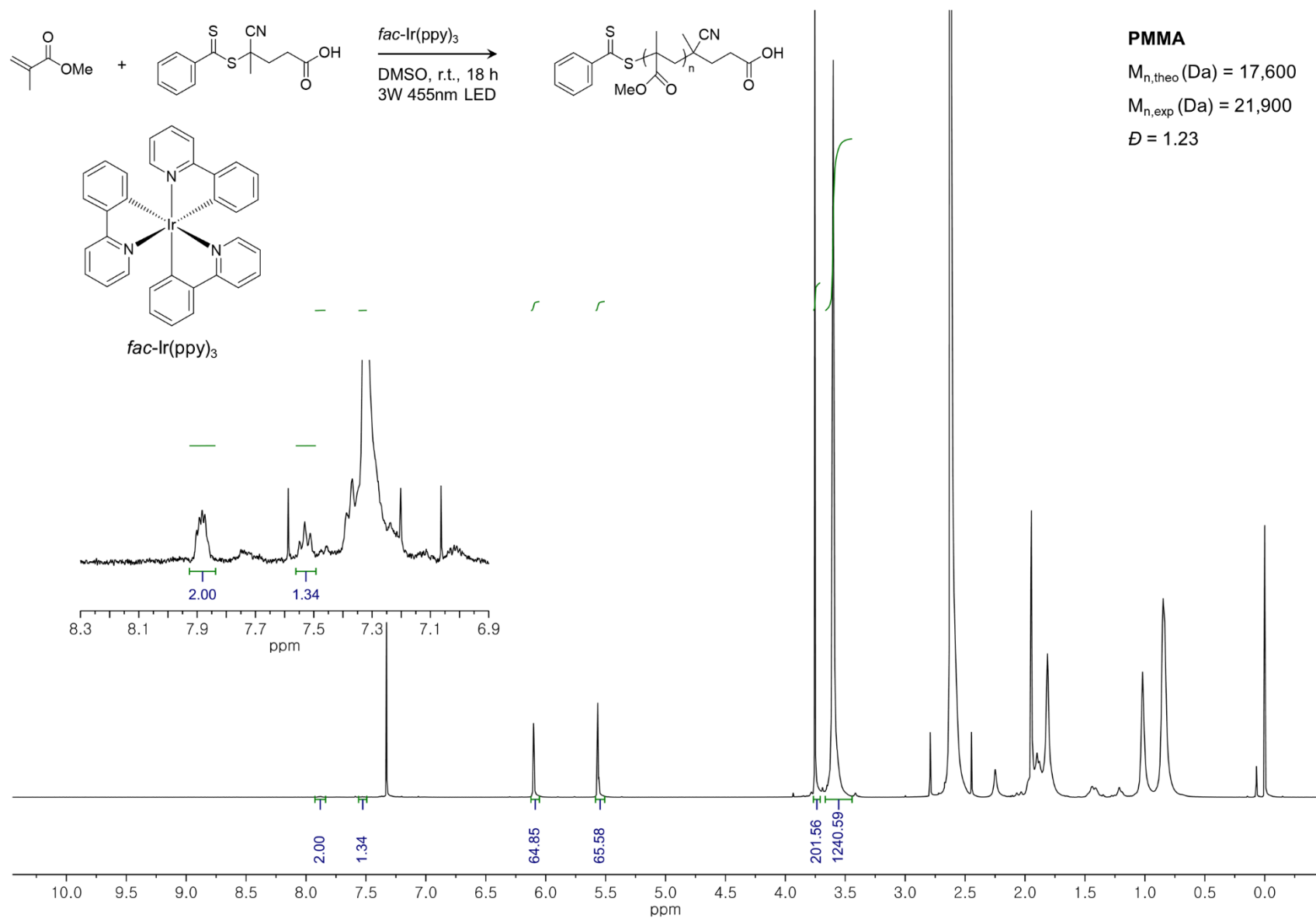


**Figure S37.** In-situ <sup>1</sup>H NMR of PMMA in the presence of CPADB, MMA, and Ir(ppy)<sub>3</sub> of 1 ppm under argon in CDCl<sub>3</sub> at r.t. (For Figure 2a. entry 1).

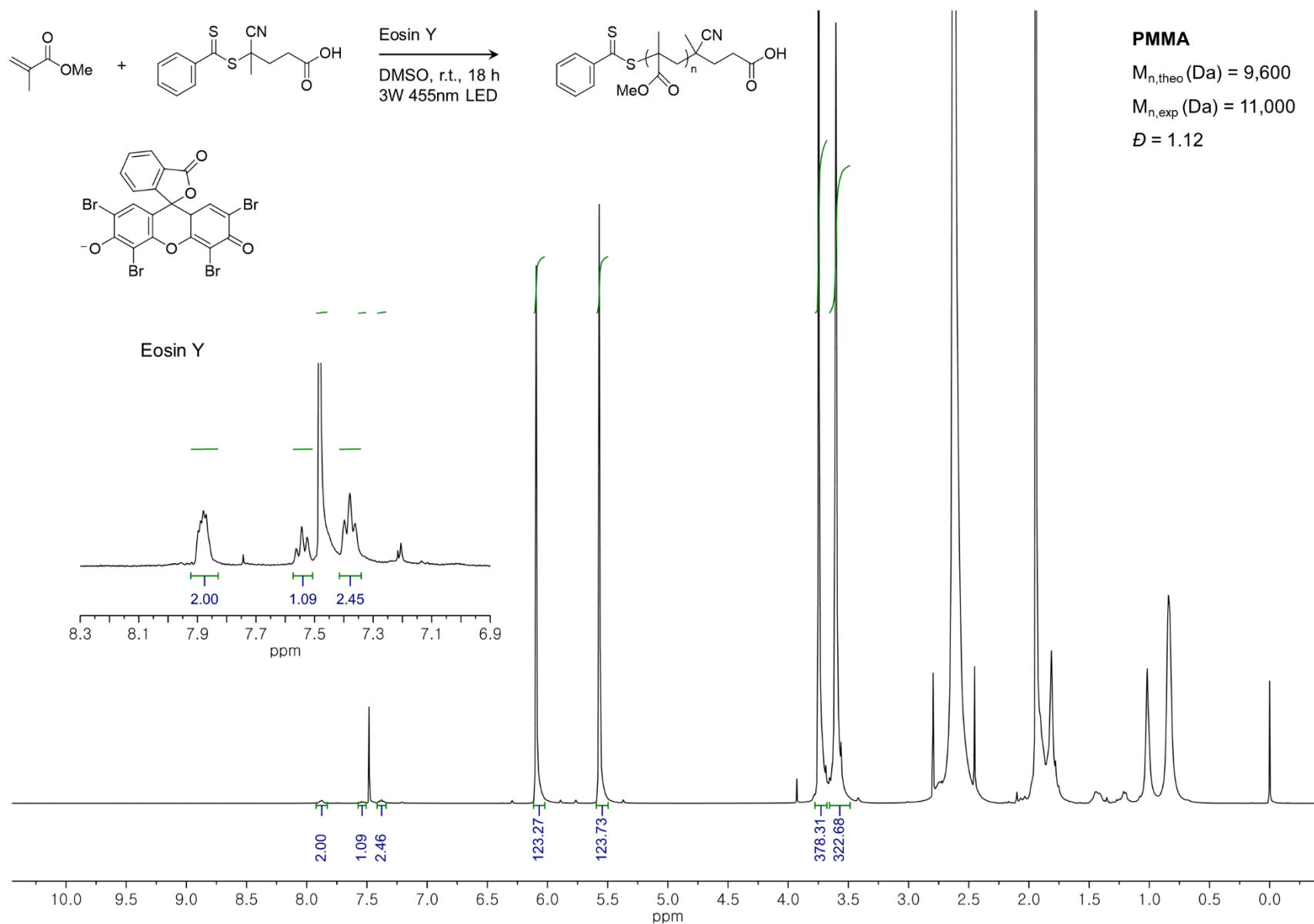


**Figure S38.** In-situ  $^1\text{H}$  NMR of PMMA in the presence of CPADB, MMA, and eosin Y of 5 ppm under argon in CDCl<sub>3</sub> at r.t. (For Figure 2a. entry 3).

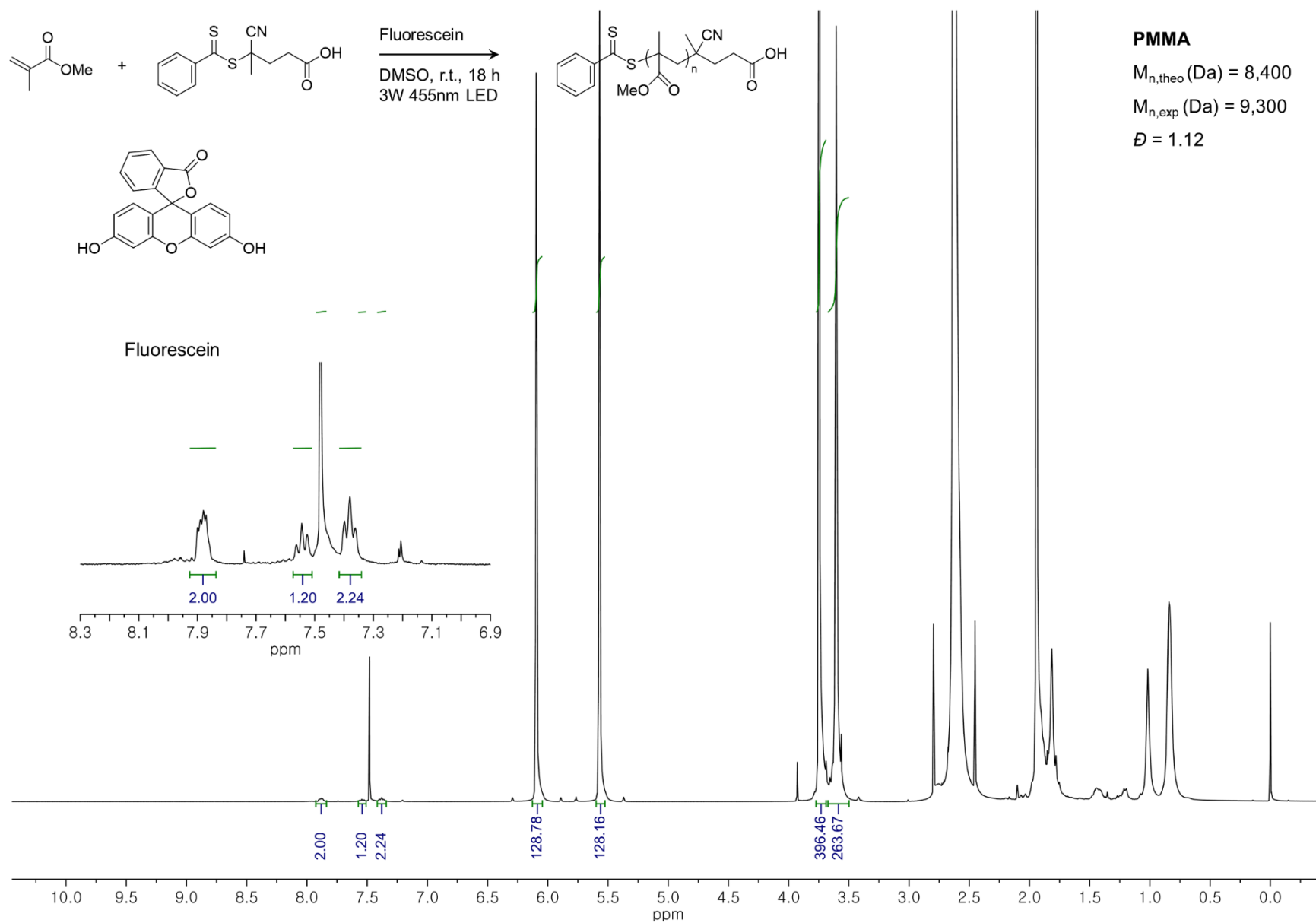


**Figure S39.** In-situ  $^1\text{H}$  NMR of PMMA in the presence of CPADB, MMA, and fluorescein of 5 ppm under argon in  $\text{CDCl}_3$  at r.t. (For Figure 2a. entry 5).



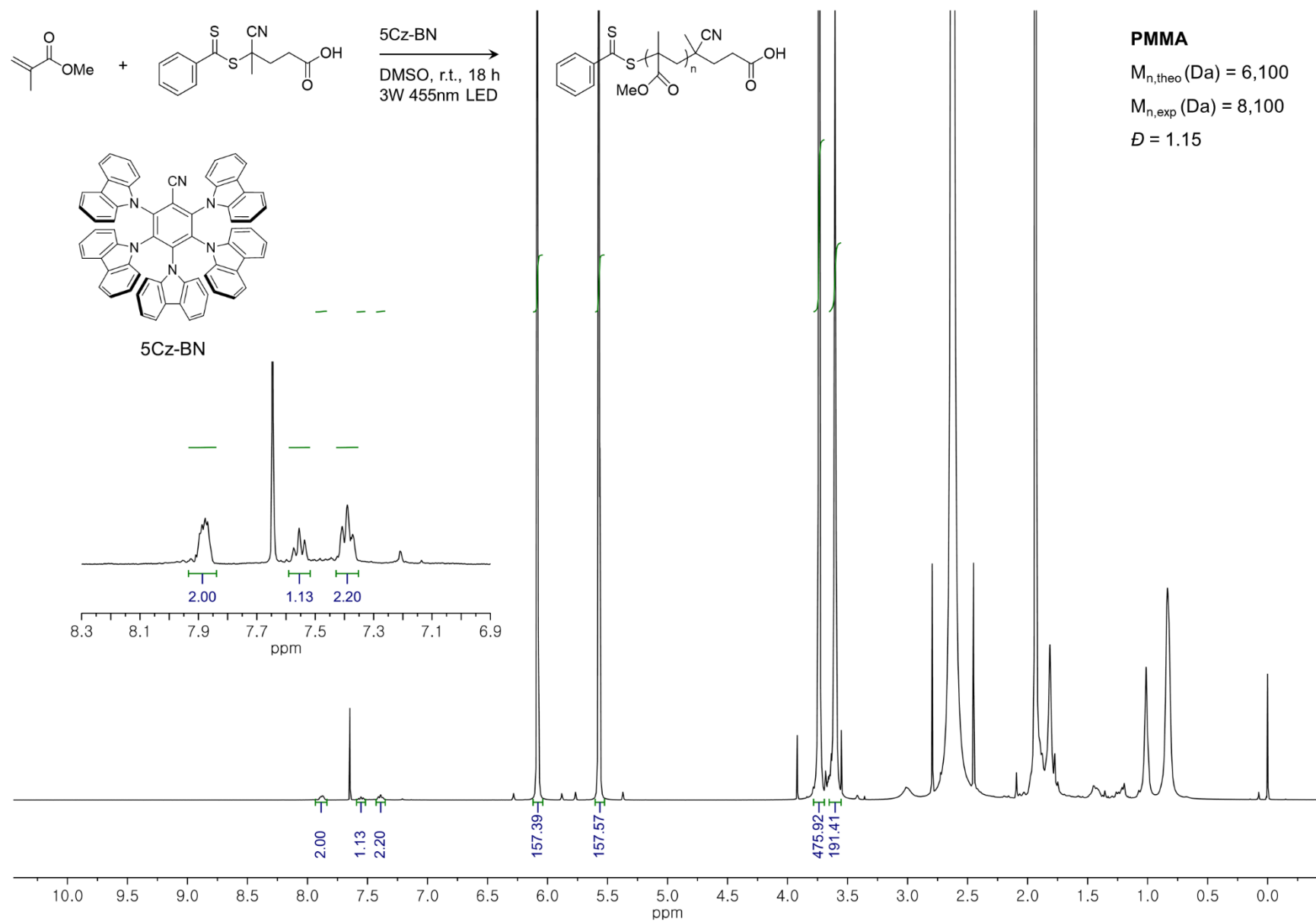


**Figure S40.** In-situ <sup>1</sup>H NMR of PMMA in the presence of CPADB, MMA, and 5Cz-BN of 5 ppm under argon in CDCl<sub>3</sub> at r.t. (For Figure 2a. entry 7).

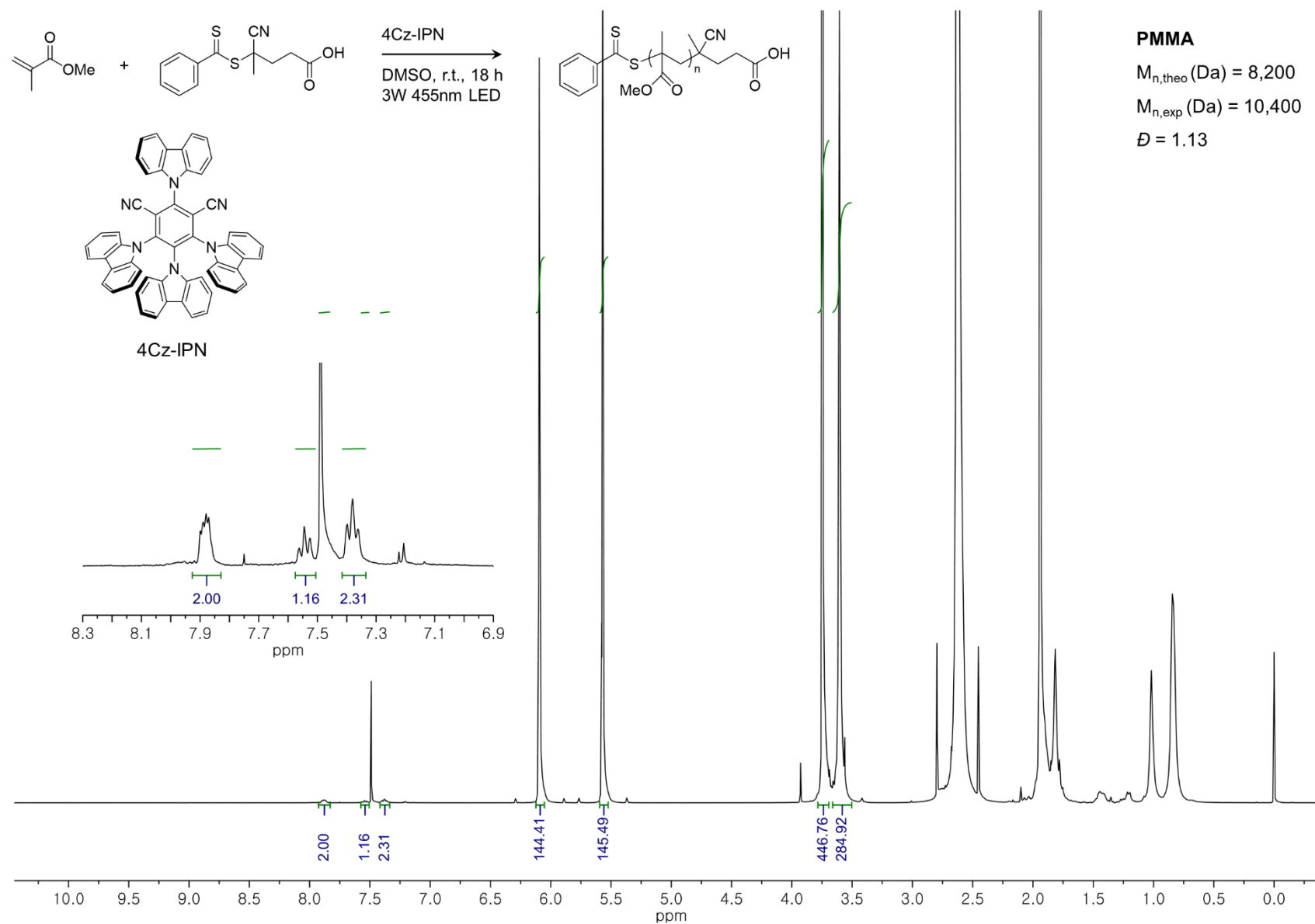


**Figure S41.** In-situ <sup>1</sup>H NMR of PMMA in the presence of CPADB, MMA, and 4Cz-IPN of 5 ppm under argon in CDCl<sub>3</sub> at r.t. (For Figure 2a. entry 9).

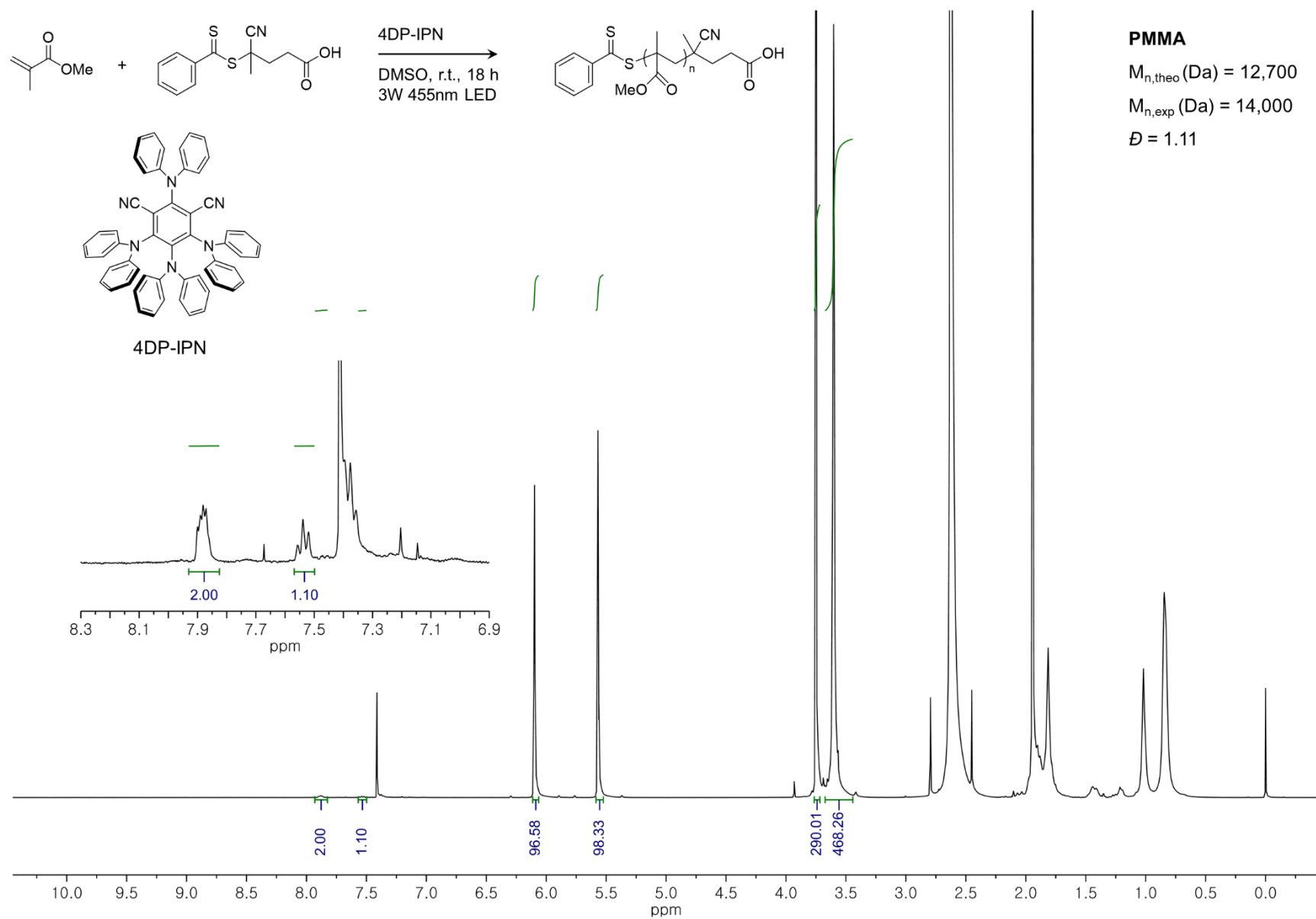


**Figure S42.** In-situ  $^1\text{H}$  NMR of PMMA in the presence of CPADB, MMA, and 4DP-IPN of 5 ppm under argon in CDCl<sub>3</sub> at r.t. (For Figure 2a. entry 11).

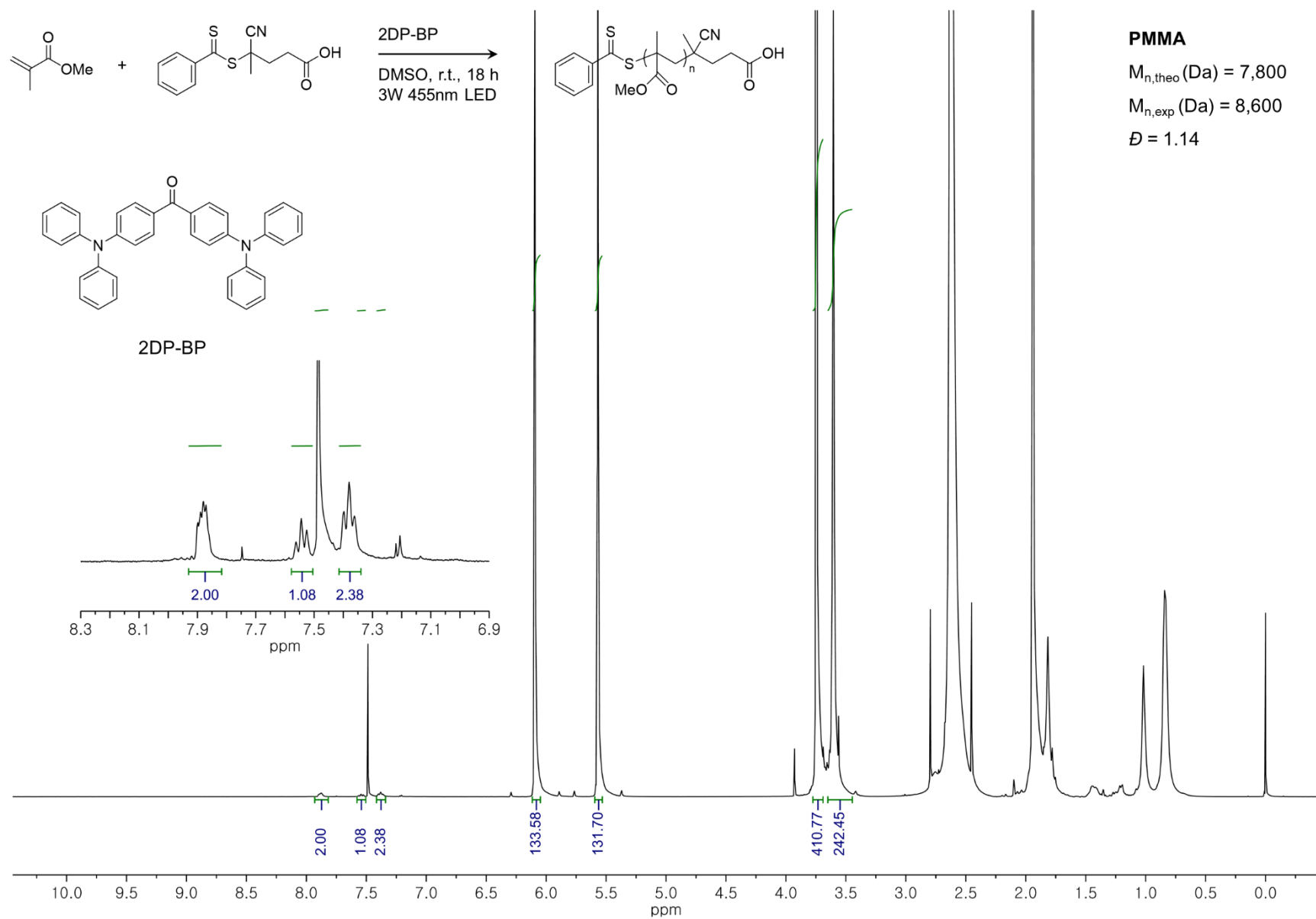


**Figure S43.** In-situ  $^1\text{H}$  NMR of PMMA in the presence of CPADB, MMA, and 2DP-BP of 5 ppm under argon in  $\text{CDCl}_3$  at r.t. (For Figure 2a. entry 13).

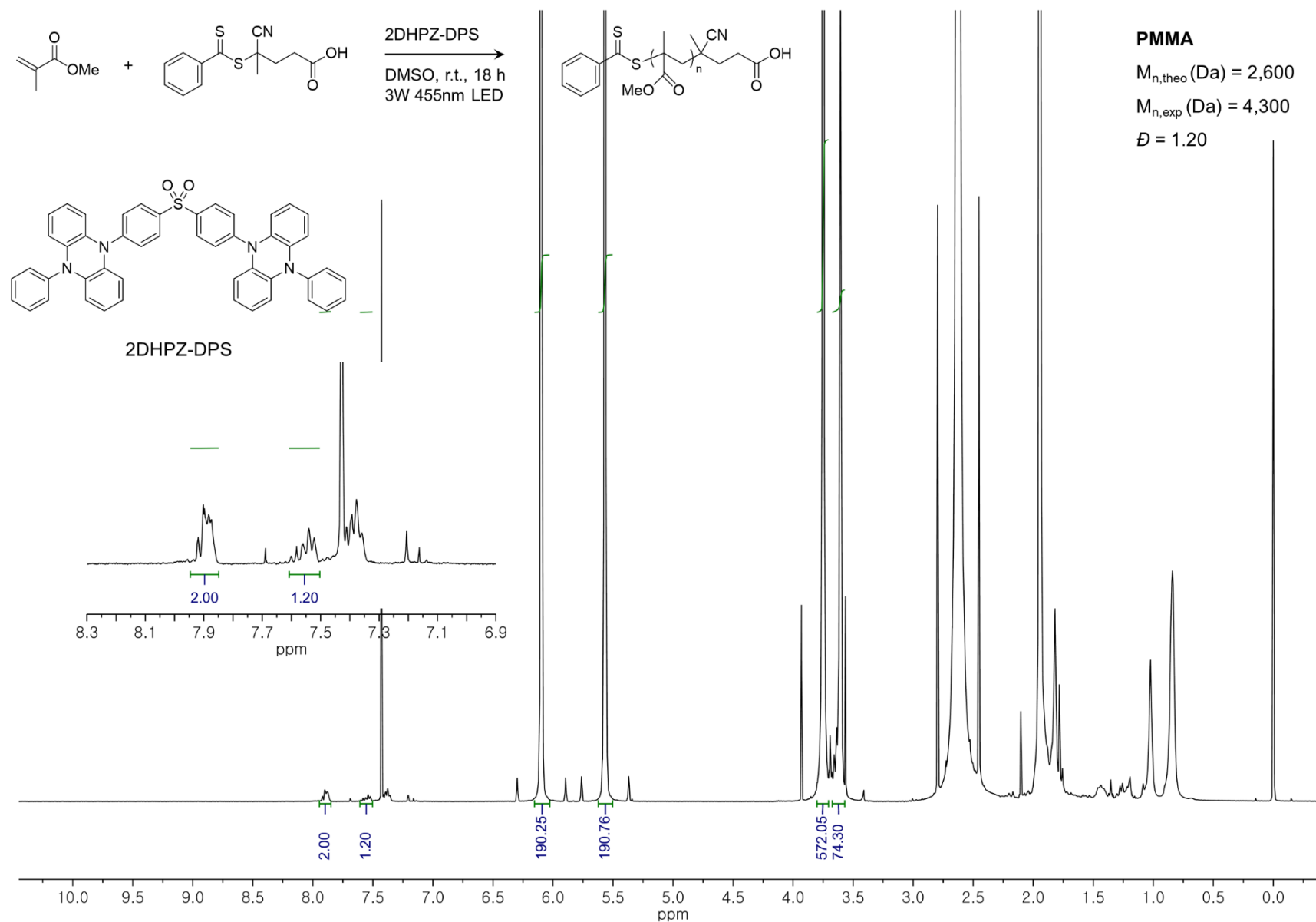


**Figure S44.** In-situ  $^1\text{H}$  NMR of PMMA in the presence of CPADB, MMA, and 2DHPZ-DPS of 5 ppm under argon in  $\text{CDCl}_3$  at r.t. (For Figure 2a. entry 15).

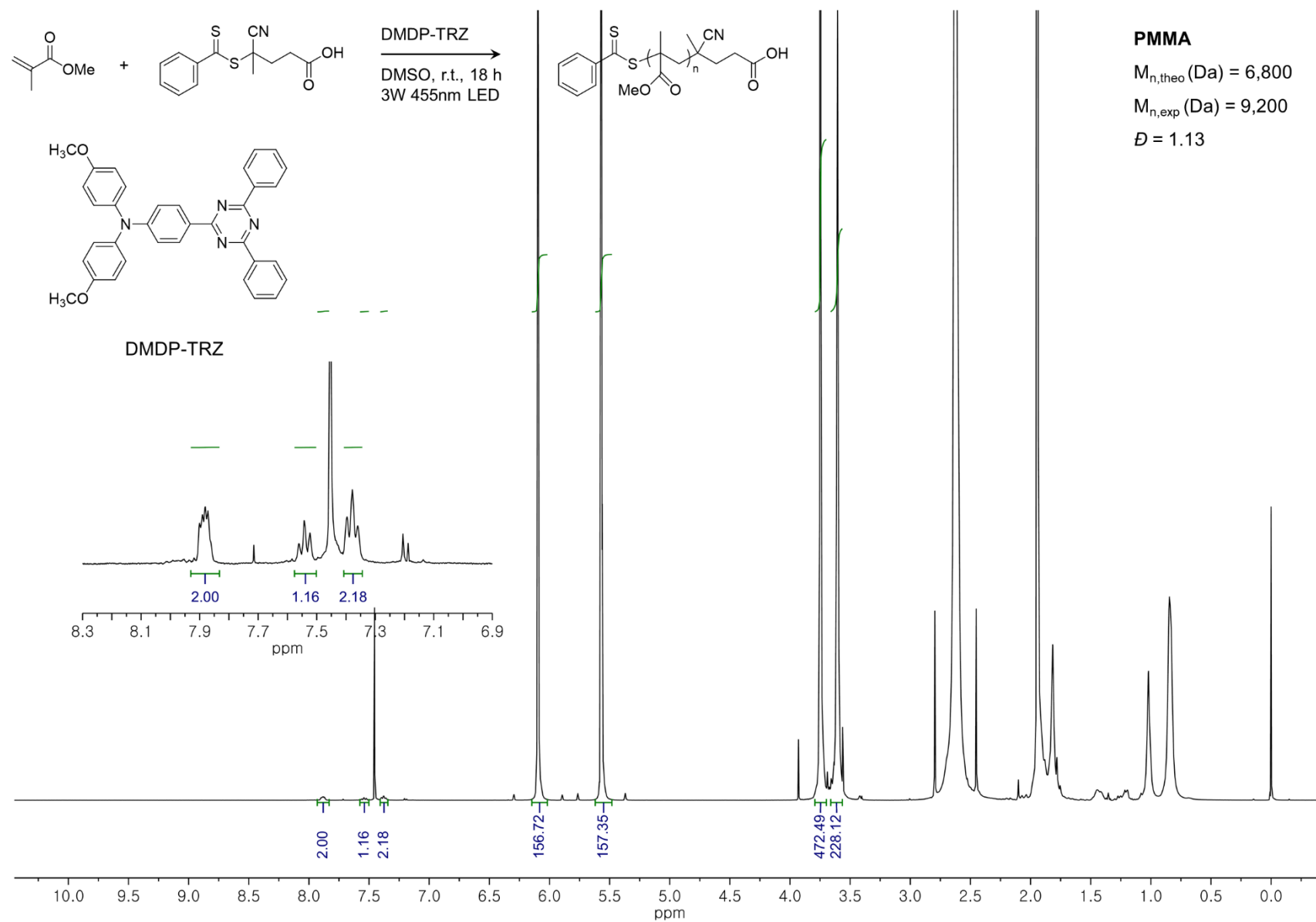


**Figure S45.** In-situ <sup>1</sup>H NMR of PMMA in the presence of CPADB, MMA, and DMDP-TRZ of 5 ppm under argon in CDCl<sub>3</sub> at r.t. (For Figure 2a. entry 17).



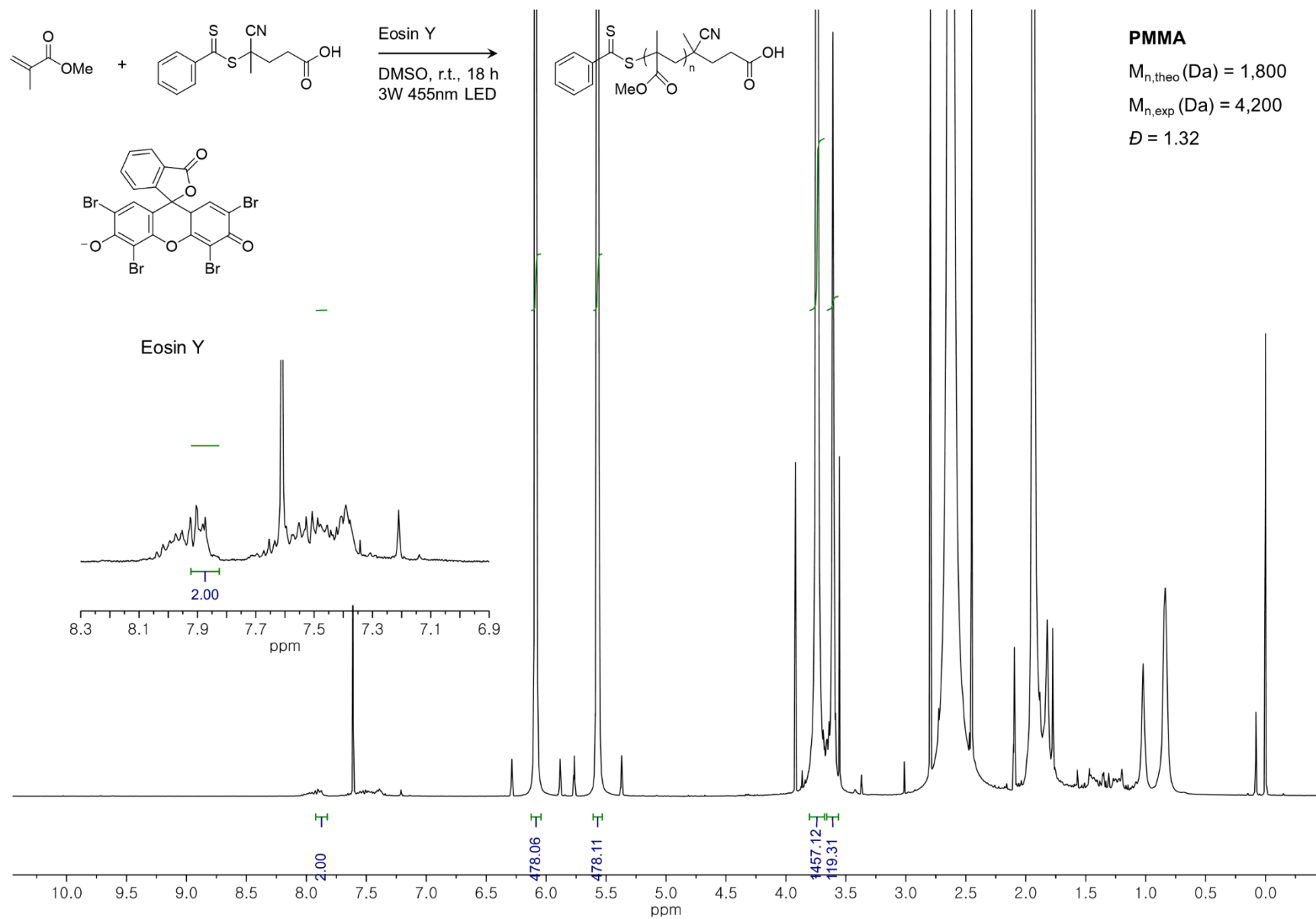


**Figure S47.** In-situ  $^1\text{H}$  NMR of PMMA in the presence of CPADB, MMA, and eosin Y of 5 ppm under air in  $\text{CDCl}_3$  at r.t. (For Figure 2a. entry 4).



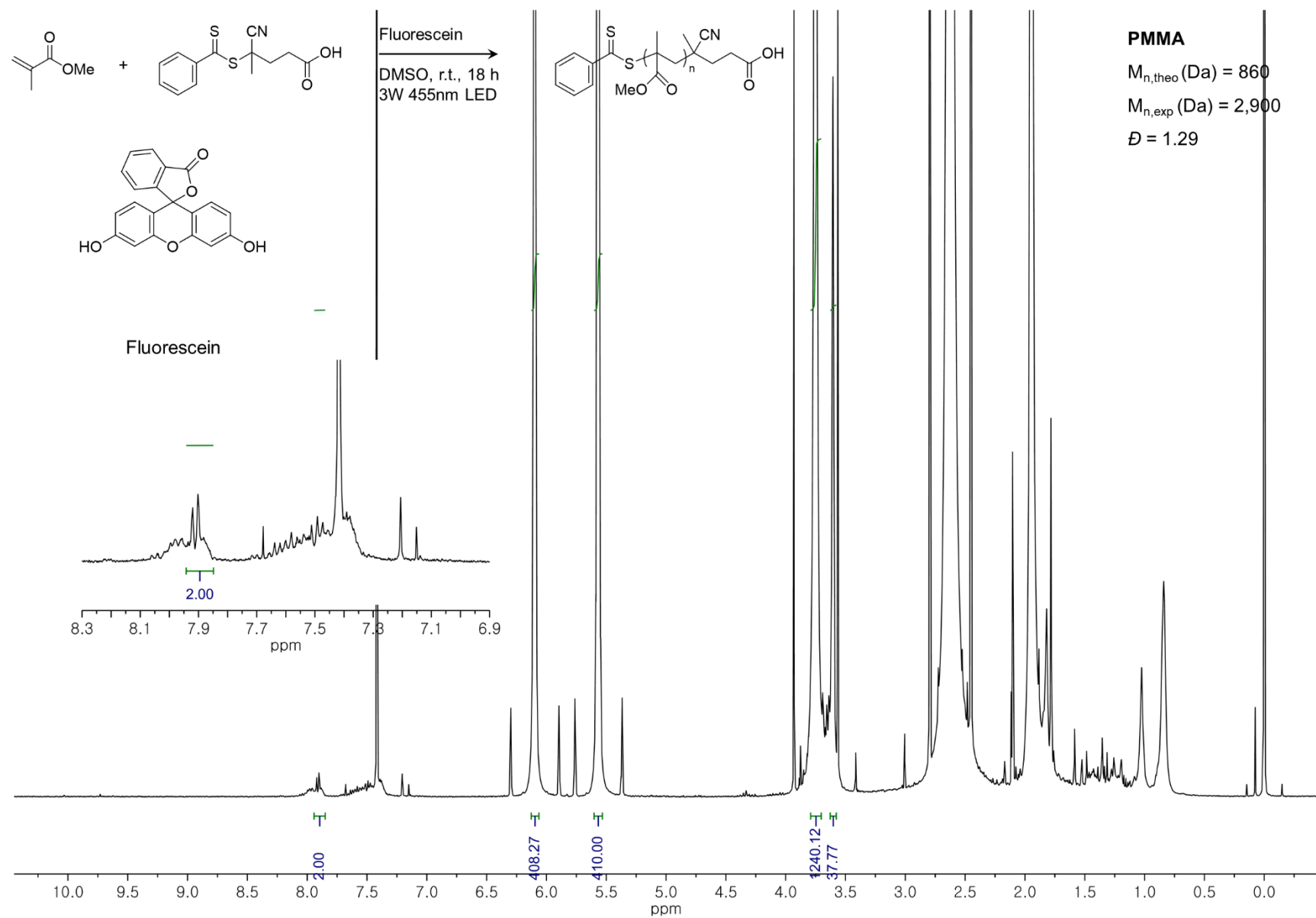


**Figure S48.** In-situ  $^1\text{H}$  NMR of PMMA in the presence of CPADB, MMA, and fluorescein of 5 ppm under air in  $\text{CDCl}_3$  at r.t. (For Figure 2a. entry 6).

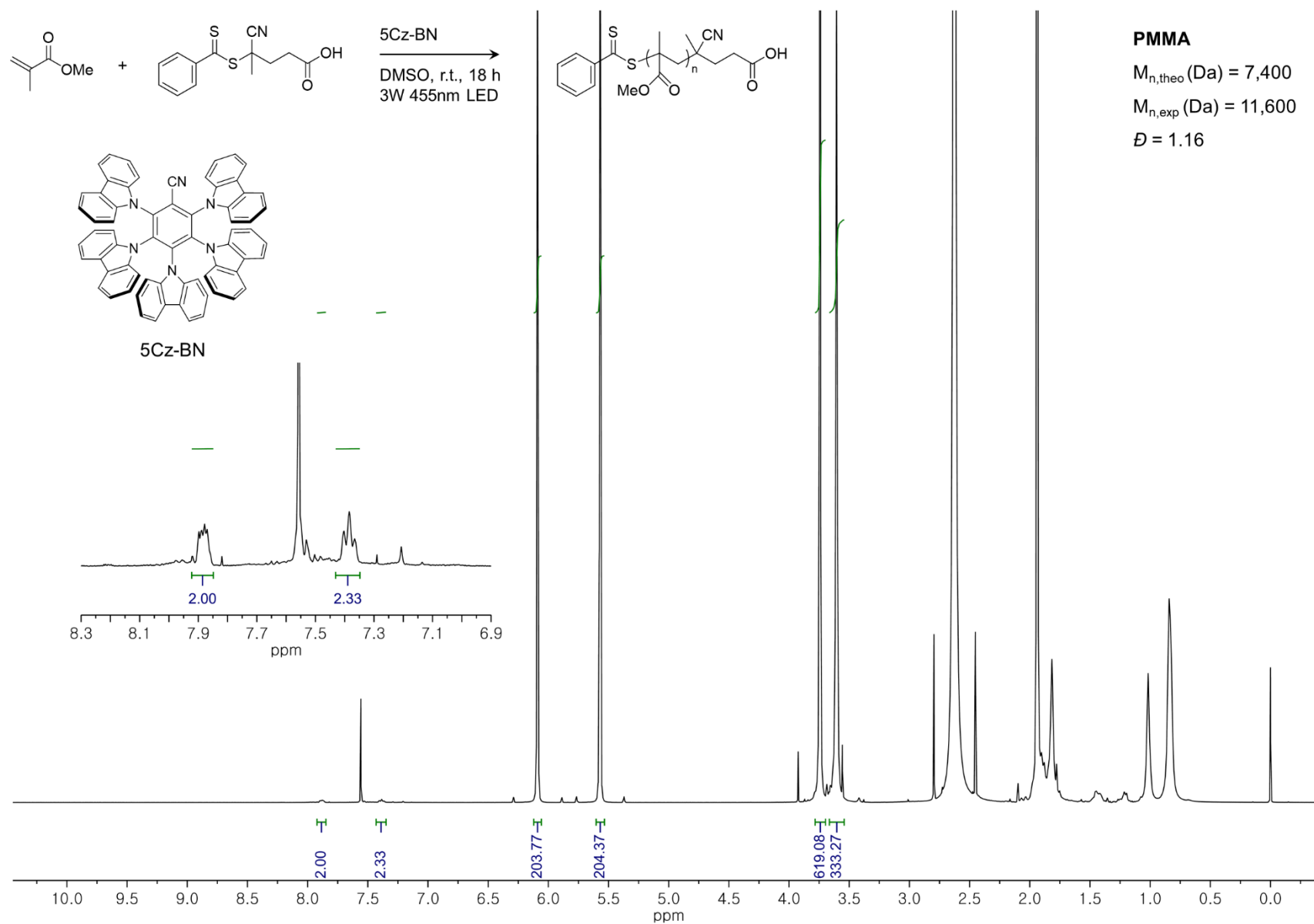


**Figure S49.** In-situ  $^1\text{H}$  NMR of PMMA in the presence of CPADB, MMA, and 5Cz-BN of 5 ppm under air in  $\text{CDCl}_3$  at r.t. (For Figure 2a. entry 8).

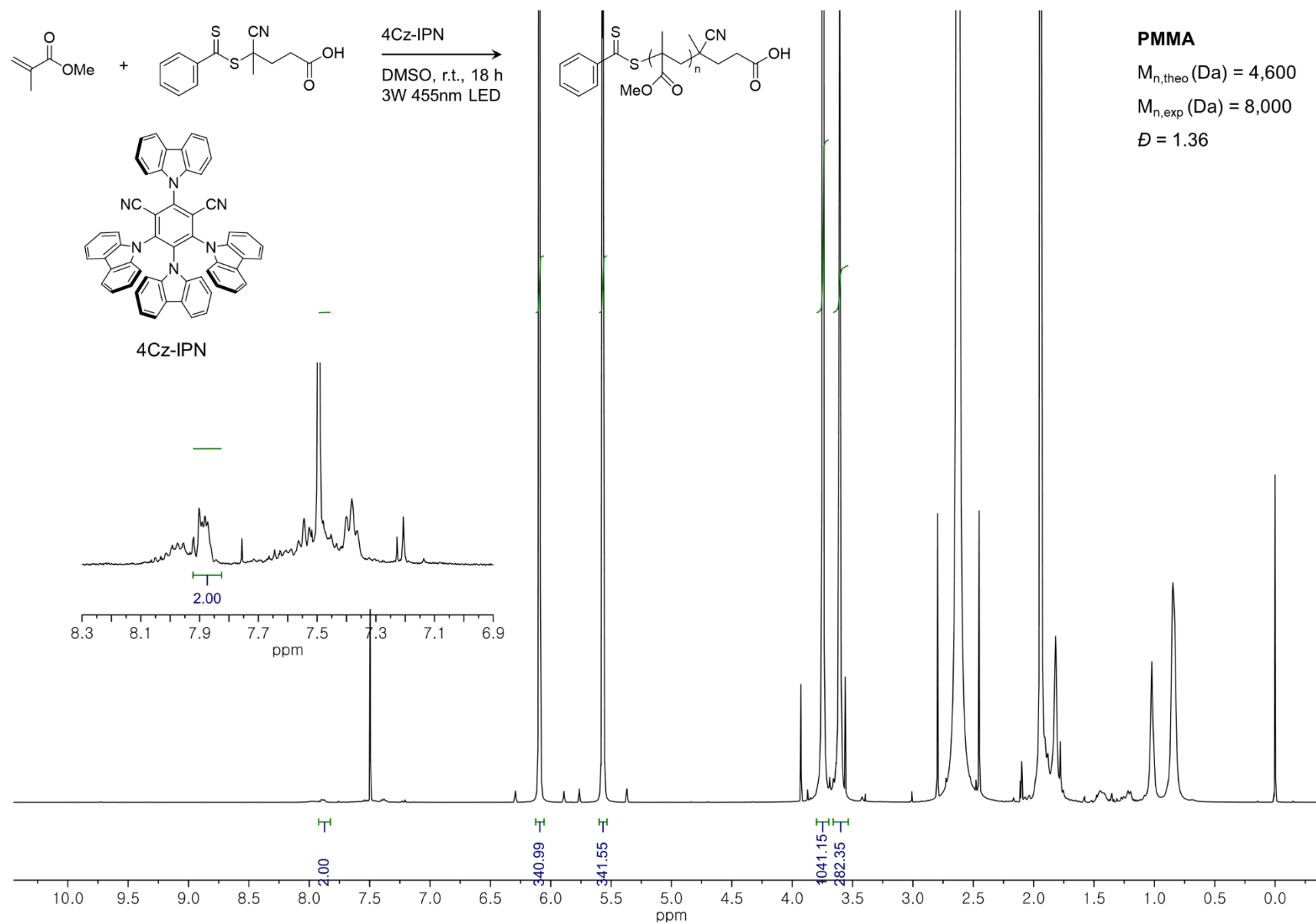


**Figure S50.** In-situ  $^1\text{H}$  NMR of PMMA in the presence of CPADB, MMA, and 4Cz-IPN of 5 ppm under air in  $\text{CDCl}_3$  at r.t. (For Figure 2a. entry 10).

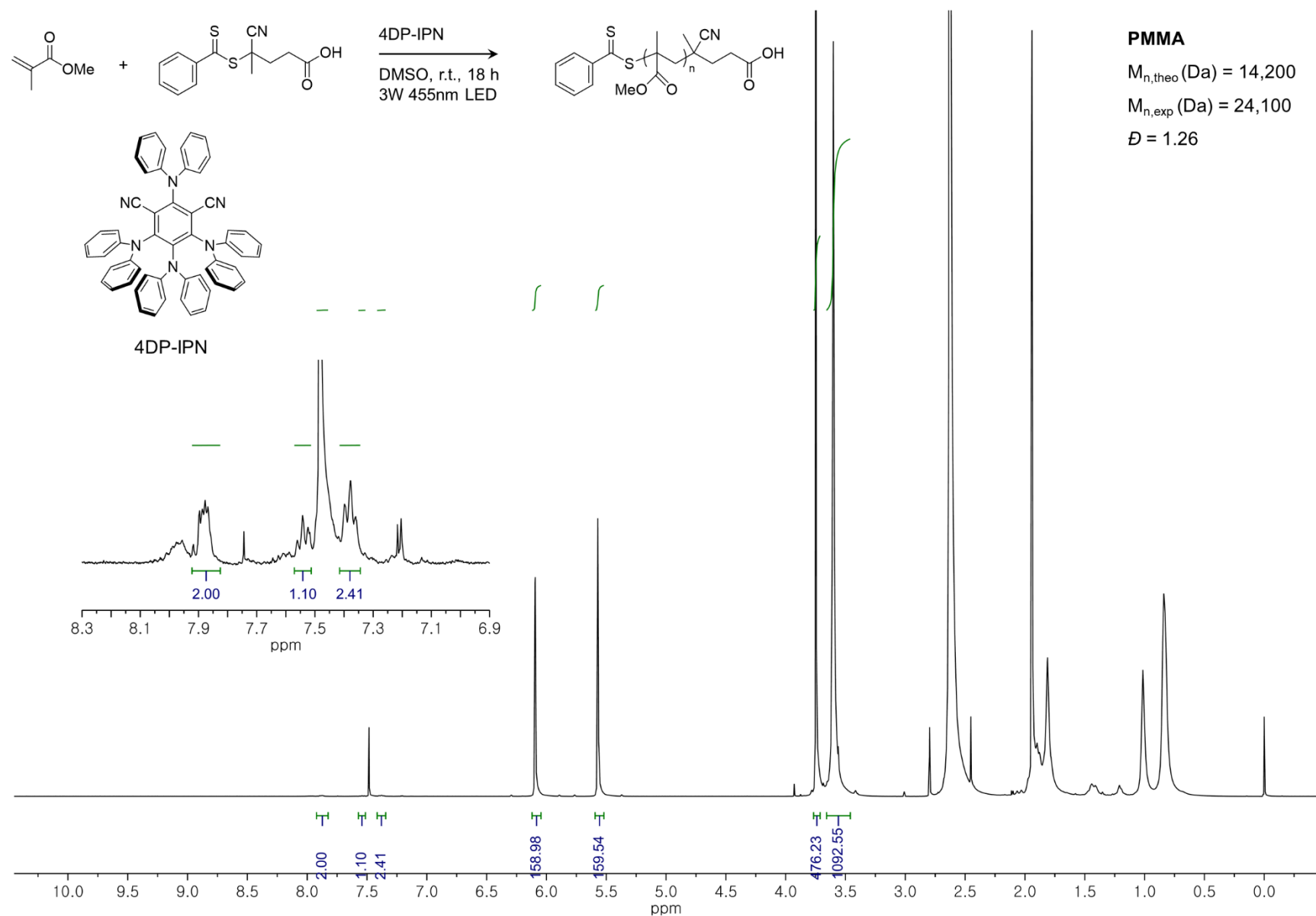


**Figure S51.** In-situ <sup>1</sup>H NMR of PMMA in the presence of CPADB, MMA, and 4DP-IPN of 5 ppm under air in CDCl<sub>3</sub> at r.t. (For Figure 2a. entry 12).

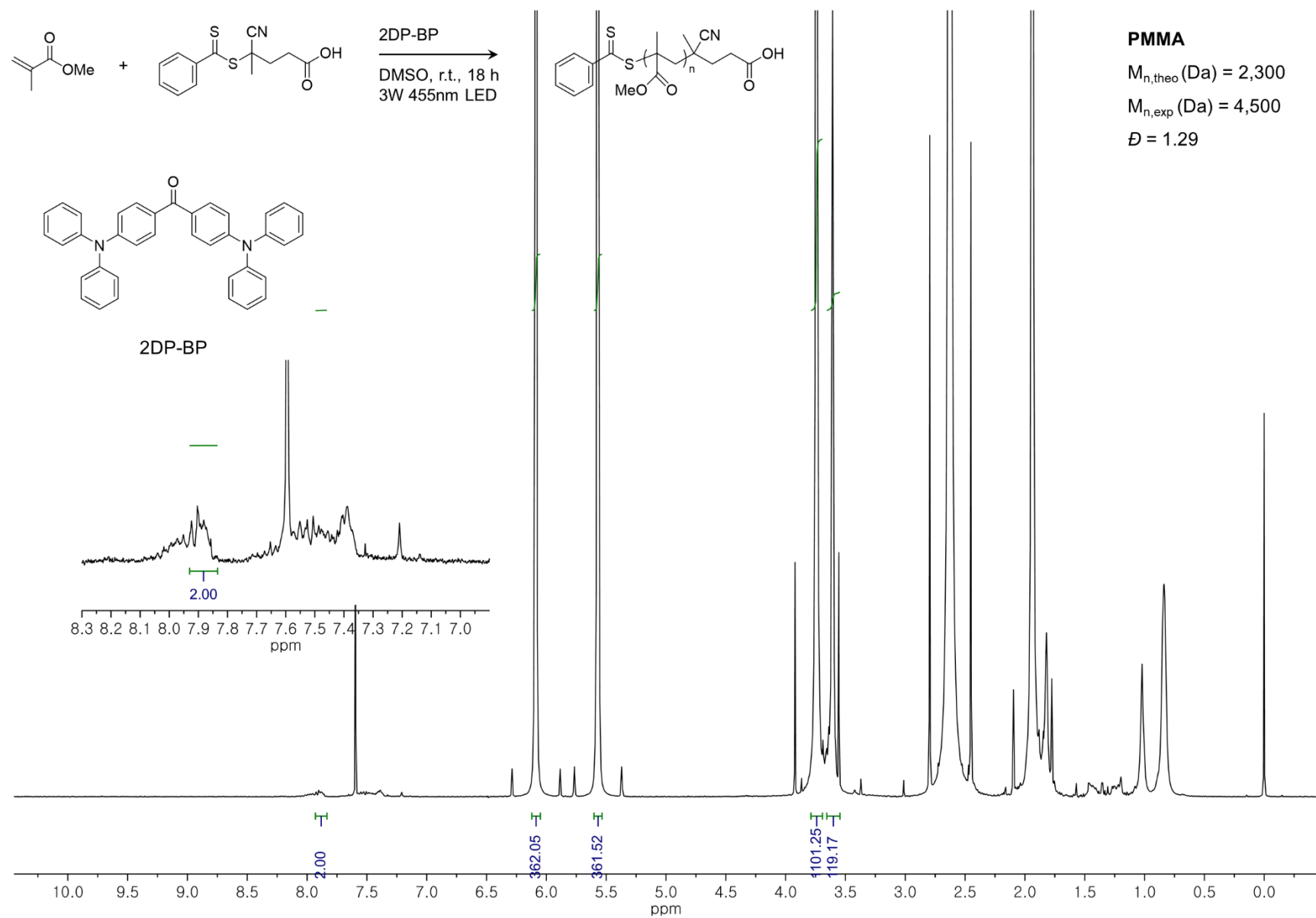


**Figure S52.** In-situ  $^1\text{H}$  NMR of PMMA in the presence of CPADB, MMA, and 2DP-BP of 5 ppm under air in CDCl<sub>3</sub> at r.t. (For Figure 2a. entry 14).

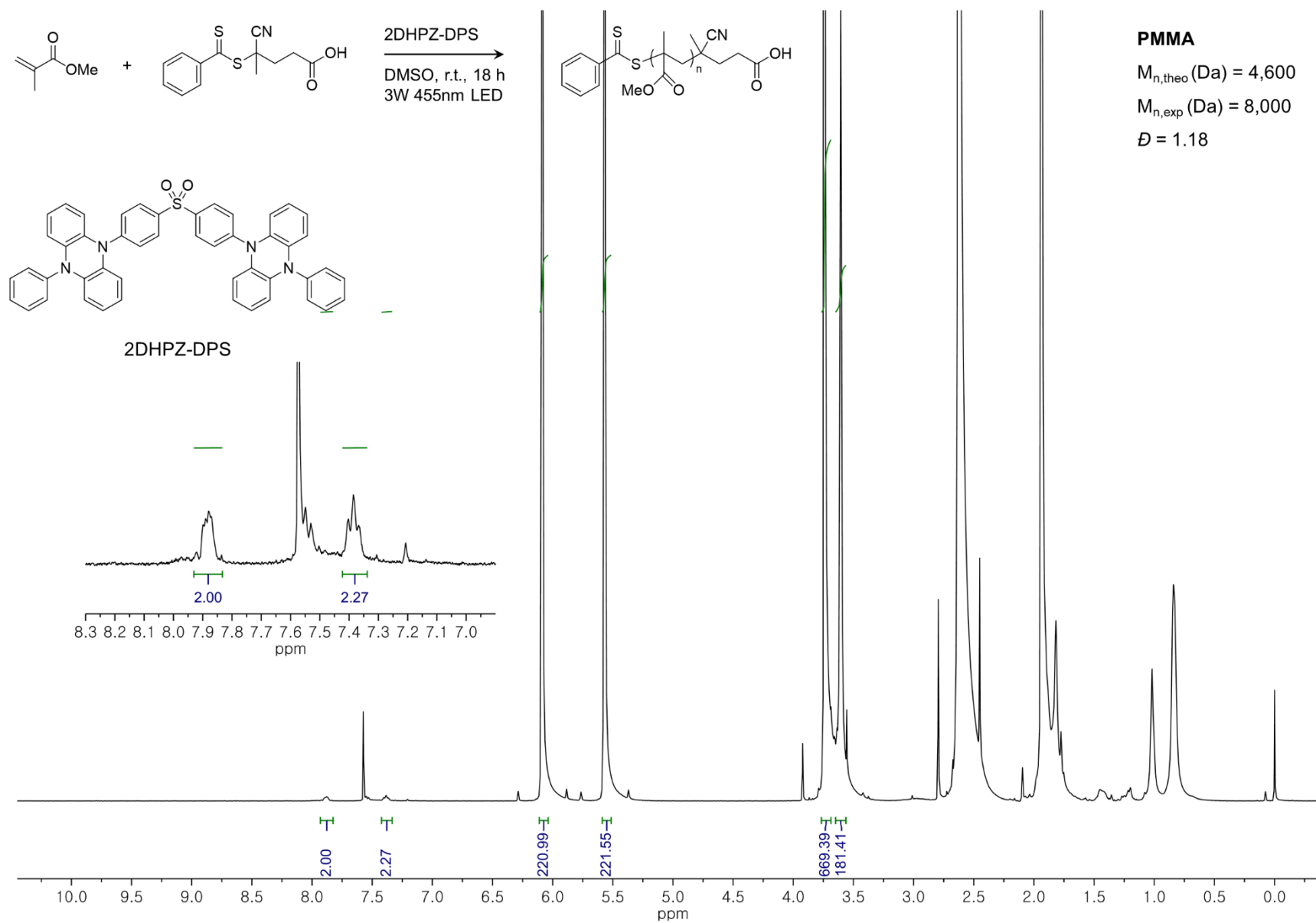


**Figure S53.** In-situ  $^1\text{H}$  NMR of PMMA in the presence of CPADB, MMA, and 2DHPZ-DPS of 5 ppm under air in  $\text{CDCl}_3$  at r.t. (For Figure 2a. entry 16).

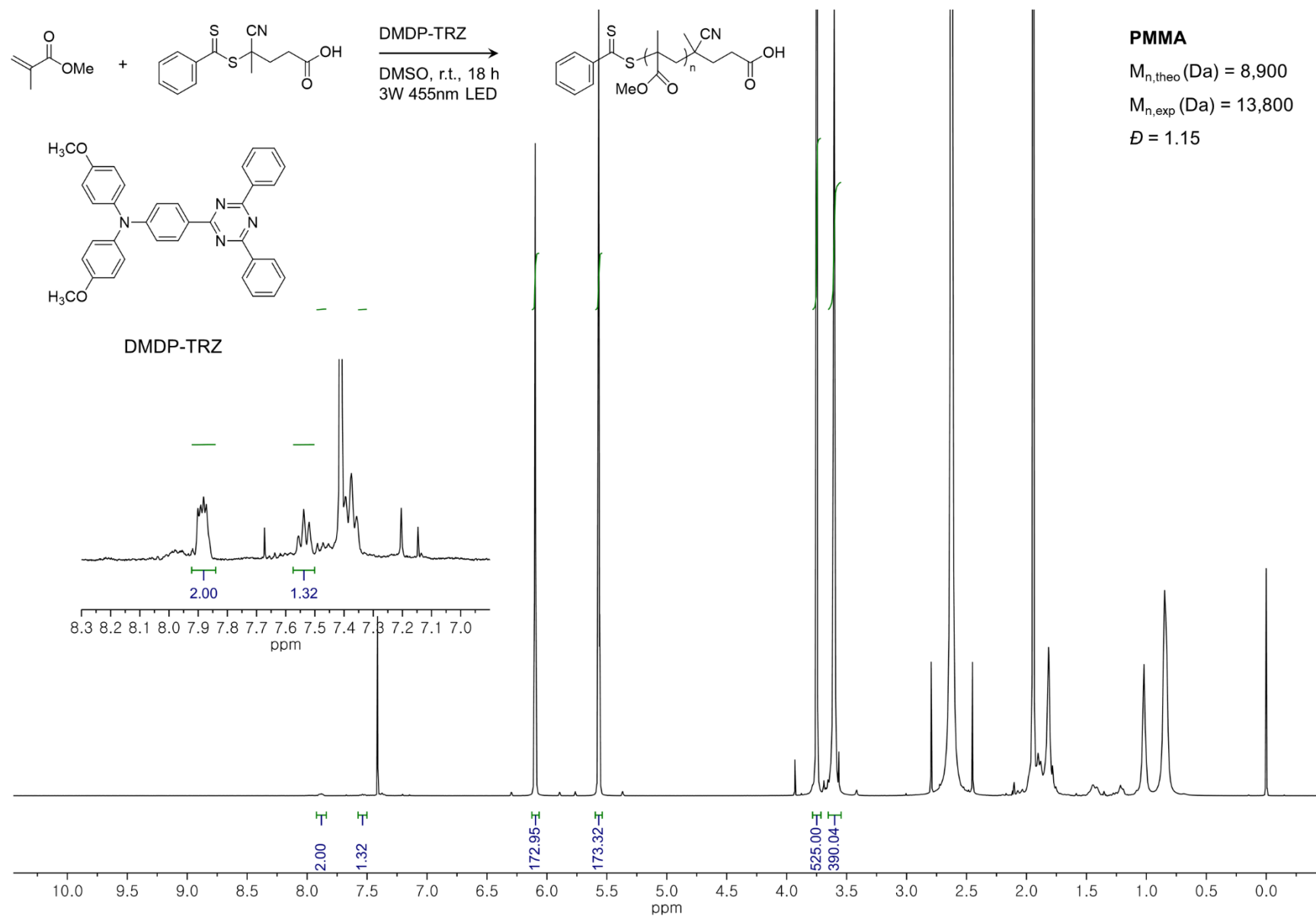


**Figure S54.** In-situ <sup>1</sup>H NMR of PMMA in the presence of CPADB, MMA, and DMDP-TRZ of 5 ppm under air in CDCl<sub>3</sub> at r.t. (For Figure 2a. entry 18).

#### IV. Supplementary References

- (1) Singh, V. K.; Yu, C.; Badgujar, S.; Kim, Y.; Kwon, Y. H.; Kim, D.; Lee, J.; Akhter, T.; Thangavel, G.; Park, L. S.; Lee, J.; Nan-dajan, P. C.; Wannemacher, R.; Milián-Medina, B.; Lüer, L.; Kim, K. S.; Gierschner, J.; Kwon, M. S. *Nat. Catal.* **2018**, 1, 794–804.
- (2) (a) Berberan-Santos, M. N.; Garcia, J. M. M. *J. Am. Chem. Soc.* **1996**, 118, 9391. (b) Baleizão, C; Berberan-Santos, M. N. *J. Chem. Phys.* **2007**, 126, 204510.
- (3) Roth, H.G.; Romero, N. A. & Nicewicz, D.A. *Syn. Lett.* **2016**, 27, A-J.
- (4) Brownson, D. A. C. & Banks, C. E. **2014**.
- (5) Pavlishchuk, V. V. & Addison, A. W. *Inorg. Chim. Acta* **2000**, 298, 97.
- (6) Gaussian 09, Revision D.01, Frisch, M. J.; Trucks, G. W.; Schlegel, H. B.; Scuseria, G. E.; Robb, M. A.; Cheeseman, J. R.; Scalmani, G.; Barone, V.; Mennucci, B.; Petersson, G. A.; Nakatsuji, H.; Caricato, M.; Li, X.; Hratchian, H. P.; Izmaylov, A. F.; Bloino, J.; Zheng, G.; Sonnenberg, J. L.; Hada, M.; Ehara, M.; Toyota, K.; Fukuda, R.; Hasegawa, J.; Ishida, M.; Nakajima, T.; Honda, Y.; Kitao, O.; Nakai, H.; Vreven, T.; Montgomery, J. A.; Peralta, J. E.; Ogliaro, F.; Bearpark, M.; Heyd, J. J.; Brothers, E.; Kudin, K. N.; Staroverov, V. N.; Kobayashi, R.; Normand, J.; Raghavachari, K.; Rendell, A.; Burant, J. C.; Iyengar, S. S.; Tomasi, J.; Cossi, M.; Rega, N.; Millam, J. M.; Klene, M.; Knox, J. E.; Cross, J. B.; Bakken, V.; Adamo, C.; Jaramillo, J.; Gomperts, R.; Stratmann, R. E.; Yazyev, O.; Austin, A. J.; Cammi, R.; Pomelli, C.; Ochterski, J. W.; Martin, R. L.; Morokuma, K.; Zakrzewski, V. G.; Voth, G. A.; Salvador, P.; Dannenberg, J. J.; Dapprich, S.; Daniels, A. D.; Farkas, O.; Foresman, J. B.; Ortiz, J. V.; Cioslowski, J.; Fox, D. J. *Gaussian, Inc., Wallingford CT* **2009**.
- (7) (a) Macchi, G.; Milián Medina, B.; Zambianchi, M.; Tubino, R.; Cornil, J.; Barbarella, G.; Gierschner, J.; Meinardi, F. *Phys. Chem. Chem. Phys.* **2009**, 11, 984; (b) Milián Medina, B.; Wasserberg, D.; Meskers, S. C. J.; Mena-Osteritz, E.; Bäuerle, P.; Gierschner, J. *J. Phys. Chem. A* **2008**, 112, 13282.
- (8) Milián-Medina, B.; Gierschner, J. *Org. Electron.* **2012**, 13, 895.